Universitat de Girona

Elvis Amoah Ofosu

Design and Numerical Analysis of Composite Deployable Lightweight Bridge Structures for Emergency Applications



FRP++
Advanced structural analysis and design using composite materials

Master Dissertation
European Master Advanced Structural Analysis and Design using Composite Materials

Work developed under the supervision of
Assistant Professor José Manuel Guerrero (PhD)
Assistant Professor Cristina Barris Peña (PhD)



Funded by the European Union

September 2026

DECLARATION

Name: Elvis Amoah Ofosu

Email: oamoah.elvis@gmail.com **Phone number:** +34 611009446

Citizen Card Number: G4476784

Title of the Dissertation: Design and Numerical Analysis of Composite Deployable Lightweight Bridge Structures for Emergency Applications

Supervisors:

Assistant Professor José Manuel Guerrero (PhD)

Assistant Professor Cristina Barris Peña (PhD)

Year of Conclusion: 2026

Master Course in Advanced Structural Analysis and Design using Composite Materials

THE ENTIRE REPRODUCTION OF THIS DISSERTATION IS AUTHORIZED ONLY FOR RESEARCH PURPOSES, UPON WRITTEN DECLARATION BY THE INTERESTED PERSON, WHICH IS COMMITTED TO.

University of Girona, 01/09/2026

Signature: 

ACKNOWLEDGEMENTS

I first express my profound gratitude to Almighty God for His grace, strength, and good health throughout this master's programme. His guidance has sustained me through every stage of this academic journey and enabled me to complete this research successfully.

I extend my sincere appreciation to my supervisors, Dr. Cristina Barris Peña and Dr. José Manuel Guerrero, for their continuous guidance, support, and constructive feedback. Their expertise and encouragement have been invaluable to the development of this thesis. I am also grateful to all the professors of the FRP++ Erasmus Mundus Master's Programme for their dedication, teaching, and motivation.

My heartfelt thanks go to my classmates for their collaboration, support, and friendship, which made this international experience both enriching and memorable.

I would like to acknowledge the AMADE Research Group at the University of Girona for providing essential technical support and access to research facilities during the development of this work. Their assistance contributed significantly to the successful completion of the experimental and numerical components of this thesis.

I also thank the partner universities of the FRP++ programme: the University of Toulouse (France)**,** the University of Girona (Spain), the University of Naples Federico II (Italy), and the University of Minho (Portugal) for offering an excellent academic and research environment.

Finally, I gratefully acknowledge the Erasmus Mundus Scholarship Award for the financial support, which made it possible for me to pursue this master's degree across multiple institutions.

Diseño y análisis numérico de estructuras ligeras de puentes compuestos desplegables para aplicaciones de emergencia

RESUMEN

En situaciones donde infraestructuras de caminos como puentes se ven alteradas tras un desastre natural y eventos climáticos extremos como inundaciones, tormentas y terremotos, la restauración del acceso se convierte en un objetivo urgente a alcanzar. Las soluciones convencionales de puente de emergencia suelen fabricarse en acero o aluminio. Aunque son efectivas, su masa limita la transportabilidad y la facilidad de despliegue en entornos post-desastre con recursos limitados.

Esta tesis investiga el uso de un perfil de polímero reforzado con fibra de carbono (CFRP) pulverizado para un puente tijera desplegable, destinado a mejorar la transportabilidad sin comprometer el rendimiento estructural.

Se evaluó un modelo global de elementos finitos tanto de CFRP como de secciones equivalentes de aluminio en función de los estados límite de deflexión, resistencia última y pandeo global bajo un vehículo de diseño real y combinaciones de cargas extremas, de acuerdo con el Código Trilateral de Diseño y Prueba (TDTC) para equipos militares y de cruce de huecos. La conexión central de pivote del puente de tijeras se analizó utilizando modelos locales de elementos finitos, evaluando dos soluciones: un pasador convencional perforado y un conector giratorio con sujeta externa

El puente CFRP cumplió el límite de deflexión aunque permaneció aproximadamente un 19% más ligero que la alternativa de aluminio y conservó una reserva de resistencia máxima sustancial, aunque con un margen global de pandeo reducido. A nivel de conexión, se comprobó que la unión de pasadores perforada fallaba en el rodamiento transversal en la perforación, mientras que las ojones metálicas del conector giratorio cedían bajo la misma caja de carga.

PALABRAS CLAVE: Puente desplegable; Mecanismo de tijera; Compuesto CFRP pulverizado; Conexiones; Modelado por elementos finitos.

Disseny i anàlisi numèrica d'estructures lleugeres de ponts compostos desplegables per a aplicacions d'emergència

RESUM

En situacions on infraestructures viàries com ponts es veuen alterades després d'un desastre natural i fenòmens meteorològics extrems com inundacions, tempestes i terratrèmols, restablir l'accés esdevé un objectiu urgent a assolir. Les solucions convencionals de ponts d'emergència solen fabricar-se d'acer o alumini. Tot i ser efectives, la seva massa limita la transportabilitat i la facilitat de desplegament en entorns postdesastre amb recursos limitats. Aquesta tesi investiga l'ús d'un perfil de polímer reforçat amb fibra de carboni polvoritzada (CFRP) per a un pont de tisora desplegable, amb l'objectiu de millorar la transportabilitat sense comprometre el rendiment estructural.

Es va avaluar un model global d'elements finits tant de seccions transversals CFRP com d'equivalent d'alumini basant-se en els estats límit de deflexió, resistència última i pandeig global sota un vehicle de disseny real i combinacions de càrregues extremes, d'acord amb el Codi de Disseny i Prova Trilateral (TDTC) per a equips militars i de creuament d'espais. La connexió del centre de pivot del pont de tisora es va analitzar utilitzant models locals d'elements finits, avaluant dues solucions: un pin convencional foradat i un connector giratori amb pinça externa

El pont CFRP va complir el límit de deflexió tot mantenint-se aproximadament un 19% més lleuger que l'alternativa d'alumini i va conservar una reserva de resistència màxima substancial, tot i que amb un marge global de caiguda reduït. A nivell de connexió, es va comprovar que la junta perforada dels pins fallava al coixinet transversal del forat, mentre que els ulls metàl·lics del connector giratori cedien sota la mateixa caixa de càrrega.

PARAULES CLAU: Pont desplegable; Mecanisme de tisora; Compost de CFRP en pols; Connexions; Modelatge per elements finits.

Design and Numerical Analysis of Composite Deployable Lightweight Bridge Structures for Emergency Applications

ABSTRACT

In situations where pathway infrastructures like bridges are disrupted in the aftermath of a natural disaster and extreme climatic events such as floods, storms and earthquakes, access restoration becomes a pressing goal to be achieved. Conventional emergency bridging solutions are typically fabricated from steel or Aluminium. While effective, their mass constrains transportability and deployability in resource-limited, post-disaster settings.

This thesis investigates the use of a pultruded carbon-fibre-reinforced polymer (CFRP) profile for a deployable scissor bridge, intended to improve transportability without compromising structural performance.

A global finite element model of both CFRP and equivalent Aluminium sections were evaluated against deflection, ultimate strength, and global buckling limit states under a real design vehicle and extreme load combinations in accordance with the Trilateral Design and Test Code (TDTC) for military and gap-crossing equipment. The central pivot connection of the scissor bridge was analysed using local finite element models, evaluating two solutions: a conventional drilled pin and an externally clamped swivel connector

The CFRP bridge met the deflection limit while remaining approximately 19% lighter than the Aluminium alternative and retained a substantial ultimate-strength reserve, though at a reduced global buckling margin. At the connection level, the drilled pin joint was found to fail in transverse bearing at the perforation, while the swivel connector's metallic lugs yielded under the same load case.

KEYWORDS: Deployable Bridge; Scissor Mechanism; Pultruded CFRP Composite; Connections; Finite Element Modelling.

TABLE OF CONTENTS

Acknowledgements III
Resumen IV
Resum V
Abstract VI
Table of Contents VII
List of Figures XI
List of Tables XIII
List of Abbreviations and Symbols XIV
1. Introduction 1
1.1. Background and Motivation 1
1.2. Problem Statement 5
1.3. Aims and Objectives 6
1.4. Scope and Limitation 6
1.4.1. Scope of Project 6
1.4.2. Limitations 7
1.5. Thesis Structure 7
2. State-of-the-art review of deployable bridges 9
2.1. Evolution of Deployable Structures 9
2.2. Deployable Bridges: Typologies and Development 11
2.2.1. Military Inventions and Description 11
2.2.2. Civilian Deployable Bridges. 13
2.2.3. Deployment Mechanisms 15
2.3. Scissor Bridge Mechanism 16
2.3.1. Structural Performance of Deployable Scissor Bridge. 19
2.4. Materials In Deployable Bridge Systems 19
2.4.1. Metallic Materials 20
2.4.2. Fibre Reinforced Polymer (FRPs) Composites 22

2.4.3. Transition from GFRP to CFRP 23
2.4.4. Hybrid FRP-Metal Bridge Systems 24
2.5. Existing Case Studies 25
2.5.1. Case Study 1: CFRP rapid portable bridge. 25
2.5.2. Case Study: Hybrid GFRP-Steel Bridge 27
2.6. Design Standards and Codes for Deployable Bridges 28
2.7. Connections in deployable bridges. 30
2.7.1. Introduction to Connection Systems in Deployable Bridges 30
2.7.2. Functional Categories of Connections 31
2.7.3. Material-Specific Connection Behaviour 33
2.7.4. Mechanical behaviour of Connections 36
3. Conceptual Design 39
3.1. Design Philosophy 39
3.2. Design Requirements and Constraints 42
3.2.1. Functional Requirements 42
3.2.2. Governing Standard 42
3.3. Material Constraint 44
3.4. Scissor Bridge Geometric Configuration 45
3.5. Material Selection 46
3.6. Preliminary Load Definition and Analysis 47
3.6.1. Dead Load 47
3.6.2. Hypothetical Design Vehicle 47
3.6.3. Pedestrian Load (P) 50
3.6.4. Wind Load 51
3.7. Design Load Combinations 51
4. Global Structural Design of the DCS 53
4.1. Scope of Global Design 53
4.1.1. Preliminary Sizing of primary Scissor Members. 53

4.2. Finite Element Model in Abaqus 55
4.2.1. Element Selection 56
4.2.2. Material Properties 57
4.2.3. Material Orientation and Section Properties 60
4.2.4. Interactions 61
4.2.5. Boundary Conditions 62
4.2.6. Load Definition 63
4.2.7. Analysis Step Definition 64
4.2.8. Mesh 67
5. Connection Design 69
5.1. Basis of Connection Design 69
5.2. Detailed Description of the selected Joint 70
5.2.1. Concept 1: Metallic Pin Connection 70
5.2.2. Concept 2: Externally Clamped Metallic Swivel Connector 70
5.3. Local Finite Element Sub Model Development 71
5.3.1. Selection of the Local Model Unit 71
5.3.2. Geometry and Material Definition 72
5.3.3. Interaction Modelling 75
5.3.4. Loading and Boundary conditions. 76
5.3.5. Meshing 78
6. Results and Discussion 81
6.1. SLS Performance 81
6.1.1. Iterative section-selection 81
6.1.2. Load-Deflection Response under Traversing Load 82
6.1.3. Load-Deflection Response Under Extreme Load Combination 83
6.1.4. Deployment displacement under self-weight 84
6.1.5. Load-Deflection Response under Convoy Wheeled Loading 85
6.1.6. Comparative SLS check for CFRP and Aluminium 86
6.2. ULS Performance 87

6.2.1. Global Stress Analysis 87
6.2.2. Bending Analysis 88
6.2.3. Buckling Performance 90
6.3. Local Structural Response of Connection 93
6.3.1. Simple metallic pin connection 93
6.3.2. External clamped metallic swivel connector 97
6.3.3. Comparison of Global Displacement Behavior 99
6.4. Failure Assessment of Connection 100
6.4.1. Pin Bearing Failure 101
6.4.2. Metallic Yielding 102
7. Conclusions and further developments 103
7.1. Main Conclusion 103
7.1.1. Global Bridge Model 103
7.1.2. Local connection model 103
7.2. Further developments 104
7.3. References 105

LIST OF FIGURES

Figure 1.1: Scenarios of climate-driven bridge collapse in Europe. 2
Figure 2.1: Historical Images of Deployable Structures. 10
Figure 2.2: Main Categories of Military Bridges 13
Figure 2.3: Civilian Deployable Bridge Structures 14
Figure 2.4: Schematic Description of Deployable Mechanisms [36] 16
Figure 2.5: Scissor Lift Structure 17
Figure 2.6: Deployable Aluminium Scissor Bridge [40], [41] 18
Figure 2.7: Hybrid FRP-Metallic Truss Bridge[60] 25
Figure 2.8: CFRP rapid portable bridge [58] 26
Figure 2.9: Hybrid GFRP-Steel bridge[61] 28
Figure 2.10: Tensile Pin Joint[58] 35
Figure 3.1: Geometric Configuration of the deployed Scissor Bridge 45
Figure 3.2: Hypothetical Design Vehicle: Nissan mini Urvan[88] 48
Figure 3.3: Tracked Load Representation 49
Figure 3.4: Wheeled Load Representation 50
Figure 4.1: Initial Geometry of DCS bridge 55
Figure 4.2: Global Model of scissor bridge 56
Figure 4.3: Material Properties 58
Figure 4.4: Material and section definition for elements 61
Figure 4.5: Interaction definition for DCS 62
Figure 4.6: Definition of Boundary conditions 63
Figure 4.7: Load definition 64
Figure 4.8: Definition of general static step 65
Figure 4.9: Definition of buckling step 65
Figure 4.10: Linear Buckling Model of DCS Bridge. 66
Figure 4.11: Definition of Mesh 67
Figure 5.1: Schematic representation of simple pin connection 70
Figure 5.2: Selected scissor unit 71
Figure 5.3: 3D model of pultruded CFRP diagonal members 72
Figure 5.4: 3D model of Pin and bushing assembly 73

Figure 5.5: 3D modelled parts of external swivel connector 74
Figure 5.6: Contact interaction in the drilled pin connection 75
Figure 5.7: Contact definitions assigned to swivel connector 76
Figure 5.8: Connection design boundary conditions and load definitions. 78
Figure 5.9: Creation of mesh for the connections 78
Figure 6.1: Mid-span deflection under different load combinations 81
Figure 6.2: Mid-span vertical deflection under traversing loads 83
Figure 6.3: Maximum deflection under extreme load case 84
Figure 6.4: Deformed configuration during deployment 85
Figure 6.5: Deformed shape of the DCS bridge under LC5 85
Figure 6.6: Comparative Load-Deflection response for CFRP and Aluminium models 86
Figure 6.7 : Deformed stress contour plot of bridge models 88
Figure 6.8: Deformed bending contour plot of bridge models 89
Figure 6.9: Comparative linear buckling response 91
Figure 6.10: Longitudinal stress (S11) distribution around the pin hole 94
Figure 6.11: Transverse Stress (S22) Distribution around the pin hole 94
Figure 6.12: In-plane shear stress (S12) distribution in the CFRP connection. 95
Figure 6.13: Von Mises stress distribution in the steel pin and bushings 96
Figure 6.14: Contact pressure (CPRESS) distribution between the bushing and the CFRP hole. 96
Figure 6.15: Stress distribution of unperforated CFRP pultruded members 97
Figure 6.16: Von Mises stress of the swivel connector 98
Figure 6.17: Contact Pressure (CPRESS) within the swivel connector 99
Figure 6.18: Displacement results of the two connection solutions 100

LIST OF TABLES

Table 3.1: Specifications of the Hypothetical Design Vehicle[88] 47
Table 3.2: Summary of Design Load combinations 51
Table 4.1: Pultruded CFRP mechanical properties 59
Table 4.2: A6NO1 Aluminium alloy mechanical properties[40] 59
Table 4.3: Wooden deck mechanical properties [90] 60
Table 5.1: Al 7075-T6: High yield Aluminium material properties 73
Table 5.2: Connector Loads from Global FE model 77
Table 6.1:Geometric section dimensions of materials 82
Table 6.2: Comparative bending verification results 90
Table 6.3: Buckling Verification Results for Aluminium and CFRP for traversing load 92
Table 6.4: Buckling verification for Aluminium and CFRP at LC4 92
Table 6.5: Bearing failure verification results. 101

LIST OF ABBREVIATIONS AND SYMBOLS

Abbreviations

CEN	European Committee for Standardization
CFRP	Carbon Fibre Reinforced Polymer
DCS	Deployable Composite Scissor
TDTC	Trilateral Design and Test Code
GFRP	Glass Fibre Reinforced Polymer
FRP	Fibre Reinforced Polymer
RHS	Rectangular Hollow Section
MLC	Military Load Class
UD	Unidirectional
ULS	Ultimate Limit State
SLS	Serviceability Limit State
LC	Load Combination
EUROCOMP	European Structural Polymeric Composites Group
FE	Finite Element
GVW	Gross Vehicle Weight
CTF	Connector Total Force
CTM	Connector Total Moment
LOC	Line of Communication
DWT	Double Warren Truss
AFRP	Aramid Fibre Reinforced Polymer
CPRESS	Contact Pressure
AS	Aluminium Section
CS	Composite Section
TL	Tracked Load
WL	Wheeled Load
SW	Self-Weight

Symbols

w	wind load
H	Height
B	Breadth
t	Thickness
α	Expansion angle
S11	Longitudinal stress
S22	Transverse stress
S12	In-plane shear stress
f_{ck}	Characteristic material strength
f_d	Design material strength
γ	Reduction factor
δ	Deflection
η	Utilization ratio
E	Elastic Young's modulus
ν	Poison's ratio
G	Shear Modulus
P	Density
f_u	ultimate strength
f_y	yield strength
P_{cr}	critical buckling capacity
φ	drag coefficient
wp	wind pressure

THIS PAGE WAS INTENTIONALLY LEFT BLANK

1. INTRODUCTION

1.1. Background and Motivation

In modern societies, infrastructure access and connectivity are a cornerstone to development. Communities access relevant services including healthcare, foot supply, day-to-day movements, and other basic utilities through roads and bridges. Basically, pathways carry the flow that keeps communities thriving. However, disasters such as floods, heavy storms, extreme snowfall, among others, frequently disrupt access without warning, placing lives at serious risk. The outcome of survivors awaiting rescue mainly depends on the speed and reliability of access restoration.

Conventional bridges and river crossings are particularly susceptible, among the various infrastructure elements that are disrupted during unexpected natural disasters. Vast stretches of road networks are rendered inaccessible when flood and storm surges completely destroy existing bridge structures. In areas where alternative routes of escape are limited, the destruction of a single crossing entirely cuts off communities from their adjoints. Delayed emergency response could inadvertently lead to loss of lives.

There are several cases that illustrate the scale of vulnerability of conventional bridges. Preliminary reports from the 2021 Ahr Valley flood in Germany discloses that between 41 - 60 conventional bridges were destroyed, isolating several communities from emergency services at the moment of greatest need (See Figure 1.1.a) [1]. Similar event happened in Valencia; Spain on October 2024 parts of the region experienced 500 mm of rainfall in eight hours. This led to the destruction of the Picanya bridge over the Barranci del Poyo (Figure 1.1.d). Residents disconnected in this situation resorted to building their own improvised walkway. More recently between October 2025 and mid-February 2026, the central of Portugal recorded approximately 1238 mm of rainfall, which caused a flood-defence dyke on the Mondego River to rupture near Casais, Coimbra. The resulting erosion scoured the foundations of an elevated section of the A1 motorway, causing a section of the carriageway to collapse (See Figure 1.1. b). Traffic had to be rerouted via long detours, placing pressure on alternatives routes.

These examples give an idea of the extent of devastation caused by climate driven disasters. According to the report covered in [2], cases of floods within 2024 and 2025 have affected over 20 European countries, caused 337+ deaths and an overall cost of about €13.8 billion in damage. These floods were driven by prolonged heavy rains, causing deaths and widespread damage due to overflowing river basins and landslides, and in several cases directly destroyed temporary bridging infrastructure. Unlike many disaster-prone regions of Asia, where bridge loss is more often tied to seismic activity, one of Europe's principal drivers of bridge disruption is increasingly erratic rainfall leading to flash flooding, a pattern that climate projections suggest will intensify in frequency and severity [3].



(a) Ahr Valley Bridge Collapse (2021 flood, Germany) [4]



(b) Collapse of A1 Motorway (2026 heavy storm in Coimbra, Central Portugal)[5]



(c) Picanya Bridge Collapse (October 2024 heavy rains, Spain) [6]

Figure 1.1: Scenarios of climate-driven bridge collapse in Europe.

Infrastructure disruption response has traditionally depended on the construction of temporary bridges as a means to restore access but they present practical limitations in certain contexts of emergencies. The construction time, skilled labour and availability of certain resources in the immediate aftermath of a disaster are of much concern. Affected communities may still remain cut off from urgent assistance depending on the duration of construction.

Another remediation to these happenings is the use of deployable bridges. Deployable structures are flexible structures that can transform themselves from a compact stowed state to a predetermined operational configuration upon actuation [7]. They are widely applied in spacecraft and satellites as well as construction of modular structures. The behaviour of these structures depends also on their geometrical, material and mechanical properties. Deployable structures operate by kinetic principles which are highly influenced by their architecture. They are constantly evolving and changing due to the specific and sector of application. Deployable structures offer reusability and energy, resource, materials and space efficiency, thus promoting sustainability [8]. The inspiration of deployable structures comes from natural biological structures such as movable parts of plants and animals. Deployable structures are widely applied in temporary shelter and emergency amenities, semi-permanent buildings, space station components. Their effectiveness includes the modest storage due to their lightweight, easy transportation due to their retractable size and simple deploying process. The hurdles associated with these structures are their cost, assembly and their critical joints determine the life of the structures [9].

Stemmed from the idea of deployable structures, deployable bridge systems can be transported to any rescue ground and also be installed in a fraction of time. The idea and concept of deployable bridges traces back to military engineering, where the capability to quickly overcome obstacles such as rivers, ditches, and gaps in terrain was recognized as a tactical obligation.

From the Military perspective, deployable bridges are well established but mainly depend on specialized, heavy steel modular systems that remain constrained by logistics, transport weight, and the availability of trained personnel and haulage assets. This constraint is not merely theoretical even under expedited emergency conditions. At the Picanya bridge intervention, full service was not restored for nearly a month, because the same personnel and heavy-haulage assets were needed elsewhere for search and rescue operations. Because

the majority of existing deployable systems were developed primarily for military applications, they are not optimized for the priorities of civilian disaster response. As the frequency of climate-driven disasters increases, there is a growing need to adapt and improve upon these military-derived systems so that they specifically serve post-disaster civilian relief.

To overcome the weight constraint associated with heavy metallic bridges, there has been a raising concern of transitioning towards FRP composite materials. The potential of utilizing the unexcelled strength-to-weight ratio as well the mechanical properties of FRP composites offers promising advantages in the scope of bridge engineering. [10]. FRP composites exist in various forms and types depending on the specific manufacturing process and intended scope of application. In the Bridge engineering, protruded profiles of GFRP and CFRP are commonly used as primary structural components, and in certain cases, they are used to replace steel-concrete bridges that are subjected to corrosive environments. FRPs provide a wide range of tensile, flexural, impact and compressive strengths which makes them viable substitute to metallic structures when a specific function is of essence. Like conventional metallic profiles, FRPs are now supported by recognized with standards and codes guiding their design.

The application of lightweight FRP composite bridges is not only limited to designing the full bridge structure entirely from FRPs, rather they are optimized with conventional materials at critical parts where their properties fall short. Specifically, joint connections in FRPs are a critical design challenge due to their anisotropic nature of the material. Pultruded FRP profiles derive their strength from unidirectional fibres embedded with resin matrix, aligned predominantly along the longitudinal direction. When these profiles are joined using conventional methods that involve cutting or drilling holes, the continuity of both the longitudinal and transverse fibre directions is compromised, weakening the section at the connection point.

To this reason, several studies [11], [12], [13] [14] and research have investigated alternative joint solutions for pultruded FRP profiles which broadly falls in three main categories including purely bolted, purely bonded (adhesive) and hybrid connections.

Building on this background, this research project focuses on the design and analysis of a deployable, lightweight bridge system composed of pultruded hollow section CFRP profiles, configured as a scissor mechanism. A central focus of this work is the development of preliminary design concepts for the connectivity of the scissor composite bridge, specifically the pivot joint through which the CFRP members interact. The study adopts finite element

analysis to evaluate the global structural behaviour, considering real case loading condition and design in accordance with the TDTC standard.

1.2. Problem Statement

Rapid Deployable bridge systems for emergency use have almost entirely been built from conventional metallic materials like steel and Aluminium, and also developed for military applications. As a result, they tend to be heavy and dependent on specialized haulage vehicles and trained crews to operate. In civilian disaster response, these same crews and vehicles tend to be needed elsewhere at the same time, for search and rescue missions. This creates delay in restoring access to affected communities.

As climate-related disaster become more rampant, the gap between what current systems can offer and what disaster response actually needs is becoming more urgent to close. CFRP composite offer plausible solution to the weight problem, commending on its high strength-to-weight ratio. However, using CFRP in deployable bridge introduces hurdle to cross at the connection level. Pultruded CFRP profiles rely mainly on their fibre direction for strength, so drilling holes for bolts, which is the standard way to connect structural members, disrupts this fibre direction and weakens the member exactly where it is most needed.

The pivot joint in a deployable scissor bridge is the central connection of the primary structural members since it ensures the free rotation during deployments while still transferring loads within the structure.

At present, there is no established connection design that allows CFRP scissor members to rotate at a pivot point without relying on drilled holes through the profile, while also being simple enough to assemble and disassemble by a small, non-specialist crew in the field. This research seeks to develop a preliminary connection concept for a CFRP scissor bridge that solves the rotation and loading demands of the pivot joint without compromising the fibre integrity of the profile so that the bridge can be structurally reliable for its intended function.

1.3. Aims and Objectives

The main aim of this research is to introduce and develop a novel deployable lightweight CFRP composite bridge design to meet the requirements of immediate post disaster relief applications. To achieve this, the project seeks to satisfy the following objectives.

1) Define and evaluate novel deployable bridge solution with ease of transportability and structural efficiency.
2) Assess the global structural behaviour of the proposed system under relevant loading scenarios.
3) Design and investigate the mechanical performance of critical connection and joint regions through numerical modelling.

1.4. Scope and Limitation

1.4.1. Scope of Project

This research encompasses the conceptual and numerical design of a Deployable Composite Scissor bridge system fabricated from industry standard-sized pultruded CFRP hollow-section profiles. The scope briefly includes;

- Development of global scissor bridge configuration for a representative span of 21 m, sized for pedestrian and a specific optimal design vehicle loading.
- Global structural analysis using finite element modelling (Abaqus), including static SLS and ULS load cases and a linear eigenvalue buckling assessment in accordance with the TDTC standard.
- Comparison of the CFRP design against an equivalent Aluminium configuration from literature, on the basis of weight and SLS deflection performance.
- Development of preliminary hinge connection concepts for the scissor pivot joints compared to a simple rotating connecting pin joint in the main structural members.
- Analysis of the joint concept with local finite element modelling of the connection region behaviour under governing load case.

1.4.2. Limitations

- The study is limited to numerical modelling and analytical design; no physical prototype or scaled model is fabricated or tested as part of this dissertation.
- Material behaviour is modelled using idealized, homogenized orthotropic properties for the pultruded CFRP profile without any consideration of manufacturing defects, batch variability, and long-term degradation.
- The connection concepts developed are preliminary design proposals. Detailed fabrication tolerances, assembly procedures, and cost analysis are outside the scope of this work.
- Dynamic effects and environmental loading such as wind are only partially accounted for, based on assumed factors from the TDTC rather than site-specific data.
- The loading scenario are based on a single representative case (a mini-Nissan Urvan) as the hypothetical design vehicle for civilian application. The study does not address deployment mechanics in detail. This mean the actuation method, and time-to-deploy are acknowledged as relevant to the stated motivation but are not modelled or quantified.

1.5. Thesis Structure

The dissertation is broadly organized into seven (7) main chapters. Each chapter is well elaborated with subheadings that breaks down the knowledge of this project. Here, each chapter is summarized to give an overview of the entire dissertation.

Chapter one (1) introduces the project with detailed background and motivation while relating to the problem statement and the objectives to be achieved. It also explains the scope and limitations of the study.

Chapter two (2) reviews the existing knowledge on the state-of-the-art literature on deployable bridge systems covering the evolution of deployable structures to typologies of deployable bridges, materials, connection techniques, the scissor bridge mechanism and structural design and analysis approaches used in previous works.

Chapter three (3) also presents the conceptual design of the bridge, covering the design philosophy, requirements and constraints, scissor bridge geometric configuration, material selection, preliminary load definition, and the development of the connection concept. This chapter translates into the design that is analysed in Chapters four and five.

Chapter four (4) develops the global structural analysis of the deployable composite bridge using finite element modelling in Abaqus. This incorporates the defined load cases in chapter three to evaluate the overall structural performance

Chapter five (5) focuses on the connection design, presenting the design basis, proposed preliminary design solutions with a local finite element analysis

Chapter six (6) presents and discusses the design results from global structural performance of the bridge as well as the local structural response of the designed connection, correlating the two analyses to assess the overall design.

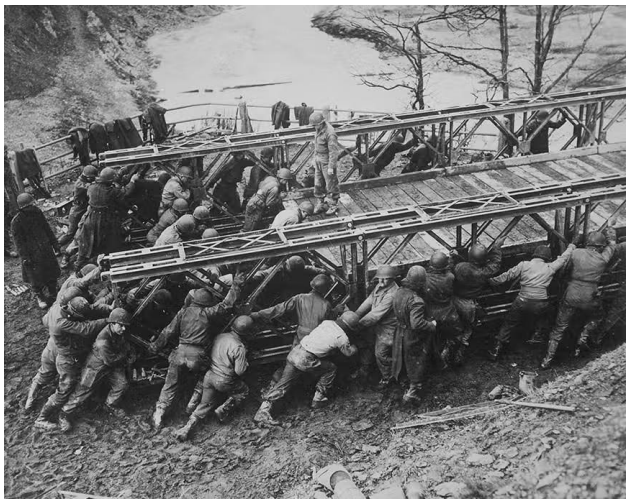
Chapter seven (7) concludes the dissertation with a summary of the key findings and the gaps for future development of the project.

2. STATE-OF-THE-ART REVIEW OF DEPLOYABLE BRIDGES

2.1. Evolution of Deployable Structures

Deployable structures are flexible structures that can transform from a simple compact state to a predetermined operational configuration upon actuation [7]. The behaviour of these structures depends also on their geometrical, material and mechanical properties. Deployable structures operate by kinetic principles which are highly influenced by their architecture. They are constantly evolving and changing depending on the specific sector of application. Deployable structures offer reusability of energy, resource, materials and space efficiency, thus promoting sustainability [8]. Throughout history, deployable structures have existed yet explored in minimal scale until the beginning of the twentieth century where industrial revolution revealed an emergence thought on them.

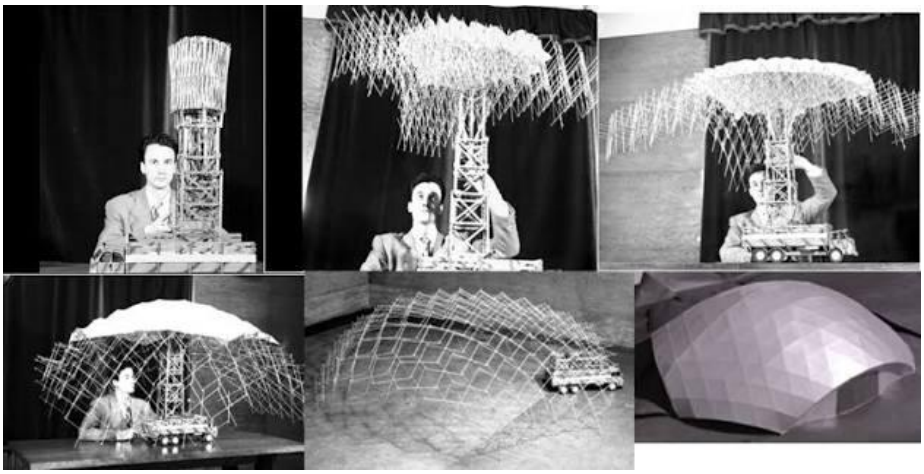
From the origin of nature-inspired retractable geometry, deployable structures evolved along emerging paths in early engineering and civilization. Tracing from the deployable bridge structures employed during the second world war, the Bailey bridge was conceived in 1936 but later developed and deployed by the British military from 1941 (See Figure 2.1 a). It was the first of its kind described as a portable modular bridge built for military application [15].



(a) Launch of Bailey Bridge in World War II, 1941 [16]



(b) Assembly of Modular Bailey Bridge Panels in 1943 [17]



(c) Emilio Piñero's Kinematic Deployable Dome Theatre [18]

Figure 2.1: Historical Images of Deployable Structures.

The aerospace industry in the 1950s hopped unto this invention, looking at how the configuration of a large structure changes in an autonomous way in any available space. Space missions increasingly required the easy mobility of large planar surfaces, a demand that propelled deployability as a core structural discipline in Aeronautics. This led to the development of spacecrafts, satellites, telescopes, solar arrays, and antennas leaving the industry to dominate and progress in this field [19], [20].

In architecture, the pioneering work of Emilio Piñero in the 1960's also translated the idea of deployability into designing a transportable theatre for Spanish festivals (See Figure 2.1 c). This innovation was recognized as the first large deployable structure actually built [18]. The concept was moved from theoretical linkage kinematics into operational architectural system [21], [22]. The kinetic principles were widely also explored in art, infrastructures and industrial design.

Piñero's kinematic deployment principle, having been refined by Hoberman, was further redirected from the track of architecture toward bridging. Although bridging has distinctly seen two eras of deployability, the premier dated back to World War II, where deployment was mainly modular with manual assembly of bridge components and the later was based on kinematic mechanism-driven, where deployment functioned from a single coordinated motion rather than sequential panel assembly [23].

With recent developments, deployable structures are widely applied in temporary shelter equipment and emergency amenities, semi-permanent buildings and space station

components [24]. Their effectiveness includes the modest storage and lightweight as well as easy transportation due to their retractable size and simple deploying process. Robotic intelligence has introduced a single button command to initiate the deployment process within a small fraction of time.

2.2. Deployable Bridges: Typologies and Development

2.2.1. Military Inventions and Description

Deployable bridges are infrastructural systems that have the potential to be easily transported to the needed grounds, assembled and disassembled, or launched to cover a specific span. They exist as temporary structures that provide access and connectivity in situations where conventional bridges are not available or disrupted. The performance of deployable bridges depends on their coverage span, rapid installation, ease of transportation with minimal logistics, load capacity and structural stability.

Deployable bridge technology has increasingly progressed from early hand-erectable modular truss system like the Bailey bridges, whose prefabricated panels, rapid assembly and adaptability revolutionized military gap crossing to sophisticated solutions designed for faster deployment, high load capacity and reduced manpower [25].

[23] presented a comprehensive historical review of how military bridging technology had progressed from simple hand-built modular trusses to highly engineered, rapidly deployable systems capable of restoring access and lifelines in emergency situations. The review categorizes deployable bridges into four main structural typologies. Rapidly erectable modular gap-crossing systems, vehicle-launched bridges, floating bridges, and ship-to-shore causeways, with each representing distinct mechanical strategies for modularity, load transfer, and deployment methodology. The geometry of the early bridge inventions utilized scalable configurations enabling variable spans lengths and load classes.

From the military perspective, these bridges transcended into three subcategories; tactical, support, and line of communication depending on their geometry and method of deployment [26].

Tactical Bridges.

These deployable military bridges, also referred as Assault bridges enable immediate manoeuvre across obstacles or gaps during combat operations (See Figure 2.2 a). They are the fastest-deploying bridge systems, designed for use under threat, often by armoured units. With a coverage span typically between 10 m and 20 m, tactical bridges usually fall within the short-span category optimized for single-span dry gaps. They usually operate hasty crossings during harsh manoeuvre, capable of handling single vehicle to high MLC loads. Tactical bridges make use of simply supported beam that require mechanized deployment ranging from hydraulic launchers, scissor mechanisms and folding girders, hence minimal manual assistance [27]. In this bridge system, deployment time is prioritized over span length. Armoured Vehicle-Launched Bridges, Joint Assault Bridge, Wolverine, Rapidly Emplaced Bridge System, scissor-type mobile bridges are typical bridges that function under this scope.

Support Bridges

These deployable military bridges provide semi-permanent, modular bridging for sustained operations once the immediate tactical phase is complete (See Figure 2.2 b). Deployment is by means of manual assembly and in some cases lightly mechanized systems. Support bridges balance span capability, modularity and deployment time. For this reason, they can be configured as single to multi-story trusses with a medium span of 20 m - 40 m single unit. Multi-span configurations are supported using piers or trestles in cases where the coverage length exceeds 60 m - 70 m. They are often used to support brigade-level movement with traffic volume higher than tactical bridges. Medium Girder Bridge, Acrow 700XS, Mabey LSB, Bailey-type modular trusses, some FRP modular systems fall within this category of operation.

Line of Communication Bridges.

The purpose of this bridge type is to establish long-term, high-capacity bridging along supply routes and logistics corridors. They are the most robust and longest-span deployable systems. LOC bridges maximize span, durability, and traffic capacity rather than rapid deployment (See Figure 2.2 c). They operate within sustained logistics movement involving high-volume and multi-lane traffic over river crossings, flooded terrain and damaged civil infrastructure [28]. Modular floating bridges, amphibious bridging vehicles, large modular causeways, semi-permanent panel bridges, and multi-span girder systems with piers, all fall under LOCs.

Due to the scope and complexity of functionality, significant planning is needed together with assisting logistics like cranes to ensure an extended coverage span of 80 m to 200 m.



(a) Tactical Bridge: M60 Armoured Vehicle Launched Bridge [29]



(b) Support Bridge: 40-meter Dry Support Bridge [30]



(c) LOC : Acrow Line of Communication Military bridge [31]

Figure 2.2: Main Categories of Military Bridges

2.2.2. Civilian Deployable Bridges.

Bridge engineers incorporated deployability into the scope of conventional bridges which are also framed under broad category of movable or foldable bridges. This smart introduction had the primary function to reconcile continuous ground traffic with navigable waterways or constrained urban spaces. The main typologies gave rise to bascule, vertical lift, swing and

retractable or folding bridges, each defined by their own deployment kinematics and operational context [32].

The iconic London Tower Bridge shown in Figure 2.3 (a), and famous pedestrian deployable bridge at Paddington Basin in London (See Figure 2.3 b) are civilian bridges that utilize smart deployable scheme. These movable structures have been integrated into permanent transport networks that allow intermittent passage of vessels, vehicles or pedestrians without interrupting overall connections. Unlike deployable military bridges that are transportable to obstacle grounds, these bridges are typically installed in dense waterfronts attached to permanent structures [32]. They provide variable clearance which enables ships of different heights and widths to pass as well as maintaining reliable road or pedestrian access during normal operation. In many European cities, deployable bridges of this sort are part of cultural and architectural identity that function as traffic-management tool by combining engineering performance with aesthetic expression [33]. These civil deployable bridges are characterized by their dual role. They form permanent components of the transportation system yet capable of transforming to accommodate alternating spatial environmental and operational demands.



(a) Bascule Bridge Type: Tower Bridge of London (b) Paddington rolling Bridge

Figure 2.3: Civilian Deployable Bridge Structures

2.2.3. Deployment Mechanisms

Deployable bridges are only efficient when there are systems and techniques that enable the structure to transition between a compact or closed configuration to an expanded operational configuration. Across the range of deployable bridges discussed above, the deployment mechanism can be understood in a broad description. From the core idea that a bridge could be built from small identical, man-portable panels rather than a one large prefabricated span. Deployment was achieved from hand lifted assembly and progressively launched across a gap by pushing into position using rollers and a launching nose [23]. Deployment earlier relied on human labour with no mechanical transformation of the structure.

With time, the application of modular assembly shifted to rapid assembling mechanisms based on kinematics. The principle of kinematics characterizes deployment into rigid-body rotation, rigid-body translation, and scissor articulations. Each method solves the same underlying problem from moving a load-bearing span into and out of operation through different geometric strategies.

Civilian deployable bridges often rely on rigid-body rotation and translation which uses counterweight to move the structure smoothly and safely. The idea of utilizing balanced lever to rotate a bridge into position instead of lifting it with heavy machinery has been adopted for rapidly deployable origami-inspired structures [34].

In bascule bridges such as London's Tower Bridge, the erection strategy applies a large mass fixed to a detachable lever to balance the mass of the structure as it rotates. The motion is balanced naturally which allows the bridge to open and close efficiently, eliminating the need for external equipment. Contemporary bascule bridges also rely on double-leave rolling designs with pulley rope mechanism and electrical motors to lift the bridge span. The integration of a three-hinged system in rolling bascule designs enhance structural integrity, stability, and precision [35]. Figure 2.4 shows a summary of schematic deployment mechanism applicable in various structures.

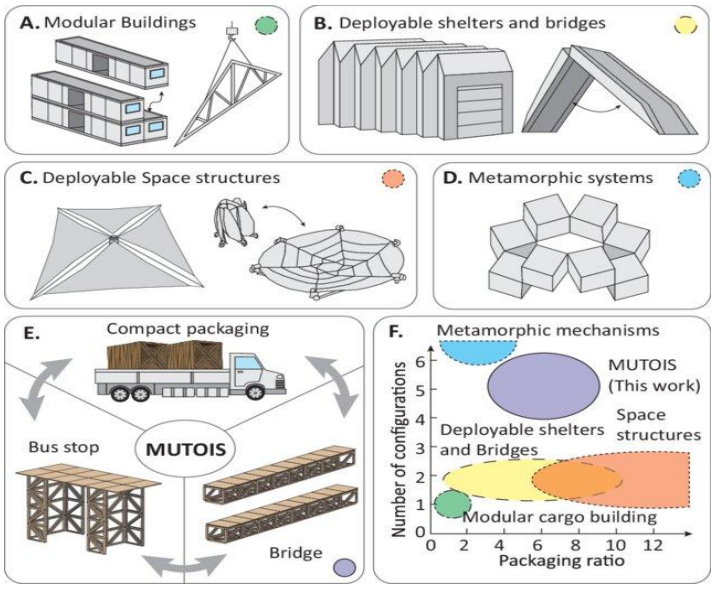


Figure 2.4: Schematic Description of Deployable Mechanisms [36]

The folding mechanism is also among the well-established mechanisms of deployment. This mechanism traces back to the early kinematic principle adopted by Piñero, Escrig, Hoberman and Gantes for deployable lattice structures. From a single rigid element with many small hinged links, load and rotation are distributed across dozens of smaller pivot connections, allowing the whole structure to be compacted for transport and rapidly expanded by manual, mechanical or smart material means [37].

The fold-to-deploy operation offers major logistical benefits for transportation and site installation, particularly in emergency conditions and extreme geology [38]. While bascule bridges used a hinged counterweight to clear vertical navigation channels, modern deployable structures adapt this rotational folding logic for rapid disaster relief and temporary crossings [34], [39].

2.3. Scissor Bridge Mechanism

The scissor mechanism stands out to be an efficient innovative structural concept for deployable bridges given its simplicity. The architecture of this system consists of two straight members linked at their midpoints by a rotating pivot joint. The mechanism has a simple operation of changing its global geometry in two main ways. The pivot joint allows the linkage

members to rotate relative to each other by compacting or extending the structure. This configuration allows the structure to form an *X-shape* when fully deployed.

A single unit is made up of two linkage members which can also be connected end to end to adjoining units through hinge joints forming an extendable chain of structural elements. The entire assembly transitions from a compact, readily transportable to a fully extended in-service configuration through a controlled rotation within the pivot joints. Load bearing structures used in industrial machinery makes use of the scissor mechanism due to its flexible operation. A common real life practical application of the scissor mechanism is seen in the scissor lift shown in Figure 2.5.



Figure 2.5: Scissor Lift Structure

Chikahiro et al adopted this mechanism in the design and testing of the a full-scale two-unit scissor bridge model which was named as Mobile Bridge (MB 1.0) [40]. The structural members of this prototype were made from extruded Aluminium alloy. This bridge spanned 7.0 m with a height of 2 m when fully deployed into a simply supported structure.

They further developed their previous MB 1.0 to MB 4.0 which was experimentally tested at a full scale over a river in Japan, demonstrating the practical use of the scissor bridge as a gap-crossing equipment [41]. This new bridge model had an overall span of 20 m and deployed height of 2 m (See Figure 2.6).

The compacted state of the bridge was transported by a trailer vehicle and connected to a robotic hydraulic pump for deployment. While the main structural members were made from

extruded Aluminium alloy, the frame for the hydraulic deployment was also made of steel (S 400). In all these models, the pivot joints as well as the linkage-to-deck joints were designed with simple metallic pins.



Figure 2.6: Deployable Aluminium Scissor Bridge [40], [41]

When fully deployed, the linkage members extend and lock into position as the deck panels lie completely horizontal. This full horizontal alignment of the deck ensures the stability of the bridge. The in-service span is fully achieved from the deployed configuration when the decks are level with the linkage members fully interlocked.

Also, within each scissor unit, the adjacent deck panels are connected by a transverse shaft rod across the width. This transverse member exists in two positions, connecting the diagonal members at the top and serving as a hinge between adjoining deck panel allowing them to fold relative to one another during the stowing and deployment process. The characteristic capacity to deploy with minimal operational resources is the exceptional attribute that makes the scissor mechanism efficient for emergency bridge applications. However, as the span increases, deflection becomes a concern that leads to the design with bigger sections.

2.3.1. Structural Performance of Deployable Scissor Bridge.

The structural capacity of scissor bridge is usually compared with the Double Warren Truss due to their geometric similarity. The DWT is made of horizonal upper and lower chord members that ran parallel to each along the span and vertical members at their end supports. Unlike Double Warren truss, which relies on a series of horizontal chord members, the scissor bridge achieves its structural form entirely through the interlocking of the diagonal linkage members at their central pivot.

The fundamental distinction between both structures lies in their force resistance. While the scissor structure resists maximum of shear force and bending moments as a sectional force, the truss bridge is mainly axial force dominated [42]. Despite the difference in internal-force pathways, both structural forms exhibit influence lines with similar qualitative trend. This correspondence allows a scissor bridge to be analysed and designed for moving loads [43].

Scissor bridges offer superior deployability but exhibit lower stiffness and higher deflection than the DWT. To this, several studies propose reinforcing configurations to increase the performance of the scissor bridge. The reinforcement involves introducing horizontal top chord members along the midspan and in some case, supporting the scissor bridge with cables. Conversely, Scissor-type bridges exhibit sensitivity to horizontal vibration because their structural form contains numerous nodal points and comparatively low lateral stiffness [44], [45].

The corresponding improvement in vertical stiffness is more modest, reflecting the inherently bending-dominated behaviour of the scissor members. Despite the geometric complexity of the mechanism, the dynamic characteristics of a scissors-type bridge can be approximated effectively using simplified beam-model representations. The natural frequencies predicted using this approach differ from experimental measurements by less than 3% [44].

2.4. Materials In Deployable Bridge Systems

The development of deployable bridges from materials perspective can be understood as a gradual transition from robust and modular metallic construction towards lightweight and structurally integrated systems. This can be broadly categorized into metallic, FRPs and hybrid material systems.

2.4.1. Metallic Materials

Steel

Aside stones and wood, steel has existed as one of the commonly used traditional materials from early days industrialization due to its isotropic properties. It stands out as a versatile alloy made up of Iron and carbon. Serving as a foundational backbone for global Infrastructure, it is utilized in various sectors of manufacturing, building construction and industrial machinery. The chemical composition of steel makes it distinct to manipulate its properties by adjusting the carbon content with the introduction of different alloying elements.

Early deployable bridges like the Bailey bridge relied predominantly on steel for its main structural components while timber was used as decks. The properties of steel are well suited to the needed conditions associated with military bridging. It has an elastic modulus ranging from 200 GPa - 210 GPa which provides a substantial structural stiffness. On the other hand, its ductility and durability make it ideal to redistribute stresses before collapse. Steel offers the flexibility to be manufactured in standardized structural shapes and sections which can be welded and bolted. The characteristics remained essential to be used in the early bridge systems as they also become applicable for contemporary structures.

However, the leading limitation of steel in deployable applications is its relatively high density. Structural steel has a density of approximately 7850 kg/m^3 - 7900 kg/m^3 which is about three times heavier than Aluminium and twice as titanium. While steel provides excellent absolute strength and stiffness, a considerable proportion of the logistical burden associated with deployable bridge is attributed to its own structural mass. A single Bailey panel weighed about 260 kg - 280 kg, and assembling the full span imposed high time demands and human resources.

The mass constraint of steel became significant as military bridges transitioned from manual assembly of modular units towards systems requiring rapid transportation, mechanical launching and installation. In subsequent designs, much emphasis was placed on rapid mobility and mass efficiency which created a natural motivation for lighter structural materials. Systems such as the Medium Girder Bridge, vehicle-launched bridges and dry support bridges were developed to increase deployment speed and reduce the manpower required for bridge construction. These developments are described by [23] as part of the

broader evolution from manually erected modular systems towards rapidly deployable bridge technologies.

Aluminium.

The development of deployable bridges increasingly required a material of lower density while also maintaining an effective structural performance. In effect, lightweight but structurally efficient. This technical requirement spearheaded the motivation to use Aluminium alloys.

Aluminium holds a significant intermediate stage in the progress of the lightweight deployable bridges. It has a density of 2700 kg/m$^{3`}$and elastic modulus of 65 GPa - 73 GPa, which in both cases, represent approximately one-third of that of steel. The lower density provides a reliable reduction in transportation and handling mass, while the strength-to-weight ratio makes it attractive for lightweight deployable bridge component [46].

The use of Aluminium for a rapidly deployable bridge model demonstrated in [26] revealed that Aluminium was not merely introduced to replace steel in conventional gap-crossing equipment. Instead, its lower density can be exploited in conjuction with a deployable configuration to produce an efficient bridge structure for emergency application. However, the advantage of Aluminium for lightweight deployable bridges goes beyond its lower density. Aluminium also possesses good corrosion resistance that can be readily extruded into different structural profiles, making them fit for several bridge configurations. In situations where temporary bridges are exposed to water, Aluminium is very durable. Low density, high strength-to-weight ratio, corrosion resistance and recyclability are among the principal advantages of Aluminium in bridge applications [46].

Nevertheless, Aluminium does not provide the optimal solution to the lightweight-bridge problem. Its lower elastic modulus depicts that an Aluminium structure may require large cross-sectional dimensions to satisfy stiffness and buckling requirements. Increasing the flange width by a factor of 1.6 addresses deflection and buckling challenges caused by the lower modulus [47]. This becomes essential in slender deployable structures for which stability and serviceability governs before material strength is reached.

2.4.2. Fibre Reinforced Polymer (FRPs) Composites

Fibre-reinforced polymer composites consist of high-strength fibres embedded in a polymeric matrix. Glass, carbon and aramid, producing GFRP, CFRP and AFRP systems are among the most widely investigated structural fibres. FRPs provide high strength-to-weight ratios, corrosion resistance, and fatigue resistance, making them a sustainable material in bridge engineering [48], [49]. These composites are multi-phase materials in which strong fibres provide strength and stiffness, while the polymer matrix bonds the fibres to transfer the shear forces. Glass and carbon are the most common in bridge applications. Their excellent strength-to-weight ratio makes them efficient for portable military bridge girders and beams [50].

The main interest of FRPs for deployable bridges is their combination of low density and high specific mechanical properties. Representative values reported in the literature [51] indicate densities of approximately 2100 kg/m³ - 2500 kg/m³ for GFRP and 1500 kg/ m³ - 2100 kg/ m³ for CFRP, which is about three to four times less than steel. Typical longitudinal elastic moduli of structural GFRP laminates are approximately 30 GPa - 50 GPa, whereas CFRP laminates can achieve approximately 120 GPa - 180 GPa or higher, depending on fibre type and laminate architecture [52].

Unlike conventional metals, in which the material properties are approximately isotropic, the mechanical properties of a composite can be tailored by controlling fibre orientation, fibre volume fraction and laminate stacking sequence. This allows the structural material to be preferentially oriented along principal load paths.

The operational case for composite deployable bridges had converged from military demand to civil demand. This means the bridges should be relatively light enough for less human resources and easily transportable for emergency crossings during post disaster rescue missions. In a series of studies conducted by [53] on short-span fibre-reinforced composite bridges for emergency response and military applications, it was demonstrated that GFRP sandwich and laminate construction could meet both requirements concurrently by combining a favourable strength-to-weight ratio with corrosion resistance.

In line with [53] and [54], pultruded GFRP tubular profiles were designed into full truss-girder deployable bridge systems. Pultruded FRP profiles are mainly used as primary load-carrying elements in maintenance-free structures under harsh and corrosive environments [55]. This design moved beyond composite decking alone to full composite primary load paths. Their

experimental testing established the feasibility of bearing-type steel-to-GFRP joints for dismountable, reusable connection. Alternatively, their subsequent full scale structural evaluation of a GFRP truss girder validated torsional and flexural performance for a 30 m span deployable bridge.

In [56], GFRP was used to develop a lightweight emergency bridge , looking at a civil-protection perspective. This explicitly framed composite substitution as the means of achieving erection by hand-portable equipment for spans previously requiring cranes.

2.4.3. Transition from GFRP to CFRP

In recent advancements, the use of FRPs for deployable lightweight bridges has sequentially shifted specifically from GFRP to CFRP material. The limitation that drove the shift away from GFRP was stiffness and not strength. Composite Deployable bridges are routinely deflection-controlled rather than strength. Like Aluminium, GFRP deployable bridges required deeper and heavier sections in order to achieve a desirable design span. This affects the size of the structure in its compact state, hence limiting mobility.

Pultruded CFRP presents a further step in the lightweight evolution of deployable composite bridge materials. Comparatively, carbon fibres possess greater stiffness and strength than glass fibres while maintaining a lower density. The high specific stiffness of CFRP makes it essential for deployable bridges because the structural performance is mostly serviceability-controlled rather than strength alone.

A polymeric-composite mobile army bridge was designed to provide improved tactical mobility, rapid deployment and retrieval, reduced profile depth and lower mass relative to existing metallic systems. An experimental test showed low strains and displacements in along the span of the structure, but the tested treadway eventually failed because of poor bonding during fabrication [57].

This result proved both the potential and limitations of composite military bridges. The structural material can be efficient in mass but manufacturing quality and interface integrity become critical. In contrast to metals where welding and bolting technologies are well standardized, composites require consideration of bonding and local stress concentrations.

A design, experimental testing and finite-element analysis on a CFRP rapid portable bridge was performed in [58]. Their study further demonstrated the suitability of CFRP for rapid portable bridges and reflects the ongoing trend toward highly lightweight bridge structures. However, to transition from GFRP to CFRP is mainly driven by the requirement of higher specific stiffness and strength. This is when transportation, deployment forces and structural slenderness become governing constraints.

2.4.4. Hybrid FRP-Metal Bridge Systems

The scope of material use for deployable bridges has followed a consistent logic. Each evolution of material solved the dominant limitation of the one before it as the new one is introduced. However, the successive materials also reveal a limitation which the previous material dominates.

Hybrid material systems behave like a composite where the properties of either materials compensate each other. Instead of completely displacing metallic construction, recent subset of literature has explored various applications of hybrid FRP-metal in deployable bridges. This seeks to combine steel or Aluminium, utilizing their ductility and isotropy at critical components of the bridge at the expense of the anisotropy of FRP.

Hybrid systems are seen in most FRP structures especially at the connection and highly localized load-transfer regions. In [59], GFRP-metal space-truss deployable bridge was designed for lightweight vehicular application. GFRP tubes and steel pieces of pins were used to achieve welded joint connection within the truss as shown in Figure 2.7. This demonstrated that GFRP can form the primary structural system while the metallic elements are integrated at sections where their mechanical characteristics provide advantages.

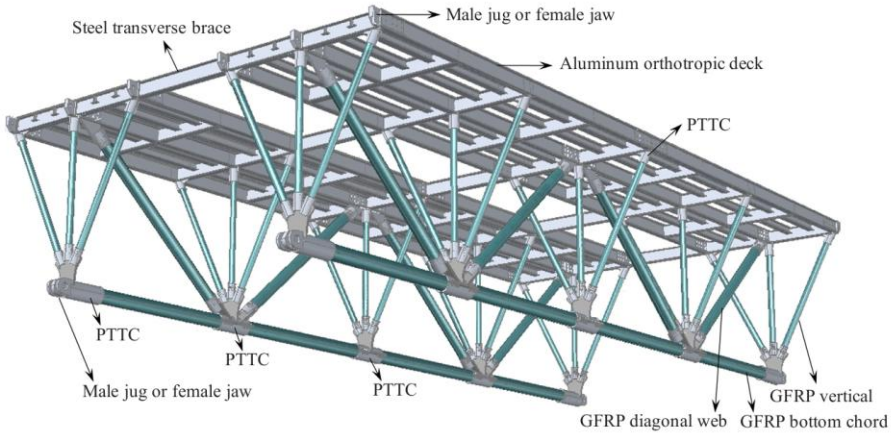


Figure 2.7: Hybrid FRP-Metallic Truss Bridge[60]

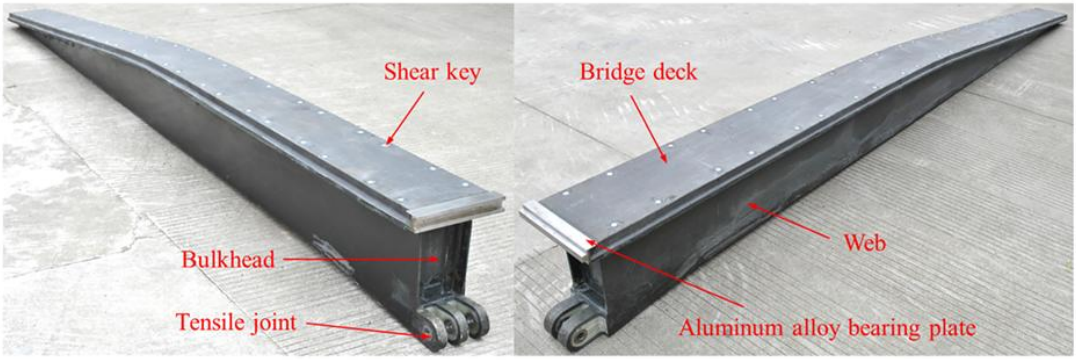
Hybrid materials in deployable bridges provide an effective compromise. It exploits the high specific properties and durability of FRP while retaining the ductility, bearing capacity of metals at regions where composite materials become complex to be designed. In a hybrid system, the structural benefits of the composite material can be partly offset by mass and complexity of metallic connection components. The literature consequently suggests that the next development in deployable bridge technology is not just simple substitution of steel or Aluminium with FRPs. It is rather an integrated design approach which considers structural geometry and connection efficiency.

2.5. Existing Case Studies

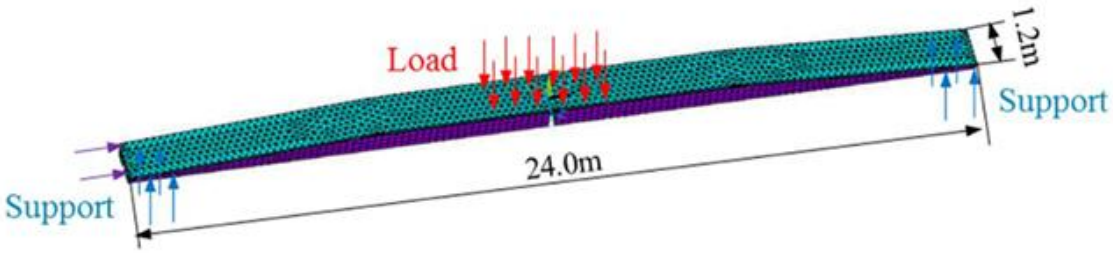
2.5.1. Case Study 1: CFRP rapid portable bridge.

CFRP rapid portal bridge was designed and tested as an alternative to conventional steel and Aluminium military bridges in [58]. The design was set to achieve the LD-60 (600kN) tracked vehicle load in accordance with the Chinese military bridging codes. The design utilized an allowable stress approach for the ULS and deflection limit of span/120 for a 24 m tactical double-box beam deck. The selection of the design cross-section was based on finite element studies in ANSYS against three loading scenarios. Figure 2.8 b shows the mid-span loading case in the FE model. A tracked vehicular load was traversed along the end supports and the mid-span to identify the extreme case. Among the various cross-section options, the double box-

beam with straight webs came out on top, satisfying the optimal combination of bending and shear performance.



(a) Small scale CFRP rapid portable bridge model



(b) FE model of the CFRP rapid portal bridge

Figure 2.8: CFRP rapid portable bridge [58]

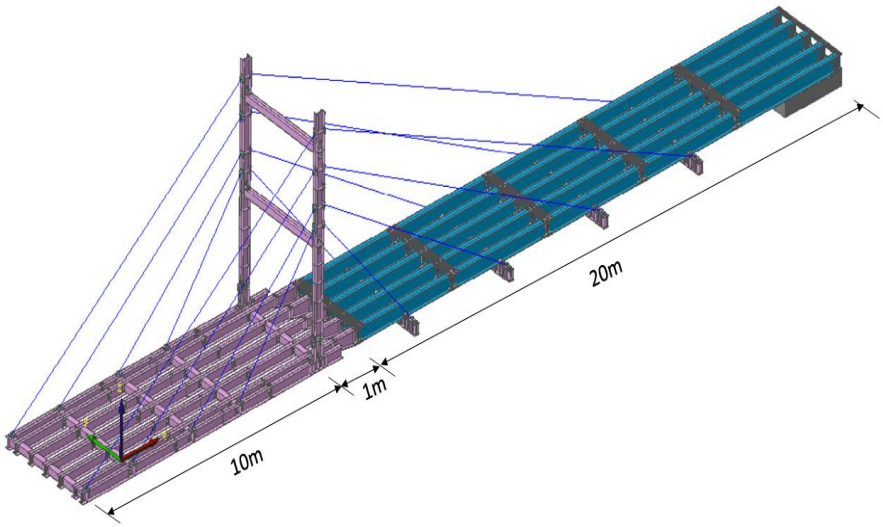
They built a small-scale laboratory model by hand-layup CFRP and GFRP using vacuum-assisted transfer moulding and loaded it to simulate track loading (See Figure 2.8 b). Using a four-point bending experimental test setup, the bridge behaved elastically. Failure occurred as the deck crushed at 157.4 kN. Deflection stayed within the serviceability limit up to 96 kN loading, representing a healthy margin.

For tactical bridge type with a single rotational joint of deployment, a tensile joint was deigned at the midspan as the most critical connection in the structure. During the experimental testing the joint held up to 902.6 kN load which was validated by an FE model. The study revealed the feasibility of an optimized CFRP box-beam deployable bridge had the capacity to meet both ULS and SLS requirements. This validated CFRP as a viable material for next-generation emergency portable bridges.

2.5.2. Case Study: Hybrid GFRP-Steel Bridge

A novel lightweight, portable and reusable composite bridge was proposed and verified in [61]. The bridge was aimed to overcome the stiffness, connection and cost challenges of FRP bridges while enabling fast restoration of access for emergency relief. An asymmetric self-anchored cable-stayed system made of heavy steel modules and GFRP composite girders were used as shown in Figure 2.9. Deployment was made through incremental launching. The heavy steel modules acted as counterweight enabling the launching process. Two prototypes were made for testing: a 10 m laboratory bridge and a 20 m field-assembled prototype. Both designs integrated pultruded GFRP girders with extensive bolted-connection testing.

After a full scale flexural, fatigue, strength and dynamic experiments, the composite girders exhibited a linear elastic response yet satisfied the deflection requirement of L/400. The proposed steel-FRP hybrid system successfully satisfied stiffness and strength requirements as it demonstrated a practical and effective composite bridge solution for emergency disaster relief.



(a) FE model of the cable-stayed GFRP-Steel bridge



(b) Assembling of bridge components for deployment

Figure 2.9: Hybrid GFRP-Steel bridge[61]

2.6. Design Standards and Codes for Deployable Bridges

Conventional bridges in Europe are mainly governed by the Eurocodes. EN 1991-2 is chosen for traffic actions while EN 1990 is used for ULS and SLS verifications. These standards provide a consistent framework for permanent actions, road traffic, fatigue, load combinations and structural safety. The Eurocodes define persistent, transient, and accidental design situations, but these refer to exceptional conditions rather than rapid-deployment emergency bridges [62] .

Applying these bridge codes to deployable structures presents significant challenges. Research on bridge construction equipment and movable scaffolding systems revealed that existing codes were not calibrated for the specificities, uncertainties and risk conditions of temporary structures [63]

Deployable bridges intended for military or emergency use operate under different set of requirements. Their loading is often governed by specific military vehicles, Military Load Classes (MLC), impact effects, eccentric vehicle positioning and temporary operational conditions that are not directly represented by the conventional Eurocode traffic models.

Among various studies on deployable bridges for emergency use, the authors apply the specific military specifications and standards in their jurisdiction [58]. Others rely on general

steel specifications and finite element analysis rather than a dedicated deployable bridge code [40], [61].

The difference between the military standard is clear in the loading philosophy considered. Eurocode 1 represents road traffic through prescribed load models intended to cover a broad range of civil traffic conditions. Deployable military bridges, in contrast, are normally designed around defined military vehicle classes and operational scenarios.

The (TDTC) was developed jointly by Germany, the United Kingdom and the United States specifically to address this problem. The TDTC covers the loading, design and testing of military clear-span bridges and other gap-crossing equipment and requires the designer to consider the user's operational requirements, military vehicle data, environmental conditions and appropriate testing. Its requirements are intended as minimum performance criteria rather than simply conventional civil structural checks.

In a study on a short-span FRP deployable bridge for emergency and military applications, the authors adopted TDTC as a principal design reference [53]. Similarly, research on modular bridge systems has identified the TDTC as an important basis for military bridge design because it specifies loading, safety and testing requirements that are more closely related to the operational function of temporary bridging than conventional civil bridge codes.

2.7. Connections in deployable bridges.

2.7.1. Introduction to Connection Systems in Deployable Bridges

Connections are essential components of every structure. From human structure to small scale and large machinery, buildings and bridges, connections play a key role in articulating the parts of the structure together. They mainly transfer forces between members enabling the structure to operate its full global performance. In bridges, connections provide reliable load paths and as well bear structural loads. Connections in deployable bridges must satisfy both structural function and mechanical function in order to allow changes in the configuration of the bridge. They permit or restrain rotation in order to allow the structure survive repeated fold-and-deploy cycles.

The significance of connection becomes very interesting when lightweight is a considering factor to be achieved. In conventional steel bridges and structures, connections are not always described as the weakest region of the structure due to the isotropy of steel. Steel is relatively high in tensile strength, shear and compressive strength. Over the past years, there have been well established guidelines and methods in steel connections.

On the contrary, connections in FRP bridges present a region whose properties differ considerably from the properties of the main member. FRP materials are anisotropic. Their through-thickness and transverse strengths are lesser than their longitudinal fibre-direction strength. For this reason, concentrated loads at jointed regions may produce local damage even when the member has high axial capacity [64].

Hybrid-FRP metal connections has also become an alternative approach in connecting composite members. This method complements the weakness in the composite with a metallic element. The main restriction to implementing hybrid steel-FRP connections lies in the knowledge deficit regarding the level of interaction and efficient connection solutions [65].

This review expounds on the broader scope of jointed connections techniques applicable in portable and deployable bridges. As far as deployable bridges are concerned, connections can be classified primarily along four complementary axes. The function, material, mechanical behaviour, and the governing design standard reveal how each classification interact with each other. The objective is to show why connections have become the limiting design

problem especially when deployable bridge material transitions from conventional metals towards FRP's and hybrid construction.

2.7.2. Functional Categories of Connections

This category describes the specific roles of the connection within the deployable structure, independent of the material it is made.

Load Bearing Connections

The primary forces or actions usually experienced in jointed components of a bridge are axial, shear and bending. Load-bearing connections transfer these actions between the members that remain fixed relative to each other once the bridge is deployed. In [66], [67], a bearing type connection between GFRP tubular profiles and steel joints were tested in three different connection details. The first test involved a composite hand lay-up reinforcement at the tube ends, the next test was an improvement with a steel splice that replaced the composite tube splice. The final test was an enhanced steel jacket connection confined internally and externally within the tips of the tube. Each joint's role was purely to maintain a continuous force along an already fixed geometry. The design, in this case was controlled by ultimate strength and stiffness compatibility in accordance with the EUROCOMP design code [68] rather than any kinematic requirement. The transition from composite-only to steel-enhanced connection significantly improved the global structural performance and load capacity. However, further tests were required to estimate rotational stiffness in order to improve correlation between theoretical FEM and experimental measurements.

Deployable mechanism connections

Deployable mechanism connections are the pivots, hinges, and revolute joints that employ certain configurations like the scissor and origami-inspired bridges to fold and unfold the bridge structure. Unlike a load-bearing connection, these mechanisms offer lower resistance of movement during deployment while maintaining sufficient structural capacity after deployment. The deployable mechanism is mainly controlled by the joint type and the member configuration. These two parameters are mostly modified across scissor structures to improve stiffness without sacrificing deployability [7].

The scissor deployable bridge consists of two linear members connected at their centres through a pivot joint. The rotation of the pivot allows the structure to change from the compact to the extended configuration. Chikahiro et al.'s full-scale Mobile Bridge™ demonstrated similar connection type carrying live vehicular load once deployed. It was also confirmed that a mechanism connection must be sized purely for kinematic freedom during folding. It must as well be re-verified as a structural pivot under service load.

Anchorage and support connections

Anchorage and support connections basically explore the interaction between the bridge and its environment. They represent the bridge's reactions into the supporting floor or abutment. Unlike the load-bearing and mechanism connections, they are designed to tolerate uneven and imperfect site conditions while providing a stable bearing point for the whole structure. This is exemplified by the Mabey Logistic Support Bridge whose ground beam and grillage systems are designed as such. The interaction between these components and the unprepared ground defies the need for tight panel-to-panel tolerances required elsewhere in the span. Military bridge manuals also treat anchorage as a separate design step. The support condition defines the boundary conditions used in the global structural analysis of the deployed bridge.

Mid-span articulation connections

Mid-span articulation connections are usually situated at the midspan rather than the support of the bridge. They combine both load-bearing and mechanism connection to transfer the midspan bending moment and shear in the fully deployed state. In most cases, they act as the folding line during the mobility of the bridge to the site. [58] adopted this connection type in their CFRP rapid deployable bridge. Designed as a hybrid tensile connector that linked two half-spans of the 9.6 m bridge, the joint transferred the full track load across the bridge. An equivalent mid-span connection exists as the pivot joint connecting the diagonal members of a deployable scissor bridge.

At this joint, maximum bending demand occurs. The scissor mechanism also depends on the rotation and lock of the pivot connection to allow deployment. The forces in this connection depend strongly on the deployment angle. As the bridge changes from folded to fully deployed configuration, the axial force in the diagonal members and the reactions at the pivot change.

Generally, a deployable connection must satisfy four main requirements. These include load transfer, controlled movement, position control or locking and durability under repeated operation. In conventional structural connections, load transfer is very common. However, the remaining three are important in deployable systems.

2.7.3. Material-Specific Connection Behaviour

Metallic Connections

Connections in metals are well established and universal in bridge engineering. They can be made of bolts, rivet, pins and welds. The behaviour of metals, particular steel and Aluminium alloys are well understood to exhibit isotropy and ductility. The Bailey bridge's steel pin joints and the Medium Girder Bridge's alloy pin joints both depended on the material's ductility to distribute and transfer stress around the pin. Ductility gives the connection a gradual, predictable load-deformation response instead of brittle failure. Steel pin joints fail either by plate bearing with large hole elongation, or by pin shear with significant plastic deformation before rupture [69].

The elongation capacity determines how much warning a connection gives before it fails. The reduced elongation capacity of a high-strength steel has a negligible effect on the ductility of a bearing-type bolted connection. In this case, net-section failure should be prevented by adequate edge distance of the plate. Hence, the ductility of a connection is governed mainly by the type of failure mode which is allowed to occur rather than the parent steel's own elongation [70].

Deformation capacity also decreases as steel strength increases, because higher-strength steels shift the critical failure mode toward the surrounding plate [71]. [72] confirmed this behaviour in the ŽM 60 demountable railway bridge. In this project the pin governed the connection capacity rather than the chord. Ductile redistribution in steel pin joints is not automatic. It requires a check for the specific pin diameter, plate thickness, and steel grade. This verification becomes impossible when one or both connected members are anisotropic FRP rather than isotropic metal.

FRP Connections

FRP connections are generally made by adhesive bonding, mechanical fastening or bolting and in some cases a combination of both. They usually represent the weakest part of load bearing structures. Adhesively-bonded joints normally exhibit higher stiffness and efficiency than bolted joints but are sensitive to fabrication process and complex to implement on-site As much as bolted joints are easier to assemble and disassemble, perforating FRP materials raises concerns about durability [73].

FRP connections behave very differently from steel. The material has high strength but low strain-to-failure and strong anisotropic property. As a result, bolted joints in pultruded FRP profiles are mainly controlled by the local stress concentrations around the perforated region rather than a ductile yielding.

Several studies consistently show that these joints can fail in different brittle modes. Bearing, net-tension, shear-out, cleavage, and block shear stand the chance of occurring depending on the geometric ratios between the width, hole diameter, plate thickness and edge distances [74].

Existing design codes incorporate methodologies similar to steel connections but account for the disparities between the materials. Most of the failure modes are sudden. It is bearing failure that provides gradual and observable deformation response. For this reason, FRP connection design deliberately aims to make bearing the governing mode. This implies that the joint geometry must be designed to suppress the brittleness since the FRP does not offer the inherent ductility like steel. The European technical specification for design of fibre-polymer composite structures defines bolted and adhesive connections should fulfil the fail-safe conditions.

Hybrid FRP-Metal Connections

Since neither an all-metal nor an all-FRP connection is superior across each functional category above, recent advancements have adopted hybrid connection approach in lightweight structures. Hybrid FRP-metal connections combine composite structural members with metallic fasteners, inserts, plates, sleeves or fittings. Drilling holes in composite may not be an ideal connection solution. However, the localized perforated region can be reinforced to drastically reduce stress concentrations. In modern high-performance composite bicycle

frames, several local attachments points and openings are designed as local structural features.

This approach generally reduces the localized weakness in pultruded composite joints because metal provide good bearing resistance compared to unidirectional composites (See Figure 2.10).

Hybrid connections are therefore considered as practical intermediate solutions in lightweight deployable bridges. However, the interface between the two connected materials plays a significant role in the efficiency of the connection. The different stiffness, coefficient of thermal expansion and the failure mechanism among the materials must be accounted in the design of hybrid connections [75].

[58] adopted a loop-type tensile connector which was made from CFRP laminates, GFRP plates, and steel components, arranged so that the CFRP carries the main tension while the steel part provided the bearing strength as well as protecting the composite from crushing. The joint outperformed the CFRP deck as discussed in section 2.5.1.

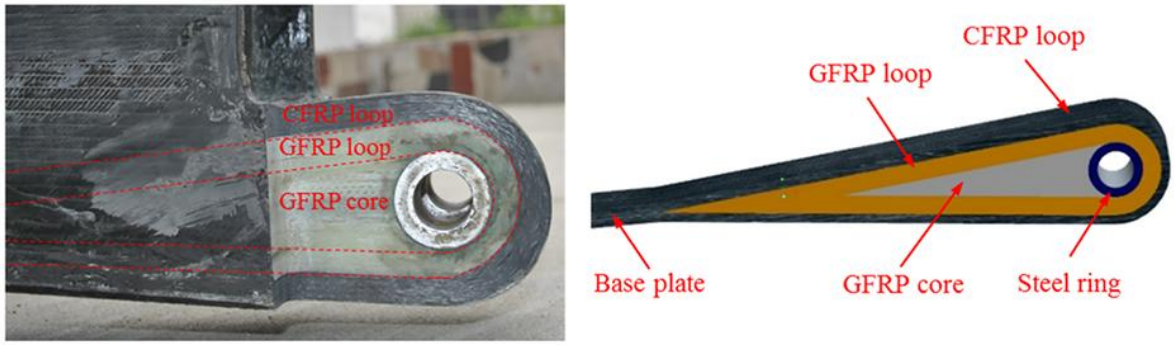


Figure 2.10: Tensile Pin Joint[58]

This indicated that the tensile joint was not the governing limit state of the bridge. A carefully detailed FRP connection can be engineered to sit comfortably at the capacity of the primary composite member rather than being the weak link as the defined principles of anisotropy predicts.

The transfer of load in perforated composite bolt connection is through bearing contact between the bolt shank and the wall in each adherend. In FRP-metallic connection, the metal is mostly stiffer than the composite material. For this reason, the adherend bears unequal share of the local deformation. This is why bearing-dominated failure dominates in composite

bolted connection. This is clearly seen in the load-displacement response of FRP bolted connection. The connection may behave nearly elastic as the initial stage until local bearing damage sets in to decrease the stiffness [76].

FRP-Steel Bolted Connection

In [77], a bolted GFRP-steel double lap joint was demonstrated to carry higher fatigue loads than GFRP-GFRP joint in static and cyclic tensile loading. The steel plate used for the joint provided a greater bearing stiffness and reduced the local compressive stress at the bolted region within the GFRP adherend. In two cases of high and low load levels the dominant failure was bearing and shear-out failure happening in the outer GFRP laminate. Alternatively, bolt fracture was observed at a high load, a situation which is avoidable by considering high-strength bolt and increased bolt diameter.

In a related study [78], three connection types between pultruded GFRP truss members and steel gusset plates were compared. The bolted-bonded hybrid joint achieved 50 % higher shear stiffness and 27 % higher ductility than the purely bolted joint. In all cases, bending failure dominated the capacity of the specimens which matched numerical predictions. It was concluded that bolted gusset plate can substantially reduce the number of cracks and improve the initial stiffness, but the maximum bearing capacity of the joints did not increase because the shear fracture of pultruded GFRP webs governs the capacity.

2.7.4. Mechanical behaviour of Connections

Across all the functional and material categories of connection, there are two main mechanical behaviours that dominate when global bridge performance is concerned.

Stiffness Characteristics of Connection

The stiffness in a connection determines how forces and deformations are distributed across the members within a bridge structure. In a deployable bridge, the configuration of the deployment mechanisms affects the stiffness of a connection. In scissor mechanisms, joint stiffness in addition to the member configuration is discussed as one of the two design variables that is mostly manipulated to improve global structural stiffness without compromising the structure's ability to fold [79].

A perfect rigid joint is known to transfer rotation and moment while a pin allows rotation but mainly transfer axial and shear forces. Deployable structures treat the joint differently from conventional bolted connections. This is because in mechanism-controlled structures, the hinge does not behave as a perfect pin. Joints constrain the relative motion through their constitutive behaviour and dimensions. However, during the deployment process, they undergo large displacements and rotations that imitates ideal pinned and rigid assumptions [80]. For a deployable bridge, the stiffness is very important during both deployment and service. Excessive joint clearance can create impact when the mechanism changes direction or reaches its deployed position. Excessive friction can increase the force required for deployment. Conversely, insufficient joint stiffness can lead to unwanted deformation and instability [81].

Failure Modes of Connections

Failure modes in connection sharply depend on the connection type and its respective material at hand, geometry and loading. Steel and FRP connections are now treated in separate design codes and each material family defines failure in different ways yet similar principles. For steel bolted and pinned joints, Eurocode 3 Part 1-8 lists five failure modes that must be checked on their own. These include bolt shear, bearing of the plate or bolt, block tearing, net-section tension, and punching shear under the bolt head or nut. All of these modes are ductile. They rely on the ability of steel to yield and redistribute stress before failure. Because of this, the design resistance is calculated from a yield or ultimate stress multiplied by an effective area. Stress concentrations are not the governing factor. The code assumes that the steel connection can redistribute stress plastically before any of these modes is reached.

FRP connections are treated very differently. CEN/TS 19101:2022 [82] is the new European document that covers bolted, bonded, and hybrid joints in composite structures. It forms the basis of the future Eurocode for pultruded composites. Instead of the five ductile steel modes, FRP joints are checked against four brittle modes: bearing, net-tension, shear-out, and cleavage. These modes are governed by stress concentrations, not by yielding.

Studies made by [83] showed that FRP bearing failure is not ductile. The laminate fails by brooming and delamination around the hole, not by plastic yielding. Their work on net-section

failure also indicated that this mode is highly sensitive to bolt spacing and edge distance, unlike the steel net-section check in Eurocode 3.

Connection Design Standards and Requirements

Steel bolted and pinned connections in bridges are designed using Eurocode 3 Part 1-8. This code assumes the ductile behaviour described earlier, where steel can yield and redistribute stress.

Alternatively, Pultruded FRP connections use a different set of rules. They were historically designed using the EUROCOMP handbook [84] for pultruded FRP structures. Designers now use CEN/TS 19101:2022. This document formalises the bearing, net-tension, shear-out, and cleavage checks that apply to FRP joints. It also forms the basis of the future Eurocode for composite structures.

Hybrid FRP-metal connections sit between these two frameworks. In practice, engineers check each interface using the provisions that govern the more critical adherend. They then support the design with project-specific tests, as seen in the studies by [77], [78]. There is no unified standard for hybrid connections. Deployable mechanism connections are the least standardised. No code provides explicit design rules for scissor or pantograph pivots. Designers therefore combine steel or FRP connection rules, depending on the material, with kinematic compatibility conditions from the deployable-structures literature. This lack of a dedicated pivot-connection standard is the reason why each new deployable composite bridge still requires case-by-case connection design. It also motivates the development of hybrid, non-drilled joint concepts for pultruded CFRP scissor pivots.

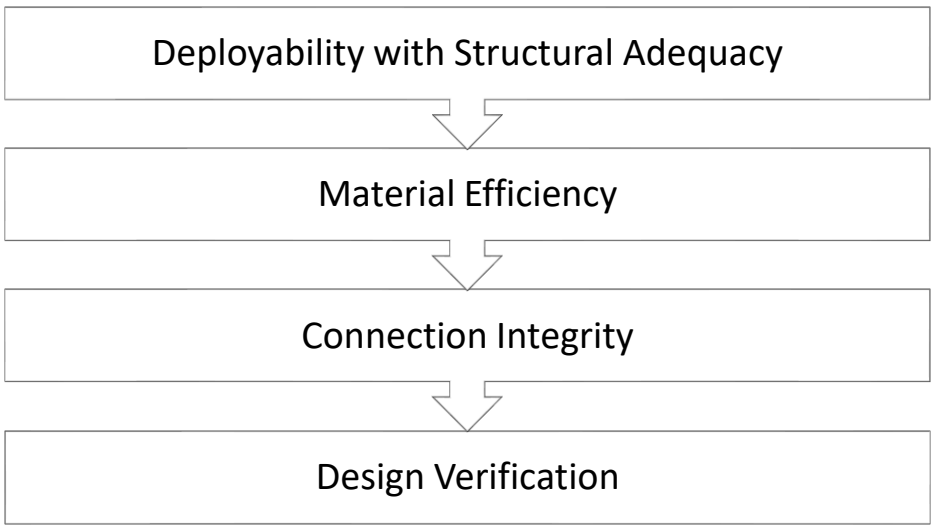
3. CONCEPTUAL DESIGN

3.1. Design Philosophy

The design Philosophy governing this project is based on the concept that deployable bridges historically depended on hand-erectable modular steel panels, constrained by weight, erection-crew size and ease of transportation. Notwithstanding, deployable bridges primarily served military applications instead of civil operations. The conceptual design of the proposed deployable composite bridge sits on the development of a lightweight and rapidly deployable structural system for emergency applications.

The principal objective is to reduce the mass of the bridge while maintaining sufficient structural strength, stiffness and stability during both deployment and full-service operation. Unlike conventional permanent bridges, the proposed system must satisfy two different structural conditions. The first occurs during deployment, when the bridge behaves as a partially supported mechanism and is subjected mainly to its self-weight. The second occurs after deployment, when the bridge forms its final load-bearing configuration and is subjected to service loading.

Reviewing various mechanisms of rapid deployment in chapter 2, this study presents a novel bridge design adopted by [40] with pultruded CFRP lightweight structural system. The philosophy is built on four main guiding principles which is developed in subsequent chapters.



The conceptual design does not aim to optimize only the primary structural members of the scissor mechanisms but also to develop a preliminary connection design in pultruded CFRP profiles.

Deployability with Structural Capacity.

The selection of the scissor configuration over panel-type, truss-type, vehicle-launched, and floating bridge typologies is due to it kinematic behaviour that allows compact fold, transportable and rapid deployment with minimal actuation effort. Scissor systems have traditionally been examined primarily as kinematic mechanisms, with their behaviour as load-bearing structural assemblies receiving comparatively limited attention [85]. This project treats both deployability and structural performance as critical design requirements. The expansion angle, module length, and member dimensions are therefore chosen not solely to satisfy geometric packaging constraints, but with explicit consideration of their influence on internal force paths and the resulting equivalent bending stiffness of the deployed structure.

This dissertation is more limited to the design of the scissor bridge structure itself. The design focuses on the geometric configuration, material efficiency, member dimensions, load-carrying behaviour, and the pivot connection. The detailed design of the actuation system is explicitly excluded.

Material Efficiency.

The behaviour of the scissor-type structure has a direct relation with its material capacity. The design adopts a material efficiency philosophy that reflects the structural demands of the scissor mechanism. The primary members of the scissor bridge are bending dominated over the axial stresses by a factor of 10 - 30 depending expansion angle and member position [86], [87].

CFRP is therefore treated in the design as bending and axial element whose unidirectional fibre and strength is selected to meet the internal force demands of the scissor mechanism. The bridge deck is specified in timber and treated as a secondary element carried by the primary CFRP members. Each material is assigned to the role for which its mechanical properties are most appropriate.

Connection Integrity.

The project adopts preliminary design solutions for the pivot connection within the CFRP DSC bridge in two fronts. First it recognizes that pultruded UD CFRP is susceptible to extreme stress concentrations at geometric discontinuities. A conventional simple drilled pin connection will be examined explicitly to establish a baseline and demonstrate the limitations identified in the literature review.

Secondly, the project adopts alternative connection design concepts that seek to bridge the gap rather than default to it. This concept replaces the drilled pin with a hybrid clamped rotating swivel pivot positioned externally to the CFRP profile. These approaches allow the project to evaluate conventional and hybrid connection strategies in pultruded CFRP composites.

Design Verification

This design philosophy commits to a staged verification procedure that progresses from preliminary configuration decisions to detailed structural assessment. The process begins with initial member sizing and selection of the geometric parameters governing the scissor mechanism. These choices establish the basis for the global FE model of the fully deployed bridge developed in ABAQUS.

Following global structural analysis, a detailed sub-model of the pivot connection is constructed to examine connection integrity under representative load transfer. This hierarchical modelling approach ensures that both system-level and connection-level performance is assessed with appropriate resolution.

3.2. Design Requirements and Constraints

The design requirements and constraints set out in this section define the quantitative and qualitative boundaries within which the conceptual design and the subsequent structural analyses (Chapters 4 - 5) are developed. This is categorized into functional requirements, governing standard, material constraints, and geometric constraints.

3.2.1. Functional Requirements

The DSC bridge is required to provide a full clear span of 21 m. This span is achieved through seven scissor units joined together with a single deployed deck length of 3 m. The bridge is intended for mixed used, accommodating pedestrian traffic and a hypothetical design vehicle described in section 3.6.2**.** In line with the bounded scope defined, the actuation system responsible for deployment is excluded from the function requirements.

3.2.2. Governing Standard

Since there is not existing code that specifically guides the design of deployable scissor bridges for emergency applications, the project adopts some guiding principles from the TDTC and reference to similar literature. The applicable ULS verification approach, design load parameters and factors are selectively picked to guide the global structural analysis. The DCS bridge is purpose-specific concept under civilian application rather than military specification.

Ultimate Limit State.

In the design of bridges, ULS refers to the conditions in which the structural safety of the bridge is not threatened. This is where the load-carrying capacity of the deployed configuration is not compromised by loss of equilibrium, excessive deformation leading to instability and material rupture. In this case, the ULS represents the ability of the CFRP members as well as the connections to resist the critical load combination and induced actions. For a DCS bridge, check on bending moment, global stresses, and buckling will be performed to ensure that the pultruded CFRP remain within its direction design strength under the governing loads. The TDTC's allowable stress method is adopted as the governing verification for the ULS.

Allowable Stress Method.

The Allowable Stress Method (ASM), also known as Working Stress Design, verifies structural adequacy by comparing the elastic stresses induced by a single design load directly against a reduced allowable material stress. Unlike Limit State Design, which separates safety margins into distinct load and resistance factors, ASM concentrates the entire margin of safety into a single reduction applied to the material strength. This results in a single verification check against a single design-load level.

Under the TDTC formulation, the governing load for ASM is referred to as Design Load as shown in Eq.(3.1)

$$F = D + A_1 + A_2 \tag{3.1}$$

where:

- F is the Design Load
- D is the dead load (self-weight)
- A_1 & A_2 are the most severe applied loads in descending order of magnitude

The stresses generated under F must remain below an allowable stress obtained by dividing the material's ultimate or yield strength by a prescribed safety coefficient. For metals, this typically corresponds to the lesser of Eq. (3.2) or Eq. (3.3)

$$\frac{f_u}{1.5} \tag{3.2}$$

$$\frac{f_y}{1.3} \tag{3.3}$$

$$\frac{P_{cr}}{1.5} \tag{3.4}$$

where:

- f_u is the ultimate strength
- f_y is the yield strength
- P_{cr} is the critical buckling capacity.

However, the allowable stress method for a pultruded CFRP profile will conform to a specific FRP criteria. These include directional fibre-strain limits and multiaxial failure criteria such as

Tsai-Wu or Hoffman-Hill, typically incorporating embedded safety factors in the range of 1.5 - 1.8 to account for anisotropy, brittle failure modes, and manufacturing variability.

Serviceability Limit State (SLS)

In this project, the SLS is defined in a narrow and structure-focused manner. This verification is limited to assessing the global vertical deflection of the deployed scissor bridge at its critical mid-span pivot location under the unfactored, in-service design load combination consistent with the Allowable Stress Method. The deflection under this load is checked directly against a single allowable limit.

Because the TDTC does not prescribe a numerical deflection limit for deployed bridges, an appropriate allowable deflection is selected from external precedent. Conventional civil engineering limits (span/400-800) for bridges are judged unsuitable, as they are calibrated for permanent bridges with decades of continuous service.

Similarly, existing scissor bridge research reports deflection only descriptively, without proposing serviceability thresholds [40]. Accordingly, the allowable deflection adopted here is span/120, following CFRP rapid portable bridge, which represents the closest published analogue in both material system and functional intent [58]. For the 21 m span of the DCS bridge, this corresponds to an allowable vertical deflection of 175 mm, stated explicitly as a project-specific design decision rather than a TDTC-mandated requirement.

3.3. Material Constraint

The design is not developed for only CFRP, but through a controlled comparison against a conventional Aluminium alloy. This material is most closely associated with lightweight, rapidly deployable bridging systems in existing practice. Aluminium is considered to set an appropriate benchmark for evaluating the performance of a composite scissor configuration in two fronts.

First, it provides a head-on reference against which the weight and stiffness advantages claimed for the CFRP scissor mechanism can be substantiated rather than assumed.

Second, the comparison constrains the scope of the material selection exercise itself. Rather than exploring a broad landscape of composite and metallic options, the project is deliberately

bounded to a direct two-material comparison. The geometric configuration and load definition are held constant as controlled variables, isolating material choice as the single differentiating parameter. Both material configurations are assessed directly against the same serviceability criterion. The results of this controlled comparison are presented in 81he Results and Discussion allowing the performance of the CFRP design to be evaluated against its established metallic counterpart.

3.4. Scissor Bridge Geometric Configuration

The geometric configuration of the DSC bridge defines the physical form within which the design philosophy and functional requirements applies. The DSC bridge covers a clear span of 21 m and comprises seven scissor units that are connected sequentially. Each single X-unit contributes to a deployed deck length of 3 m and a uniform width of 2.5 m. This subdivision allows the kinematic nature of the scissor to operate as pin-jointed modules whose deployed length is fixed once the expansion angle is defined.

The expansion angle, α, is a central geometric parameter that governs the configuration of the scissor mechanism. This is the angle of inclination between the diagonal member and the vertical axis as shown in Figure 3.1.

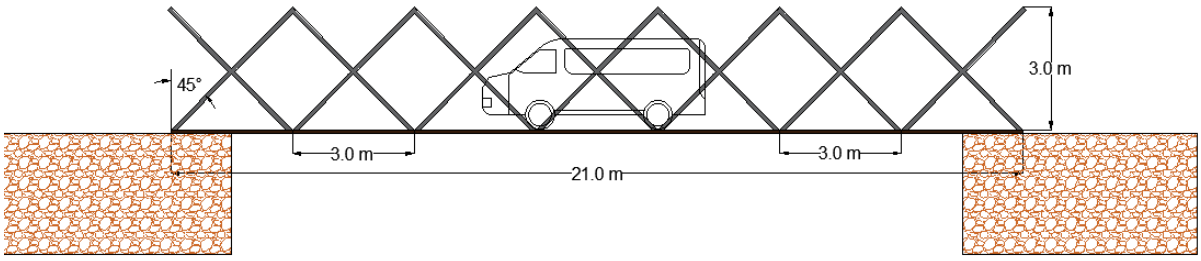


Figure 3.1: Geometric Configuration of the deployed Scissor Bridge

As established in chapter 2, α cannot be selected solely on the basis of packaging convenience but it places a strong nonlinear influence on both the internal force distribution as well as the equivalent bending stiffness of the structure [85]. It has been established that beyond 60°, axial forces rise sharply. As the angle also approaches 90°, the axial force tends towards an

extremely large value which renders the mechanism to lose stability. On the other hand, below 30°, the mechanism achieves minimal axial force but excessive global deflection. To this, a selective range of 30° to 60° is defined as optimal expansion angle.

For this reason, this DCS bridge adopts an expansion angle of 45° ensuring that the deployed structure possesses sufficient stiffness to satisfy the deflection criterion defined. With an expansion angle of 45° and single deck of 3 m, leads the DCS bridge to a corresponding deployed height of 3 m. The multi-unit configuration preserves the compact folded geometry that motivates the scissor topology, while still achieving the full 21 m deployed span required by the functional specification.

3.5. Material Selection

The selection of the material proceeds in two main directions to reflect the comparative framework established earlier. This involves a full Aluminium scissor configuration and a pultruded CFRP configuration with a shared wooden deck held constant across both. Each material choice seeks to justify the problem statement.

Aluminium is chosen as the metallic benchmark because it is the material most closely associated with lightweight, rapidly deployable bridging systems in both practice and literature. Steel on the hand seems comparable to CFRP in terms of its stiffness but its density positions it at a trivial disadvantage.

By contrast, Aluminium represents a lightweight-optimised metallic solution within the deployable-bridging tradition, making it a meaningful and literature-grounded reference against which any weight or stiffness advantage of the CFRP configuration can be rigorously assessed [41].

The selection of CFRP over GFRP or hybrid FRP-metal systems is due to the highest stiffness and strength-to-weight ratio among the available composites even though its costly. This presents CFRP as the upper bound of the weight-reduction hypothesis. Pultruded CFRP RHS profiles are industry-standardized composite products that have consistent dimensional tolerances reliable for a structural bridge application rather than wet layup or laminates.

Employing a wooden deck maintains internal validity for comparison. With the wooden deck shared across both configurations, any differences in global performance, self-weight, or deflection will be attributed solely to the scissor members.

3.6. Preliminary Load Definition and Analysis

This section establishes the load definition carried into the global structural analysis of the DCS bridge. The load definitions are categorized into the structure's own self-weight, a hypothetical design vehicle load, pedestrian load, and wind load. These loads are calculated selectively from the guiding principles of the TDTC.

3.6.1. Dead Load

In the global structural analysis discussed in chapter 4, the dead load accounts for the gravity load which is directly dependent on the section and material properties of the primary structural members.

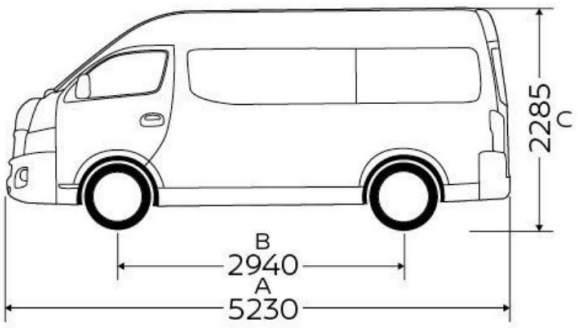
3.6.2. Hypothetical Design Vehicle

The project defines its own design vehicle to serve a similar functional role as the MLC specified in the TDTC. This dedicated vehicle represents the governing imposed action for the structural design of the DCS bridge. For emergency situation and lightweight limitation, a 14-seater Nissan mini Urvan is selected as the representative vehicle (See Figure 3.2). Its key geometric and weight characteristics are summarized in Table 3.1.

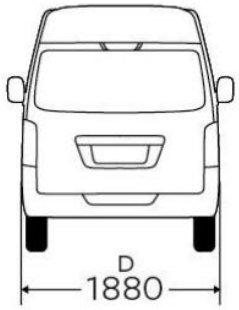
Table 3.1: Specifications of the Hypothetical Design Vehicle[88]

Parameter	Value	Unit
Wheelbase	2940	[mm]
Width	1880	[mm]
Height	2285	[mm]
Overall Length	5230	[mm]
Gross Vehicle Weight	3400	[kg]
Max. Front Axle	1600	[kg]
Max. Rear Axle	1800	[kg]
Average weight of passenger	80	[kg]
Passengers	14	[persons]

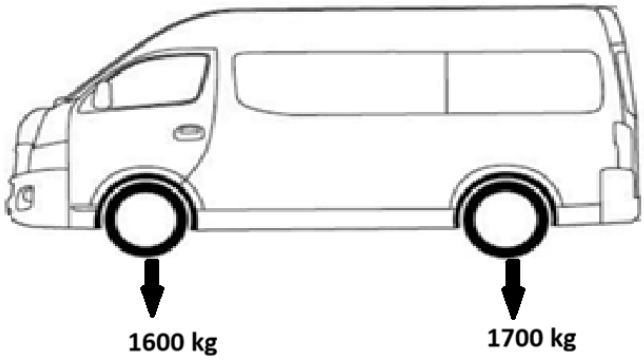
Vehicular loads are classified into wheeled loads and tracked loads. Both cases are attributed to how the axle forces are transmitted to the bridge deck. On the hand, the two cases have dynamic effects on the bridge structure. Wheeled loads produce higher dynamic effects due to the axle-by-axle impact while the tracked loads produce lower dynamic amplification due to the distribution of the load. The bridge is therefore verified against the worst-case scenario form both loading behaviours.



(a) Longitudinal section dimensions



(b) Transverse section dimensions



(c) Axle load distribution

Figure 3.2: Hypothetical Design Vehicle: Nissan mini Urvan[88]

Tracked Load Case

A tracked load represents the vehicle weight as a continuous pressure distributed over the full wheelbase or contact footprint of the vehicle. Instead of applying discrete axle forces, the GVW is spread uniformly across the area in contact with the deck (See Figure 3.3).

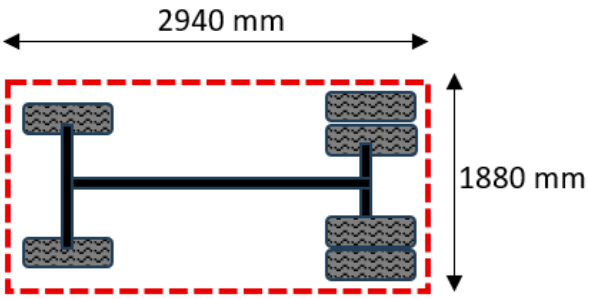


Figure 3.3: Tracked Load Representation

This produces a conservative loading condition because it assumes a larger, uninterrupted load patch, increasing the effective influence on bending and shear in the bridge. The tracked load case also accounts for the passenger load and dynamic amplification factor of 1.15. The tracked load is calculated from the equation (3.5) below.

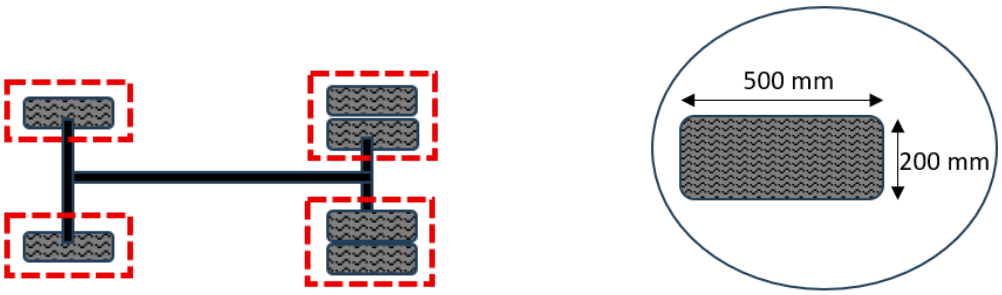
$$TL = d_T * \left(\frac{GVW + P_L}{T_A}\right) \tag{3.5}$$

where:

- d_T is the dynamic amplification factor for tracked load
- GVW is the Gross Vehicle Weight of the design vehicle
- P_L is the passenger Load
- T_A is the tracked area.

Wheeled Load Case

The wheeled-load case represents the vehicle's weight through the direct contact areas of each wheel on the bridge deck. Because the front and rear wheels differ in both contact area and axle load, their contributions are calculated separately. Passenger mass is included by distributing the passenger load equally between the front and rear axle groups, ensuring that the total imposed action reflects the full in-service vehicle weight.



(a) Contact areas of double axles (b) Contact area of single wheel

Figure 3.4: Wheeled Load Representation

To account for the higher dynamic sensitivity associated with discrete axle impacts, the dynamic impact factor applied to wheeled loads is taken as one-third greater than that used for the tracked-load case. A value of 1.5 is specified from the TDTC for the dynamic impact factor. This adjustment ensures that the wheeled-load model captures the increased dynamic amplification. The wheeled load per axle is calculated from the equation (3.6) below.

$$WL = d_w * \left(\frac{A_L + 0.5(P_L)}{W_a}\right) \tag{3.6}$$

where:

- d_w is the dynamic amplification factor for wheeled load
- A_L is the axle load of the design vehicle
- W_a is the area of a single wheel
- P_L is the Passenger load

3.6.3. Pedestrian Load (P)

The TDTC standard defines pedestrian load under the category of Foot Walk Loading (F), which covers humans, bicycles, and livestock. However, given the intended functionality of the DCS bridge a maximum uniformly distributed pedestrian load of 5.0 kN/m² is adopted for the design. This single UDL value is intended for dense foot traffic and crowd loading across the entire usable deck width and length.

3.6.4. Wind Load

The effect of wind is relevant in the load analysis due to the relatively large surface area of the bridge deck compared to the structural members. To this effect, the TDTC outlines maximum wind pressure values to which the bridge should be designed to resist. Considering an extreme case, a wind pressure value of 0.552 kN/m^2 is chosen to act on the bridge deck. In equation (3.7), the value is further multiplied by a drag coefficient of 1.4 in which accounts for diverse directional impacts from the wind.

$$w = \varphi * wp \tag{3.7}$$

where:

- φ is the drag coefficient
- wp is the wind pressure

3.7. Design Load Combinations

The design load combination discussed herein is in accordance with the TDTC guideline. The global FE model evaluates the bridge under the critical combination of the imposed actions expected during both deployment and the in-service performance. The load combinations are summarized in Table 3.2 below.

Table 3.2: Summary of Design Load combinations

Load Combination	Description	Application
LC 1	SW	During Deployment
LC 2	$SW + TL + w$	In-service
LC 3	$SW + WL + w$	In-service
LC 4	$SW + P + w$	In-service
LC5	$SW + WL + WL + WL + w$	In-service

LC5 is a special case of considering a convoy of three wheeled loads spaced per deck distance.

THIS PAGE WAS INTENTIONALLY LEFT BLANK

4. GLOBAL STRUCTURAL DESIGN OF THE DCS

4.1. Scope of Global Design

The global structural design forms the first stage of the numerical investigation of the DCS bridge. Based on the conceptual definition of the bridge geometry, material system, and the deployment mechanism established in chapter 3 above, this section develops the structural model required to evaluate the global behavior of the bridge.

The objective of the global structural design is to determine whether the proposed bridge configuration can provide adequate stiffness, strength and stability while maintaining the low structural mass necessary for rapid deployment. The analysis is carried out at the scale of the full bridge rather than at the level of individual units. Accordingly, the central pivot and other connection details are idealised at this stage, and the internal forces obtained from the global model are later used as input for the detailed design and numerical assessment of the critical connection in chapter 5.

4.1.1. Preliminary Sizing of primary Scissor Members.

The preliminary sizing of the primary structural members is taken as an initial section-selection step prior to the development of the global FE model. In conventional beam or truss design, member sizing is often estimated directly from simplified relationships and structural theories. This approach is not well suited in the case of DCS bridge because the behaviour of the scissor system depends strongly on its geometric configuration and the deployed state. The scissor bridge presents a mechanism-controlled system rather than simple pin jointed truss.

Analytical studies of scissor systems clearly define this distinction [43], [87], [89]. The structural response of the DCS is governed by the equilibrium of its mechanism. This equilibrium formulations only provide reliable means of obtaining the internal forces rather than defining the cross-sectional properties. The cross-section dimensions are provided as initial inputs within the equilibrium in order to obtain the internal forces.

For these reasons, the present study does not attempt to derive an optimal CFRP section based on the equilibrium equations. Instead, the member cross-section is treated as iterative

design variable that is chosen to satisfy three principal structural requirements specified in the equations below. However, initial section is done based on the deflection check in equation (4.1) before the remaining checks are considered in the global analysis.

$$\delta_{max} \leq \delta_{lim} \quad (4.1)$$

$$\sigma_{max} \leq \sigma_{all} \quad (4.2)$$

$$P_{cr} \geq P_d \quad (4.3)$$

where:

- δ_{max} is the maximum global vertical displacement
- δ_{lim} is the defined global deflection limit
- σ_{max} is the maximum member stress
- σ_{all} is the allowable design resistance
- P_{cr} is the critical buckling load
- P_d is the design load

Section Selection for primary structural members

The member selection procedure for both comparative material models followed the iterative section-selection approach. The candidate sections for the Aluminium bridge model started from the section properties defined in [40]. This reference section was assigned to the primary scissor members in the global FE model and checked against the target performance criteria. The section was then iteratively adjusted by selecting alternative standard Aluminium profiles and re-analyzing the global model until the bridge satisfied the deflection criterion.

For this DCS bridge, a commercially available Röchling Industrial Durostone CF pultruded CFRP RHS was adopted as the initial candidate section for the preliminary structural design. The selected profile was chosen from Röchling Industrial's catalogue of standard pultruded structural composite profiles. The geometric and orthotropic mechanical properties of the Durostone CF profile was assigned to the primary scissor members in the global finite element model developed in Abaqus.

Similar to Aluminium, the CFRP member sizing also followed an iterative process. In both models, preliminary sizing was therefore driven by the global structural response of the scissor system rather than by isolated member checks.

The resulting sections were therefore considered preliminary rather than analytically optimal. The final selected Aluminium and CFRP sections were then carried forward to the detailed structural analysis presented in the subsequent sections.

4.2. Finite Element Model in Abaqus

The global FE model presented a full 3D configuration of deployable scissor bridge similar to real prototype in section 2.3, Figure 2.6. The structure consisted of seven scissor units connected sequentially to form a fully deployed span of 21 m. Each unit comprised diagonal members with a length of 4.2 m arranged at an expansion angle of 45° .

The 3D configuration had two parallel scissor frames which formed a width of 2.5 m as shown in Figure 4.1.

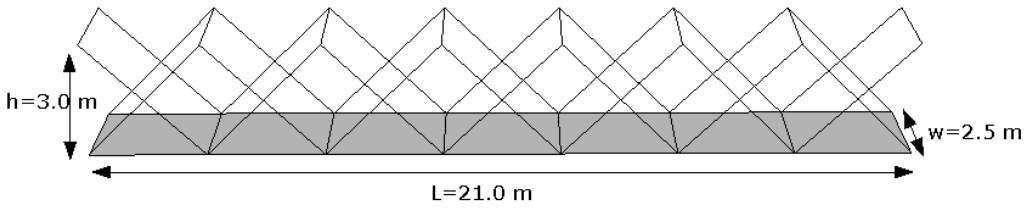
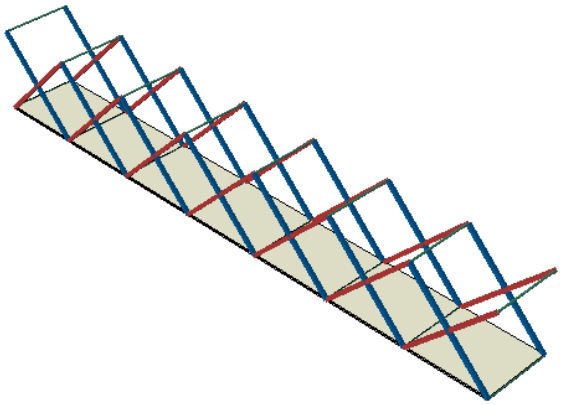


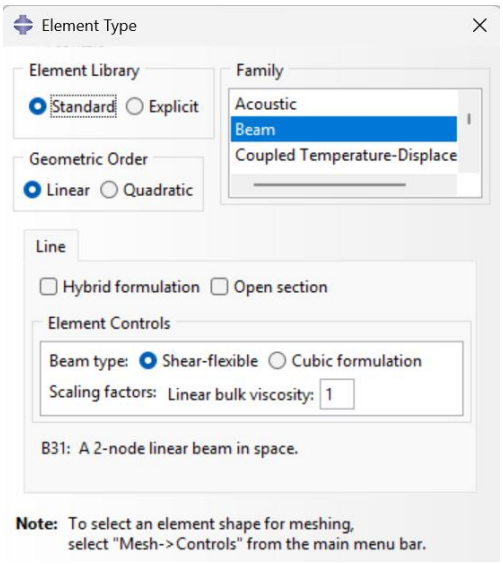
Figure 4.1: Initial Geometry of DCS bridge

These assemblies were joined by transverse members that stabilize the mechanism and support the deck system. All the joints in the structure were made of hinges that allowed a single degree of rotation to portray the scissor mechanism during deployment. This geometric definition established the basis for the whole FE model described in the next sections.

4.2.1. Element Selection

The scissor bridge geometry was built from separate three-dimensional wire parts, later assembled into the full model using hinge connectors. Each scissor unit's two diagonal members, inclined at 45°, were modelled as wire parts, as well as horizontal member represented the transverse element connecting the two parallel scissor lines. The deck was modelled separately using shell elements, which provided a surface over which the vehicular pressure loads could be applied. The different coloration in Figure 4.2 (a) shows the different parts assembled together rather than a full single rigid scissor part. Figure 4.2 (b) shows the beam element type used in the model.





(a) Full Model (b) Element type

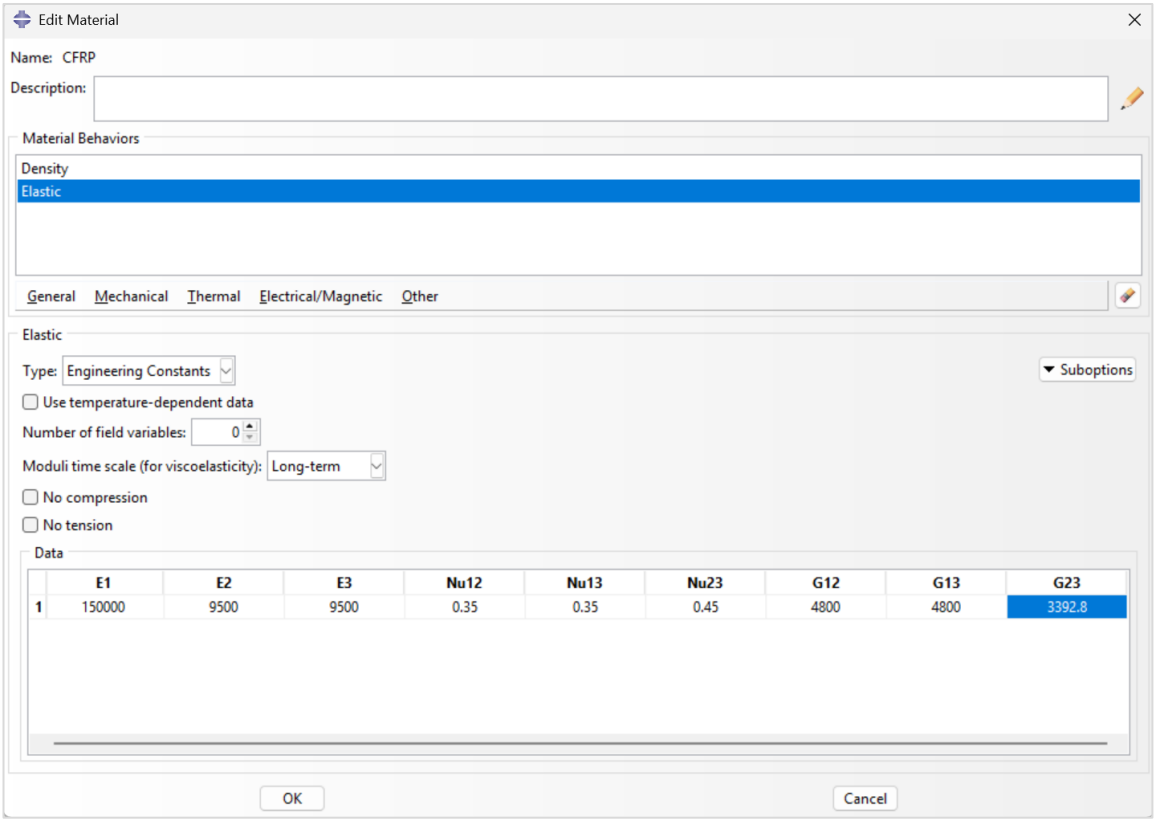
Figure 4.2: Global Model of scissor bridge

The diagonal and transverse members were assigned as B31 elements described as two-node linear beams in Abaqus. Each node has six degrees of freedom: three translational (U1, U2, U3) and three rotational (UR1, UR2, UR3). Beam elements were chosen to capture the global structural response of the scissor mechanism efficiently, without the computational cost of a full solid representation.

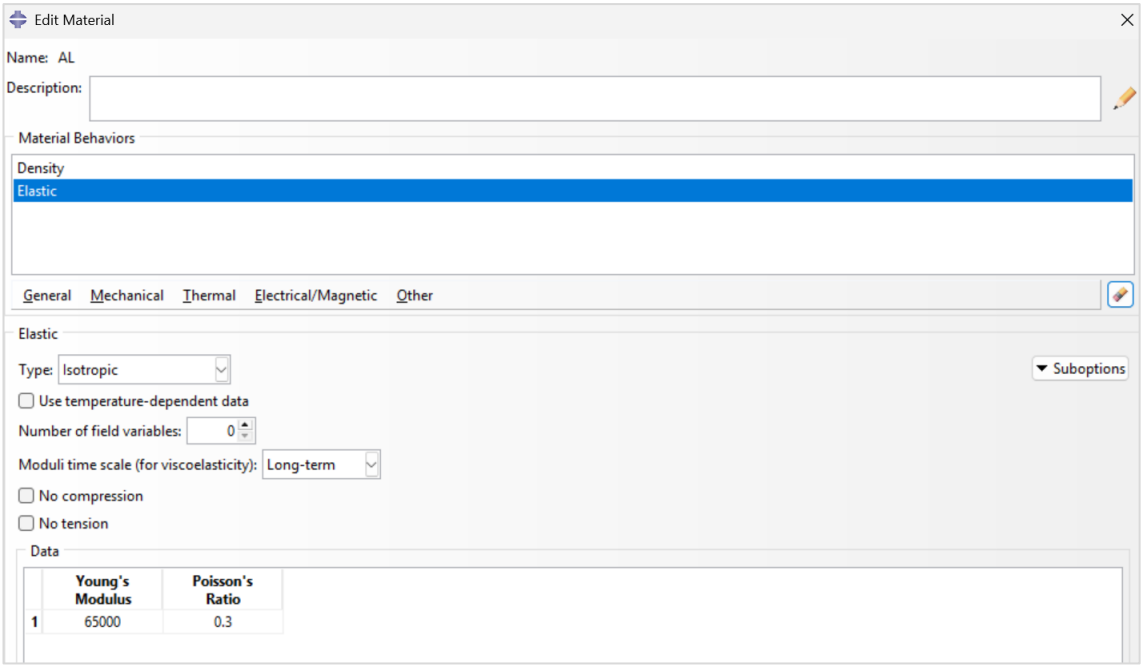
All geometric dimensions were defined in millimetres (mm), applied loads in newtons (N), stresses in megapascals (MPa), and mass properties in tonnes (t).

4.2.2. Material Properties

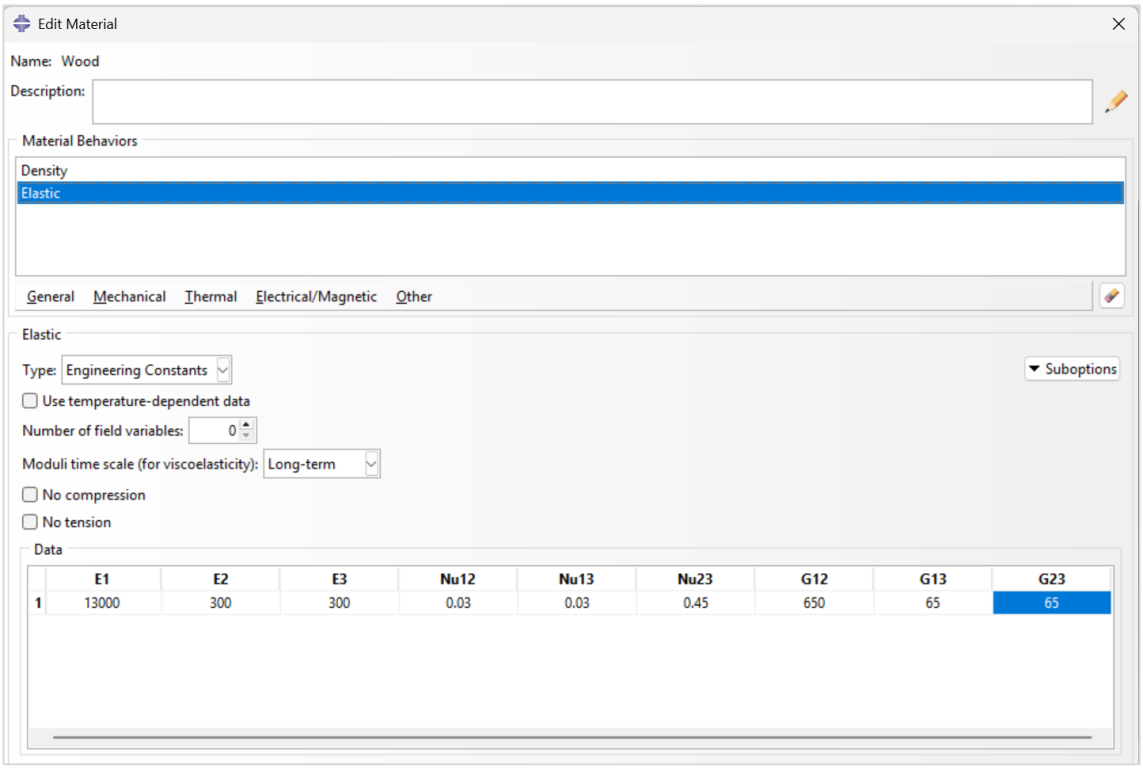
Three distinct material models were defined in the FE model: an Aluminium alloy, pultruded CFRP, and wood (for the deck). Two global models were built for comparison, one with Aluminium scissor members and one with CFRP. Each of them was assigned its corresponding material properties as the timber deck properties remained common to both. The pultruded CFRP and the wood were defined using homogenised orthotropic engineering constants as shown in Figure 4.3 below.



(a) CFRP



(b) Aluminium



(c) Wood

Figure 4.3: Material Properties

The Aluminium alloy, by contrast, was defined as an isotropic linear elastic material, requiring only a single Young's modulus, Poisson's ratio, and density. The mechanical properties

adopted for the Aluminium alloy, the pultruded CFRP, and the timber deck are summarised in Table 4.1, Table 4.2 and Table 4.3 below.

Table 4.1: Pultruded CFRP mechanical properties

Property	Symbol	Value	Unit
Longitudinal Young's Modulus	E_{11}	150000	[MPa]
Transverse Young's Modulus	E_{22}	9500	[MPa]
Out-of-plane Young's Modulus	E_{33}	9500	[MPa]
Major Poisson's ratio	v_{12}	0.35	-
Minor Poisson's ratio	v_{13}	0.35	-
Transverse Poisson's ratio	v_{23}	0.40	-
Major shear Modulus	G_{12}	4800	[MPa]
Out-of-plane shear Modulus	G_{13}	4800	[MPa]
Transverse shear Modulus	G_{23}	3392.8	[MPa]
Longitudinal tensile strength	X_t	1800	[MPa]
Longitudinal compressive strength	X_c	900	[MPa]
Transverse tensile strength	Y_t	80	[MPa]
Transverse compressive strength	Y_c	150	[MPa]
Density	ρ	1.5	[g/cm^3]

Table 4.2: A6NO1 Aluminium alloy mechanical properties[40]

Property	Symbol	Value	Unit
Elastic Young's Modulus	E	65000	[MPa]
Poisson's ratio	v	0.3	-
Yield strength	σ_y	180	[MPa]
Density	ρ	2.7	[g/cm^3]

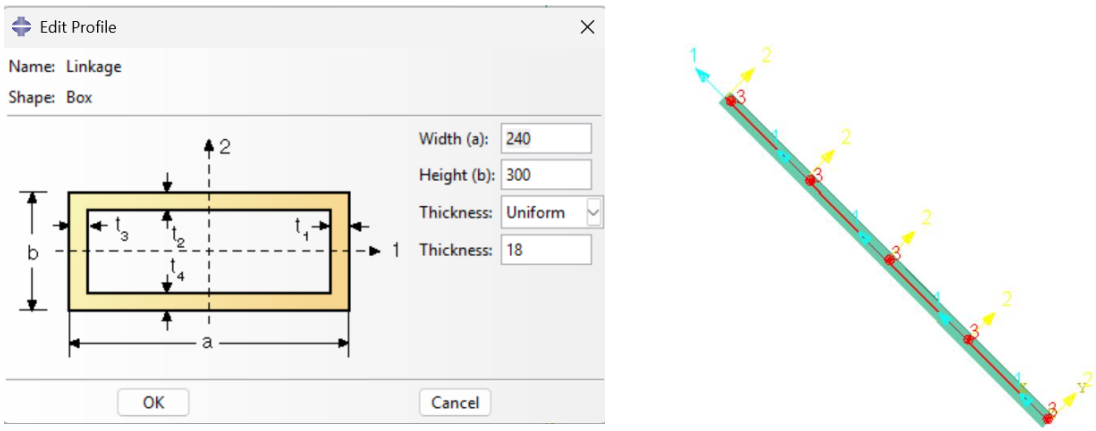
Table 4.3: Wooden deck mechanical properties [90]

Property	Symbol	Value	Unit
Longitudinal Young's Modulus	E_{11}	13000	[MPa]
Transverse Young's Modulus	E_{22}	300	[MPa]
Out-of-plane Young's Modulus	E_{33}	300	[MPa]
Major Poisson's ratio	v_{12}	0.03	-
Minor Poisson's ratio	v_{13}	0.03	-
Transverse Poisson's ratio	v_{23}	0.45	-
Major shear Modulus	G_{12}	650	[MPa]
Out-of-plane shear Modulus	G_{13}	65	[MPa]
Transverse shear Modulus	G_{23}	65	[MPa]
Density	ρ	0.46	[g/cm^3]

4.2.3. Material Orientation and Section Properties

The CFRP members were modelled as pultruded unidirectional profiles, so each beam required a local material axis aligned with its fibre direction. A local coordinate system was assigned to every member, with the local x-axis defined along the member's length to represent the strong fibre direction as shown on Figure 4.4 (b).

Both the beam orientation and the material orientation were specified for each element to ensure that the anisotropic properties were applied correctly. The same local-axis approach was used for the timber deck, which was modelled with shell elements.



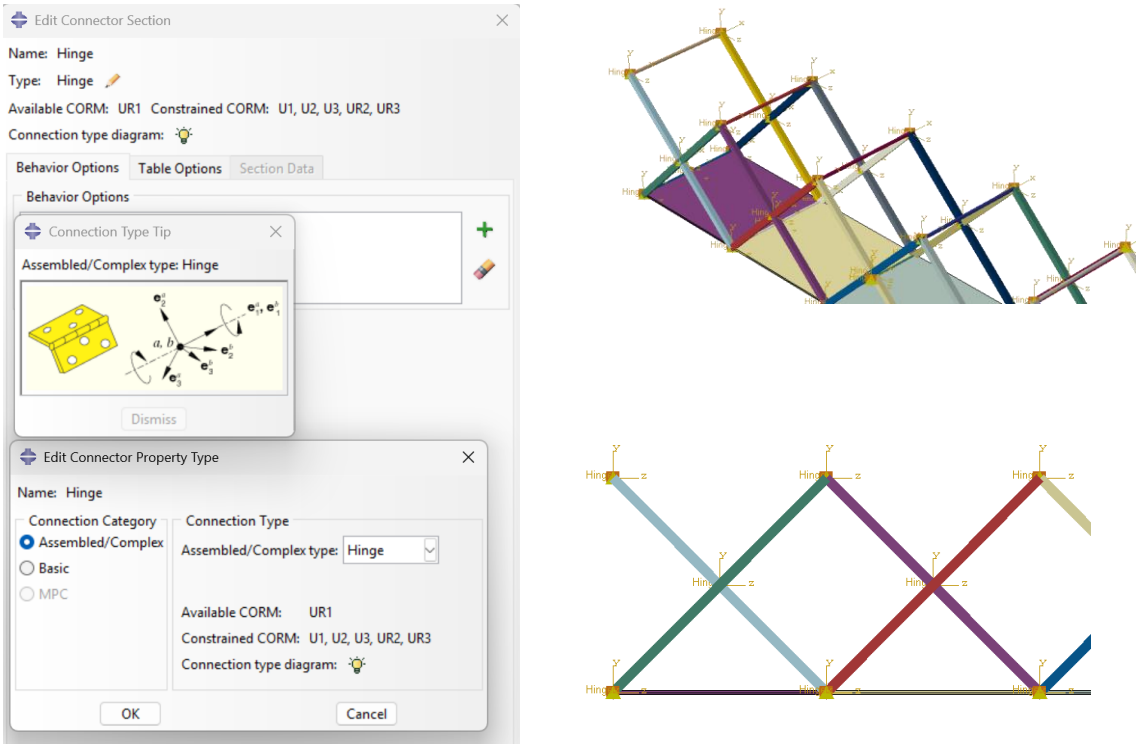
(a) Geometric section for beam element (b) Beam orientation

Figure 4.4: Material and section definition for elements

Homogeneous beam sections were created to define the geometric properties of the structural members as shown in Figure 4.4 (a). Based on the preliminary sizing stage, three standard rectangular hollow sections (RHS) were tried out for both the CFRP and Aluminium models. These sections were iterated within the global FE model until the deflection limit was first satisfied under LC4 load combination.

4.2.4. Interactions

The interaction module was among the most important parts of the FE model, since it governed how the model reproduced the actual kinematics of the scissor mechanism. Abaqus's connector builder was used to join the nodal points of the members, with a hinge connector property assigned at each joint. This connector type constrained all relative translations while leaving a single rotational degree of freedom about the local x-direction and allowing free rotation at the joint while fully transmitting force.



(a) Connector Definition (b) Hinge Joints

Figure 4.5: Interaction definition for DCS

For every jointed connection, the connector builder generated a reference point that was constrained to the nodes of the connecting elements. At the deck panels, the inner ends of each pair of meeting panels were hinged to one another, while their outer ends were hinged to the horizontal transverse member. This arrangement was chosen specifically to represent the folding mechanism that occurred during the real deployment of the bridge.

Surface-to-surface hard contact was defined between the deck and the horizontal transverse members at the bottom of the bridge, allowing load to be transferred from the deck into the supporting members. Contact controls were also introduced to add a degree of damping to the system, improving the numerical stability and convergence of the analysis.

4.2.5. Boundary Conditions

The boundary conditions were defined to represent a realistic deployment scenario. Here, one end of the bridge is assumed to be connected to an actuation system that drives the folding/unfolding motion while the opposite end is free to translate as the span extends. On

this basis, restraints were applied at three principal support edges, each comprising two joints, giving six restrained joints in total.

- **Actuation-end lower support (A) pinned support.** This joint provided the fixed reaction point for the actuated end, restraining translation in all three directions (U1, U2, U3) while leaving rotation free.
- **Actuation-end upper support (B) inclined roller.** This joint was assigned its own local (inclined) coordinate system, restraining translation perpendicular to the local axis while allowing translation along it (U2=0), so that the actuator-driven joint could move along a fixed inclined guide rather than being fixed in the global directions.
- **Trailing-end lower support (C) roller support.** Located at the opposite end of the bridge, this joint was modelled as a conventional roller, restraining vertical and transverse translation while permitting longitudinal translation along the span.

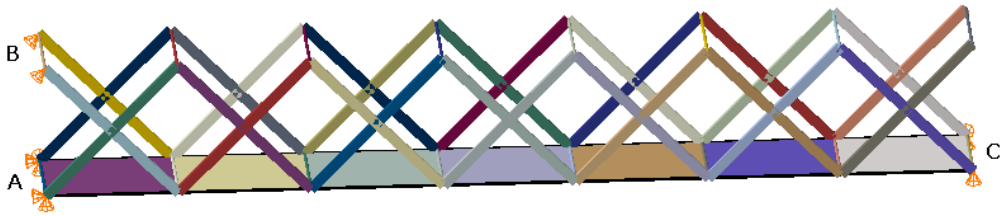


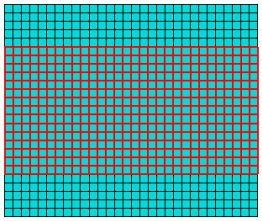
Figure 4.6: Definition of Boundary conditions

Figure 4.6 shows the full bridge assembly with the restrained node points labelled and named according to the scheme above.

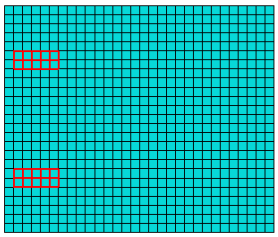
4.2.6. Load Definition

The load definition applied in the FE model followed directly from the loading description set out in section 3.6. The dead load was defined as a gravity load and assigned to the entire bridge structure. The tracked vehicle load was applied by defining a tracked-contact area on the bridge deck and assigning it as a pressure load over that area (See Figure 4.7 a), while the wheeled vehicle load was applied similarly, by defining the respective axle wheel-contact area on the deck and assigning it as a pressure load (See Figure 4.7 b & c). The wind load and

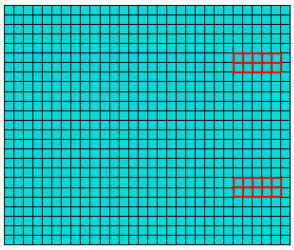
pedestrian load were both applied as pressure loads distributed over the entire deck surface (See Figure 4.7 d).



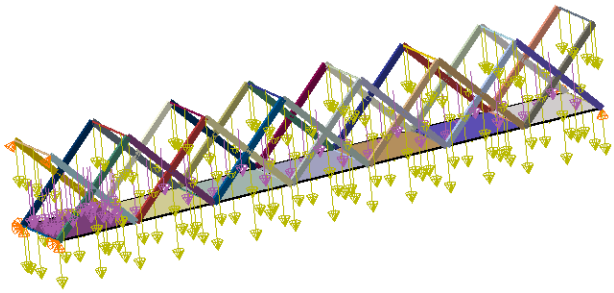
(a) Tracked load area



(b) Front axle wheel area



(c) Rear axle wheel area



(d) Total applied load

Figure 4.7: Load definition

4.2.7. Analysis Step Definition

Static Analysis

Two steps were used in the FE model: the Initial step, which Abaqus creates by default and to which the boundary conditions were applied, and a Static General step, created to apply the loads on top of those boundary conditions. Geometric nonlinearity (NLGeom) was deactivated for this analysis as shown in Figure 4.8.

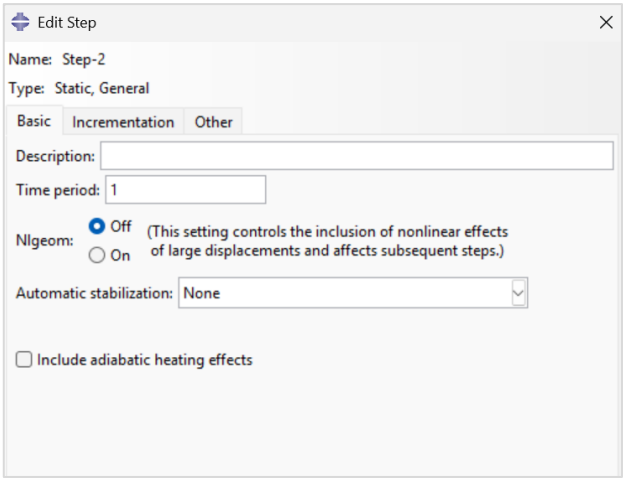


Figure 4.8: Definition of general static step

Buckling step

A separate Buckling step was also created and assigned a unit load, used to perform a linear eigenvalue buckling analysis. This step was critical to the verification process during geometry and section selection, providing a check on the elastic buckling capacity of the trial RHS sections against the applied design load. Figure 4.9 shows the creation of the buckling step.

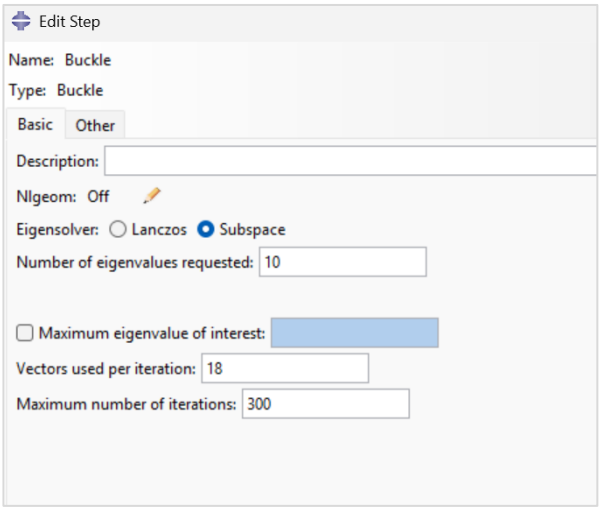
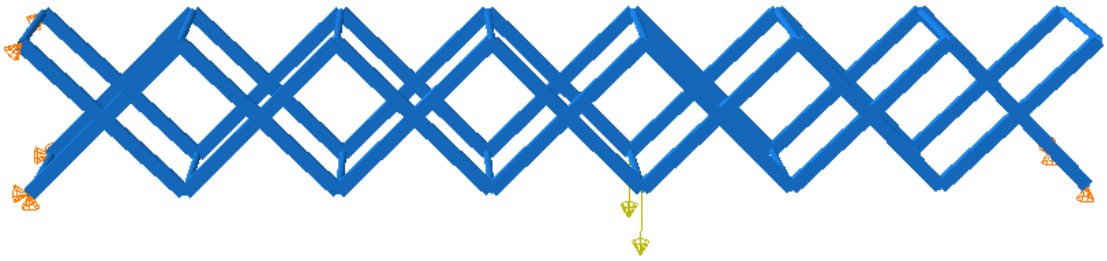
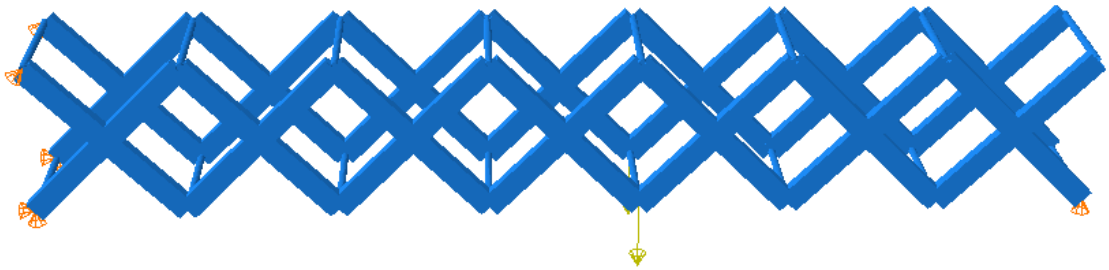


Figure 4.9: Definition of buckling step

Here, a unit traversing load was applied at intermediate points between the supports to determine the buckling capacity of the entire bridge. Because buckling mainly affects the scissor members, the deck was not included in the FE buckling model as shown in Figure 4.10.



(a) CFRP Linear Buckling Model



(b) Aluminium Linear Buckling Model

Figure 4.10: Linear Buckling Model of DCS Bridge.

Instead, the unit load was applied as a nodal force at the bottom of the DCS to represent a moving vehicle. The analysis then identified the first critical buckling mode, calculated the corresponding buckling load factor, and compared the global stability of the Aluminium and CFRP bridges before detailed member and connection checks.

4.2.8. Mesh

Each part in the assembly was meshed independently, with B31 elements assigned to the beam members and S4R elements assigned to the shell (deck) parts. Global seed size of 100 mm was applied across the model, confirmed through a mesh convergence study, with curvature control activated to refine the mesh locally around curved or transitional geometry. This resulted in a total of 1,576 linear beam elements and 5,250 linear quadrilateral shell elements across the model. Figure 4.11 shows the total meshed assembly of the DCS.

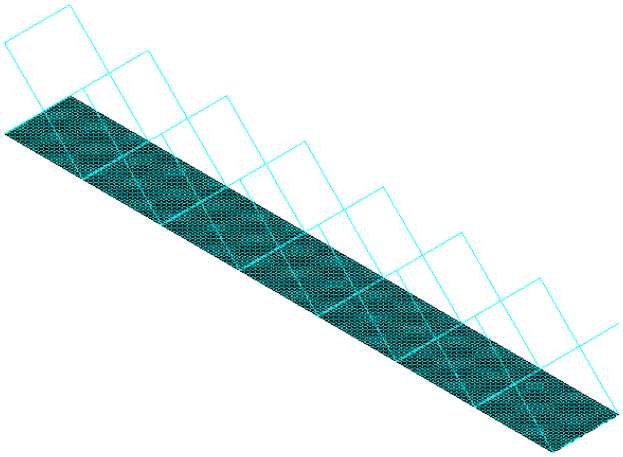


Figure 4.11: Definition of Mesh

THIS PAGE WAS INTENTIONALLY LEFT BLANK

5. CONNECTION DESIGN

5.1. Basis of Connection Design

The connection design presented in this project focuses on the pivot joint between the diagonal members of the DCS bridge. This is the central joint that enables the scissor mechanism to deploy and transmit forces between the crossing members once the bridge is locked in its deployed configuration.

The design of the pivot connection is approached in two distinct forms. The first is a conventional metallic pin, passed through perforated holes in the two crossing diagonal members to allow the pivot to rotate.

This concept is examined first because it highlights the main structural issue in this chapter: the effect of drilling a hole through a pultruded UD CFRP profile. Pultruded sections rely almost entirely on continuous longitudinal fibres for strength and stiffness. They have very little reinforcement in the transverse and through-thickness directions. Drilling a transverse hole cuts these load-carrying fibres. The remaining material must then rely on matrix-dominated and off-axis properties to resist bearing, net-tension, shear-out, and cleavage stresses. These stresses are the typical failure modes of bolted joints in fibre-reinforced composites. Pultruded UD laminates also lack the cross-ply reinforcement found in many composite laminates used to establish standard bolted-joint design rules. As a result, common guidelines such as minimum edge distances or width-to-diameter ratios cannot be assumed.

The second is a metallic rotating swivel joint, clamped externally on the diagonal members without perforation of the composite.

The scope of the connection design study is to compare the effect of these two options on the global structural performance of the bridge under extreme loading combinations. To this end, each proposed connection is developed as a local finite element sub model, loaded with the governing actions extracted from the global FE model. This is to ensure that the local response of each connection concept can be assessed under representative in-service demand.

5.2. Detailed Description of the selected Joint

5.2.1. Concept 1: Metallic Pin Connection

The first connection concept as shown in Figure 5.1 uses a single cylindrical metallic pin inserted through aligned transverse holes drilled in the webs of the two intersecting CFRP RHS diagonals. This arrangement mirrors the traditional pin-type joints commonly used in Aluminium scissor and deployable structures. The pin, together with retaining washers and a nut, forms a simple revolute joint that allows relative rotation between the members during deployment and folding while maintaining continuity of the diagonal load path.

To limit frictional resistance and reduce wear at the composite-metal interface, a low-friction bushing is proposed between the pin and the CFRP hole surface. This provides smoother rotation and improves the bearing capacity of the thin CFRP profile in contact with the pin.

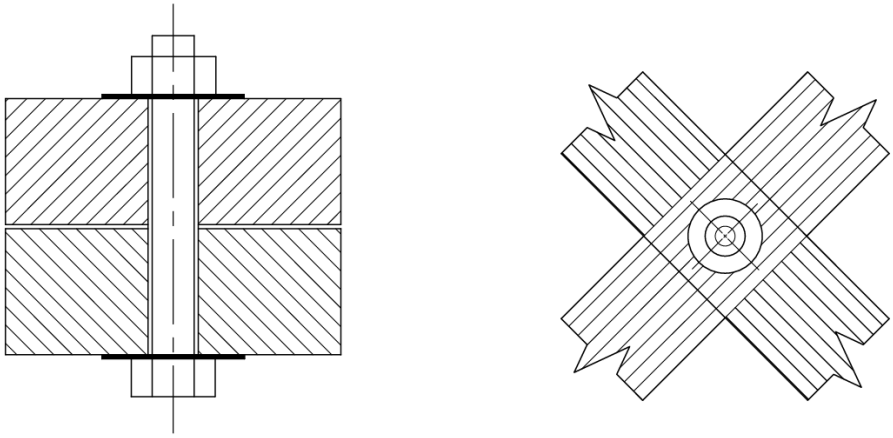


Figure 5.1: Schematic representation of simple pin connection

5.2.2. Concept 2: Externally Clamped Metallic Swivel Connector

The preliminary alternative connection solution avoids perforating the pultruded CFRP scissor members. Instead, a split metallics swivel made from two half-shells is clamped around each CFRP RHS diagonal member. Load is transferred through friction and bearing along the clamped area, rather than through a single fastener hole. Each diagonal member receives its own swivel assembly. The two swivels are then connected to each other by a single pivot pin housed entirely within the metallic hardware. The pin links the two swivel bodies directly and

never touches the composite member and preserves the full cross-section. The connection provides a single rotational degree of freedom about the pivot axis. This satisfies the kinematic requirement of the scissor mechanism. In this concept, the rotation axis is defined by the geometry of the connector rather than by a hole through the composite member. Any offset between this axis and the theoretical scissor node used in the global model is checked during the connector design.

5.3. Local Finite Element Sub Model Development

Following the description of the two proposed connection concepts, a local finite element model was developed to assess the structural behaviour of each joint under the internal actions obtained from the global bridge analysis. The scope, geometry, and material assignment adopted for this local model are described in this section.

5.3.1. Selection of the Local Model Unit

The scissor bridge is composed of multiple interconnected scissor units spanning between the two supports. Instead of modelling the full assembly, the local finite element model focused on a single crossing unit isolated from the global structure as highlighted with red colour in Figure 5.2 . The first crossing unit was selected because the global FE analysis identified it as the most critical location in the bridge. Using this unit, the local model represented the governing combination of internal actions acting on the pivot connection.

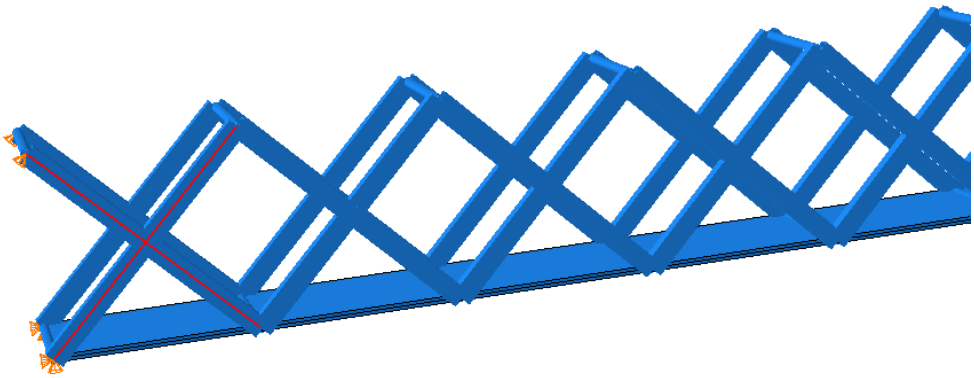
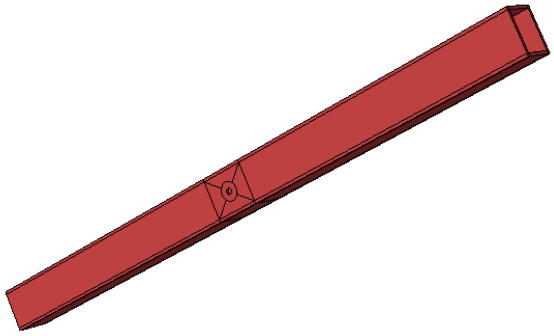


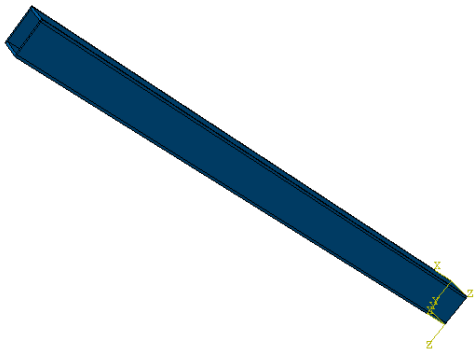
Figure 5.2: Selected scissor unit

5.3.2. Geometry and Material Definition

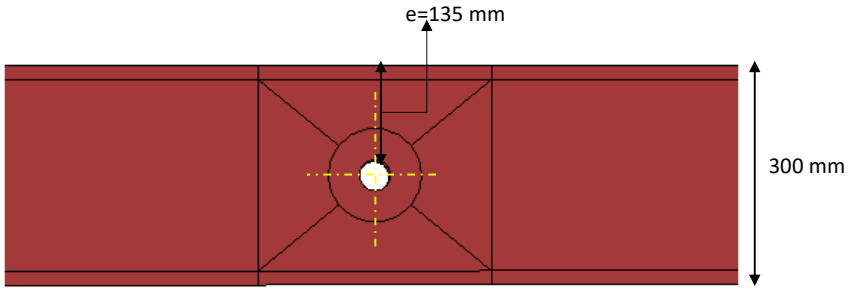
The two crossing diagonal members in the selected unit were modelled as 3D extruded solid parts. Their geometry was generated directly from the hollow rectangular cross-section used for the CFRP RHS profile in the global FE model. With this, the local model reproduced the exact profile dimensions and the same inclination assigned to the diagonals in the global analysis. Figure 5.3 shows the modelled pultruded CFRP members of the perforated and undrilled parts for each connection design solution.



(a) Perforated CFRP diagonal member



(b) Undrilled CFRP Diagonal member



(c) Dimensioned section of the perforated CFRP region

Figure 5.3: 3D model of pultruded CFRP diagonal members

The CFRP members were given the same orthotropic material properties used in the global model for the pultruded UD profile. Homogeneous solid sections were assigned with careful attention to fibre orientation and wall thickness. The local material axes were aligned with the member's longitudinal direction so that the fibre direction in the local model matched the

orientation used globally. This maintained consistency between the global and local representations of the CFRP behaviour.

Local Model of Connection Concept 1: Pin Connection

In the first connection concept, a 30 mm metallic pin and its bushing were modelled as additional three-dimensional solid parts positioned within the crossing CFRP diagonals (See Figure 5.4).

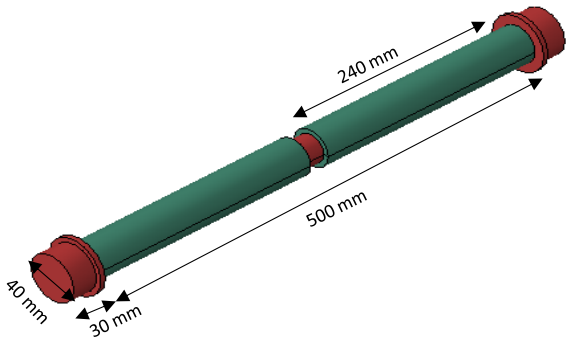


Figure 5.4: 3D model of Pin and bushing assembly

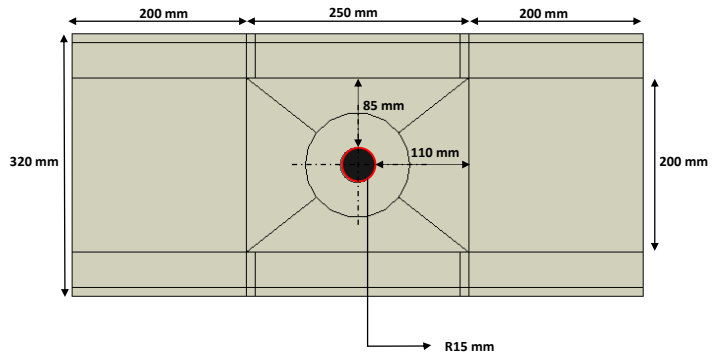
These components represented the physical pin assembly used to form the rotational joint. Both the pin and the bushing were assigned the engineering properties of a high-strength aluminium alloy in Table 5.1, consistent with the lightweight metallic material identified earlier in the material selection.

Table 5.1: Al 7075-T6: High yield Aluminium material properties

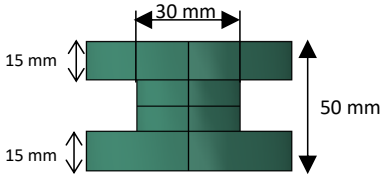
Property	Symbol	Value	Unit
Elastic Young's Modulus	E	71700	[MPa]
Poisson's ratio	v	0.33	-
Yield strength	σ_y	503	[MPa]
Density	ρ	2.82	[g/cm^3]

Local Model of Connection Concept 2: External Swivel Connector

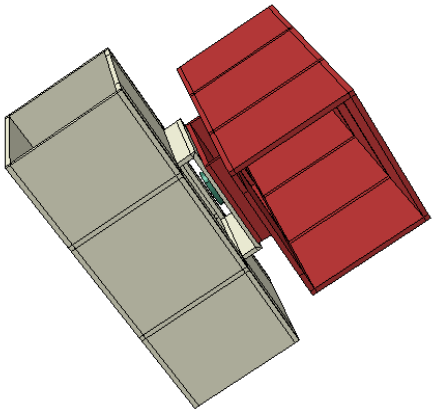
In the alternative connection concept, the two-half swivel connector and the pivot bolt were also modelled as 3D solid parts as shown in Figure 5.5. All metallic components were assigned the same high-strength aluminium alloy properties used in the pin-connection model. With this, the structural performance of the two concepts could be compared under a common material assumption.



(a) Single swivel collar



(b) Connecting swivel Pin



(c) Rotating Swivel Connector

Figure 5.5: 3D modelled parts of external swivel connector

5.3.3. Interaction Modelling

Interaction behaviour was a key aspect of the local finite element model because both connection concepts involved several three-dimensional components in contact. Appropriate contact definitions were therefore required to capture bearing stresses, frictional transfer, and relative motion between the metallic hardware and the CFRP members.

Concept 1: Pin Connection

In the pin-based concept, multiple contact interfaces were present (See Figure 5.6). The bushing was in contact with the inner faces of both CFRP diagonal members, and the pin was in contact with the bushing. Two distinct contact formulations were assigned:

- **Pin - bushing interface:** A metal-to-metal, frictionless, surface-to-surface contact was defined.
- **Bushing - CFRP interface:** A metal-to-composite contact was used, with a friction coefficient of 0.315. This value is consistent with published data for dry contact between steel/aluminium and CFRP surfaces and aligns with values reported in composite bolted-joint literature [91]. All contact pairs used hard contact in the normal direction to prevent penetration while allowing separation when unloaded.

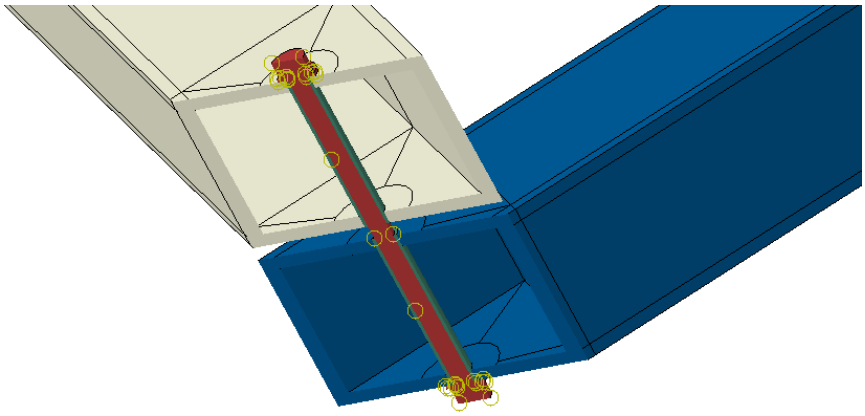


Figure 5.6: Contact interaction in the drilled pin connection

This combination of frictional and frictionless interfaces reflected the intended mechanical behaviour: rotation at the pin, and friction-based load transfer between the bushing and the composite member.

Concept 2: Swivel Connector

For the swivel-connector concept, all external metallic components attached to the CFRP profile were modelled using explicit contact interactions. This approach allowed the model to capture realistic load transfer through friction and bearing at the collar-CFRP interface.

The two metallic halves-shells forming the swivel collar were assigned metal-to-composite surface-to-surface contact with hard contact in the normal direction and a friction coefficient representative of dry aluminium-CFRP interaction.

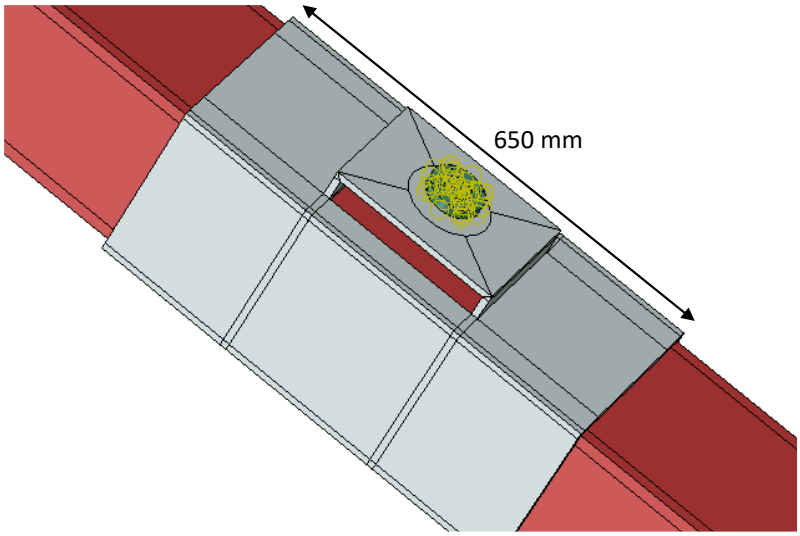


Figure 5.7: Contact definitions assigned to swivel connector

The pivot pin connecting the two collar halves was modelled with a metal-to-metal frictionless contact (See Figure 5.7). This ensured free rotation about the bolt axis and reproduced the intended kinematic behaviour of the swivel connector without introducing artificial resistance.

5.3.4. Loading and Boundary conditions.

The boundary conditions and loading applied to the local finite element model were taken directly from the global bridge analysis. Because the first scissor unit was identified as the most critical from the global bridge, its true support conditions and internal actions were reproduced in the local model. Two diagonal ends in the local model corresponded to the physical supports of the bridge while the other two ends to the hinge-connector nodes.

Boundary Conditions

The two diagonal ends that coincide with the physical supports: the pinned support and the inclined roller were modelled using displacement restraints rather than applied loads. Each CFRP cross-section was coupled to a reference point located at the corresponding global support node. The connecting pin was also restrained in its translational movements (U3=U1=0).

Loading

The remaining two diagonal ends corresponded to the hinge-connector nodes linking this unit to the next scissor unit. These ends were loaded using the internal actions extracted from the global model as presented in Table 5.2. These internal actions corresponded to the local axis defined for the global FE bridge model.

Table 5.2: Connector Loads from Global FE model

	Internal Force (N)			**Connector Moments (N.mm)**		
	CTF 1	**CTF 2**	**CTF 3**	**CTM 1**	**CTM 2**	**CTM 3**
Node 1	16.84	36622.70	-1630.36	0.00	17273.49	16304.67
Node 2	39.07	125306.18	-51300.08	0.00	-67804.62	-74255.42

The extracted forces and moments were applied at reference points coupled to the CFRP cross-sections, ensuring that the loads were distributed across the full section rather than applied as concentrated point loads. The local coordinate system was aligned with the fibre direction to maintain consistency with the global model as shown in Figure 5.8.

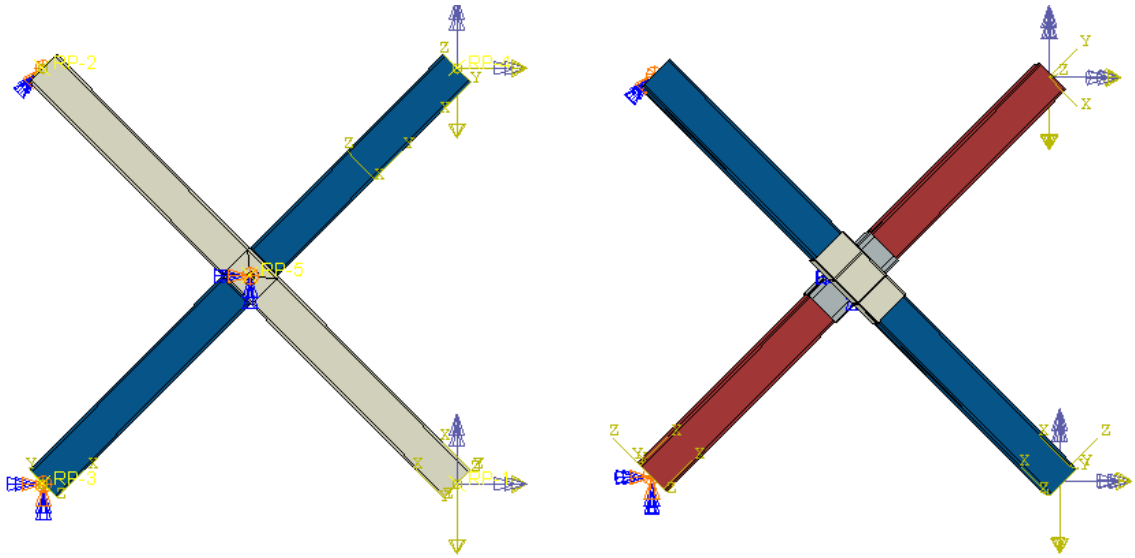
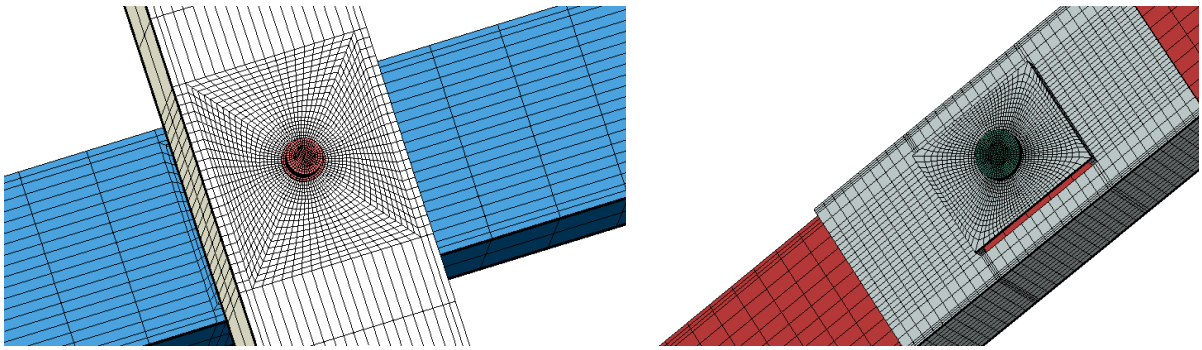


Figure 5.8: Connection design boundary conditions and load definitions.

The analysis followed the same step sequence as the global model: boundary conditions defined in the Initial step, followed by a Static, General step in which the extracted loads were applied.

5.3.5. Meshing

A refined 3D mesh was generated for all components in the local finite element model to ensure accurate representation of stress concentrations and contact behaviour. Solid elements were used throughout, with mesh density increased in regions where high gradients were expected particularly around curved geometries as shown in Figure 5.9.



(a) Drilled CFRP mesh (b) Swivel connector mesh

Figure 5.9: Creation of mesh for the connections

This approach followed established practice in joint modelling, where fine meshes are required to capture localised bearing stresses, frictional transfer, and the interaction between metallic hardware and composite members. Element sizes were reduced around circular features such as pins, bushings, and bolt holes, and along the CFRP surfaces where fibre interruption or clamping effects occurred.

THIS PAGE WAS INTENTIONALLY LEFT BLANK

6. RESULTS AND DISCUSSION

6.1. SLS Performance

6.1.1. Iterative section-selection

The serviceability performance of the DCS bridge is first governed by its global vertical deflection, which must remain within the allowable limit of 175 mm (span/120). The iterative section-selection process for both material configurations was driven by this requirement, evaluated under the critical load combination. Figure 6.1 compares the maximum mid-span deflection of the global scissor bridge for the different load combinations considered in the finite element analysis.

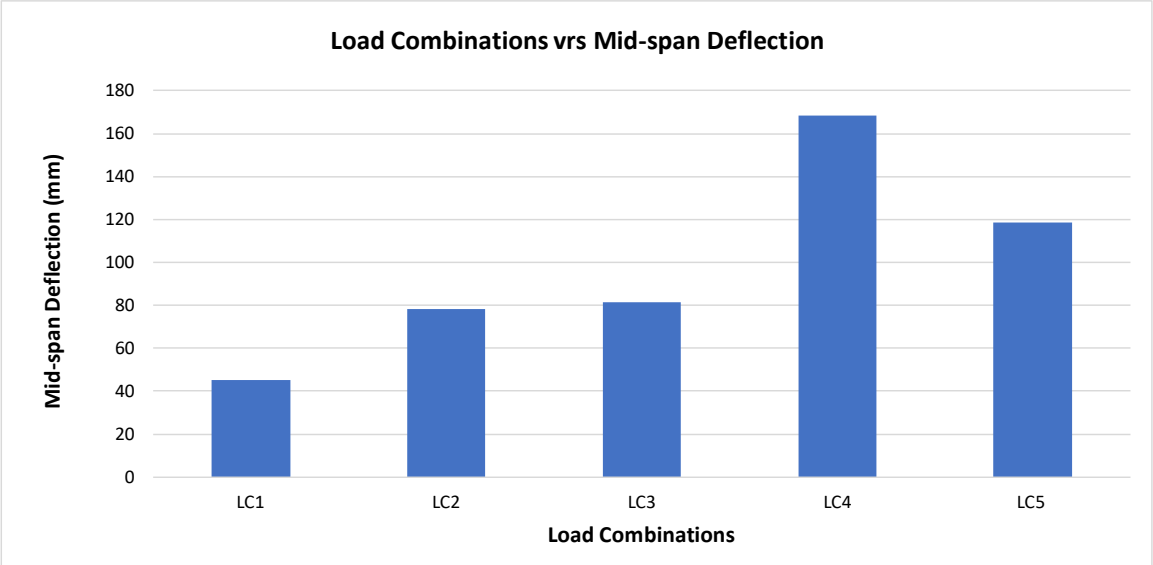


Figure 6.1: Mid-span deflection under different load combinations

LC4 represented the most demanding serviceability condition, consisting of the self-weight**,** full pedestrian loading**,** and wind pressure acting simultaneously. This combination reflected the worst-case scenario which governed the serviceability load case for the preliminary sizing of the bridge members. LC4 was adopted as the governing condition for verifying member

stiffness, stability, and connection performance in the subsequent FE design checks. Table 6.1 summarizes the selected sections and their deflections.

Table 6.1: Geometric section dimensions of materials

Material	Section Name	Dimension: (H x B x t) [mm]	Global Vertical Displacement, δ [mm]
Aluminium	AS1	200 x 100 x 10	1316.51
	AS2	350 x 200 x 10	235.57
	AS3	450 x 250 x 10	171.08
CFRP	CS1	154 x 94 x8	1441.71
	CS2	240 x 240 x 6	613.56
	CS3	300 x 240 x 18	168.45

Based on the serviceability performance of the selected sections for both material configurations, AS3 and CS3 satisfied the deflection requirement, as each produced a maximum vertical deflection below the 175 mm allowable limit. These sections were chosen to proceed in the comparative global performance between Aluminium and CFRP.

6.1.2. Load-Deflection Response under Traversing Load

The influence-line approach was adopted in the load-deflection response to determine the maximum mid-span vertical deflection as well as the governing vehicular load impact.

Figure 6.1 presents the mid-span vertical deflection as a single wheeled and tracked vehicle traverses the bridge, together with the 175 mm serviceability limit. The wheeled vehicle produced the largest deflection at mid-span at 81 mm, slightly higher than the tracked vehicle (78 mm), a difference of about 3 mm or 4%. This small gap remained across the span, narrowing near the supports where both cases dropped to roughly 45 mm.

The wheeled load gave a slightly larger response because its axle loads act over a smaller, more concentrated contact area, creating higher local bending effects than the broader footprint of the tracked vehicle. Even so, both load cases remained well below the

serviceability limit, using only about 45 % - 46 % of the allowable deflection and demonstrated a comfortable reserve in performance.

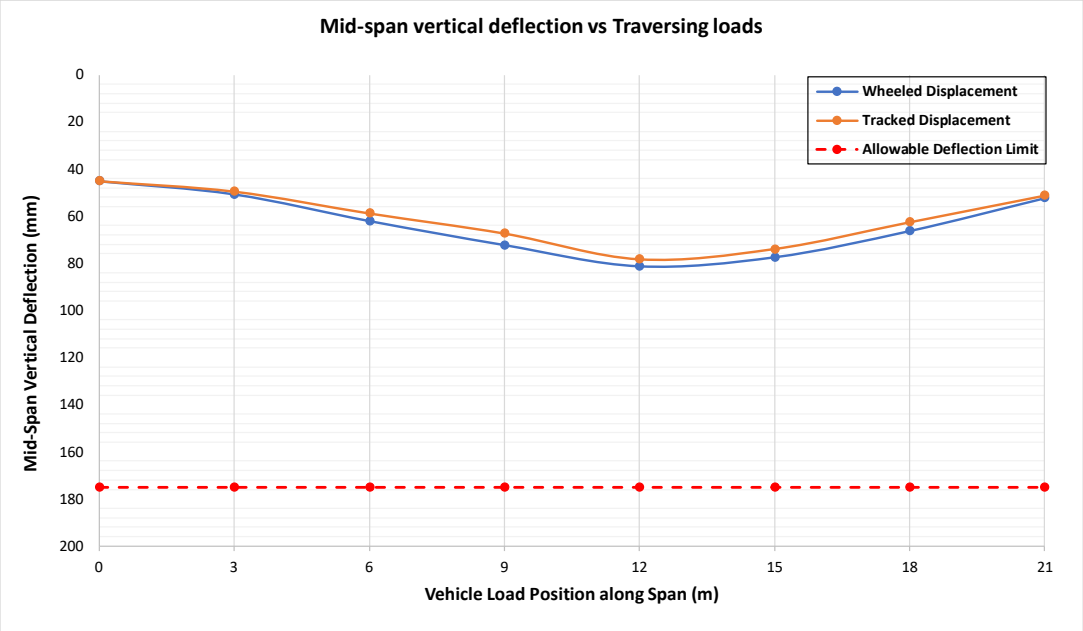


Figure 6.2: Mid-span vertical deflection under traversing loads

6.1.3. Load-Deflection Response Under Extreme Load Combination

The FE model visualization shown in Figure 6.3 presents the deformed shape of the DCS bridge under the governing in-service load combination. The analysis predicted a mid-span deflection of 168 mm, compared with the adopted serviceability limit of 175 mm. This confirmed that the bridge met the serviceability requirement defined in equation (4.1). The difference between the obtained peak deflection and the allowable deflection limit corresponded to roughly 96% utilisation of the permitted deflection. This implies that deployable scissor bridge is sensitive to deflection.

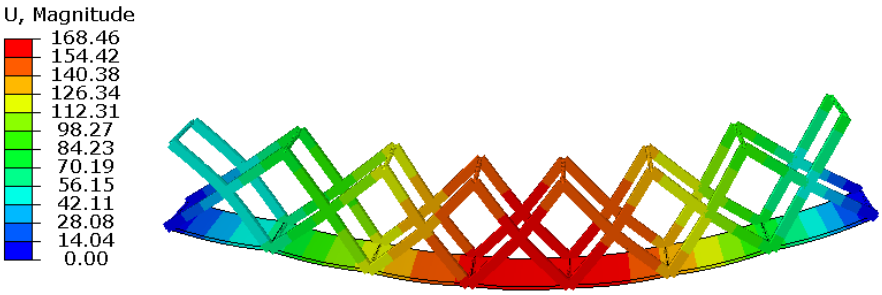


Figure 6.3: Maximum deflection under extreme load case

Although the loading was applied as a uniform pressure load on the deck instead of the nodes of the scissor joint, the resulting deformation transferred throughout the scissor members. This confirmed that the DSC behaved as a single integrated system while the implemented joint in model also ensures structural continuity and transmission of force during the in-service loading.

6.1.4. Deployment displacement under self-weight

Figure 6.4 shows the deformed configuration of the deployable CFRP scissor bridge during the deployment stage under the action of self-weight, LC1. In this configuration, the bridge behaved as a cantilever structure, with one end restrained while the free end remained unsupported during deployment. The displacement contour indicated a progressive increase in vertical displacement from the supported end towards the free end, where the maximum deformation occurred. The relatively large displacement predicted by the finite element model was expected because the analysis considered only the gravitational self-weight of the bridge and did not include the stabilising action of the deployment actuation system or counterweight mechanism.

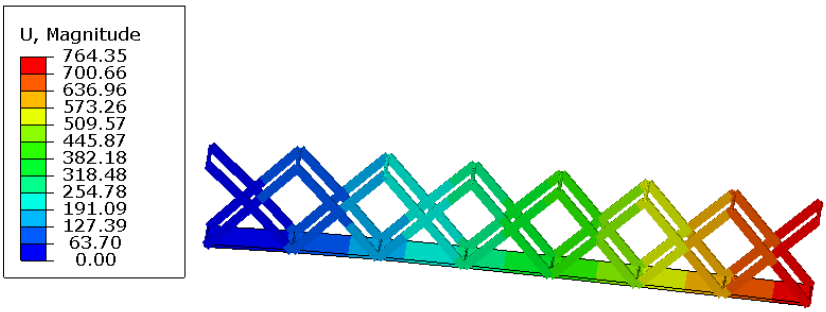


Figure 6.4: Deformed configuration during deployment

In practical deployment, the actuator and counterweight provide balancing forces that reduce cantilever deflection and improve stability throughout the deployment sequence. Therefore, this analysis represents a conservative assessment of the bridge behaviour during deployment and highlights the importance of the actuation system in controlling displacement before the bridge reaches its fully deployed configuration.

6.1.5. Load-Deflection Response under Convoy Wheeled Loading

Figure 6.5 illustrates the vertical displacement response of the DCS bridge under an exceptional load combination consisting of a convoy of three wheeled design vehicles simultaneously positioned on the bridge and spaced at 3 m intervals, LC5. This loading configuration represented an operational scenario in which multiple vehicles occupy the bridge at the same time, producing a substantially higher distributed live load than the standard traversing vehicle case.

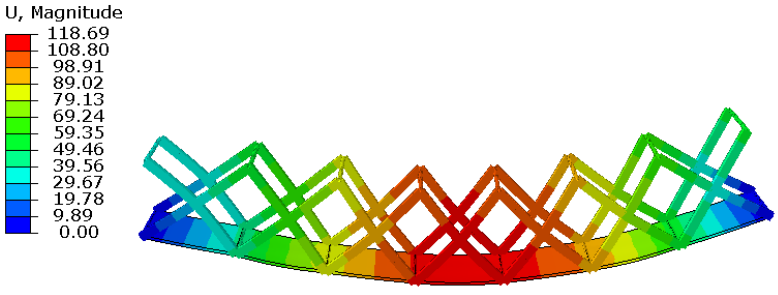


Figure 6.5: Deformed shape of the DCS bridge under LC5

The maximum displacement obtained under the convoy loading was approximately 118.7 mm, which was significantly greater than the single wheeled traversing load case but still

remained below the adopted serviceability deflection limit of 175 mm. This indicated that the bridge retained adequate global stiffness even under an exceptional loading scenario and satisfied the prescribed serviceability criterion with a reserve margin of approximately 56 mm.

6.1.6. Comparative SLS check for CFRP and Aluminium

The Aluminium and CFRP bridge models were sized using equivalent RHS sections that met the serviceability deflection limit of 175 mm. The Aluminium bridge weighed 72.24 kN, while the CFRP bridge weighed 58.59 kN, giving a 19% difference in weight. Because the wheeled vehicle produced the largest mid-span deflections, it was used as the governing serviceability load for comparing the two materials. As shown in Figure 6.6, both bridges displayed a similar and symmetrical deflection profile, with peak displacement at mid-span when the vehicle was positioned at 12 m.

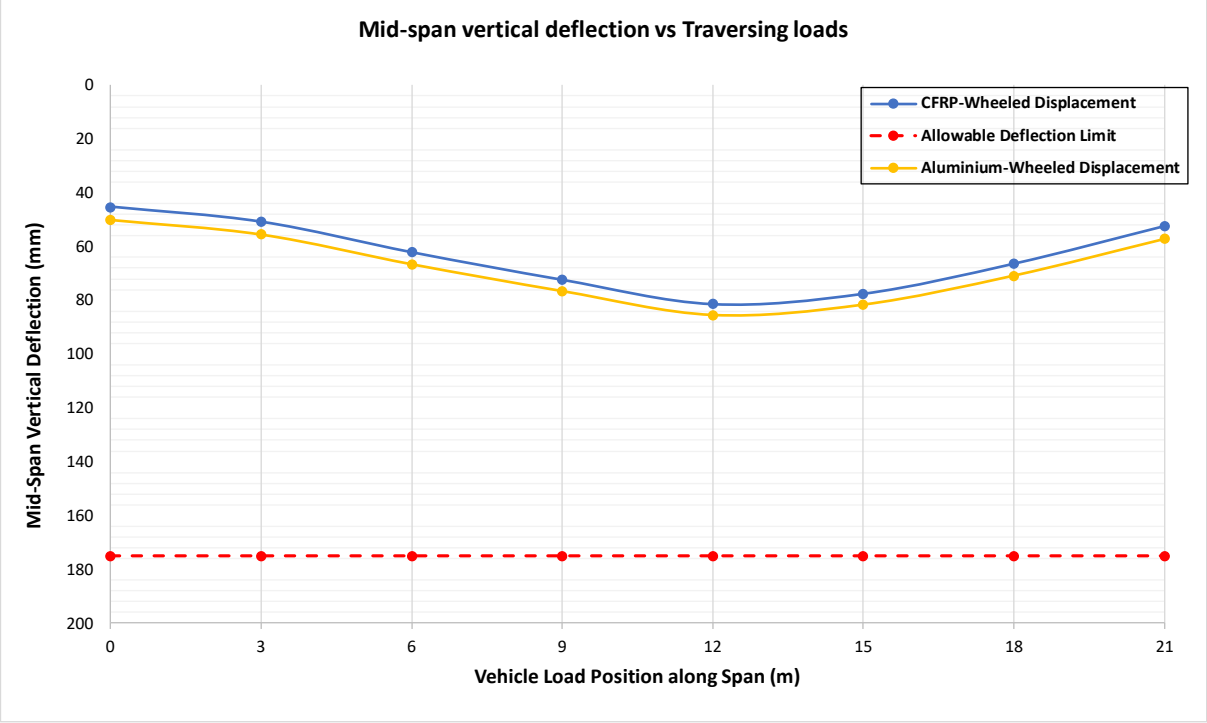


Figure 6.6: Comparative Load-Deflection response for CFRP and Aluminium models

The CFRP bridge reached a maximum deflection of about 81 mm, slightly lower than the Aluminium value of 86 mm. Although the difference was small, it showed that the CFRP system achieved comparable and marginally better serviceability performance while carrying significantly less weight. This reflected the higher stiffness-to-weight efficiency of the

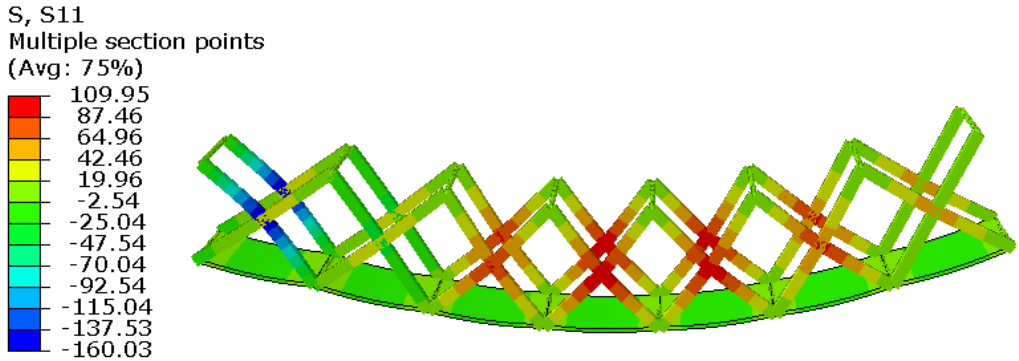
pultruded CFRP members and confirmed that the section-selection process produced equivalent global behaviour for both materials. The CFRP bridge provided a more weight-efficient solution while still satisfying the serviceability requirements.

6.2. ULS Performance

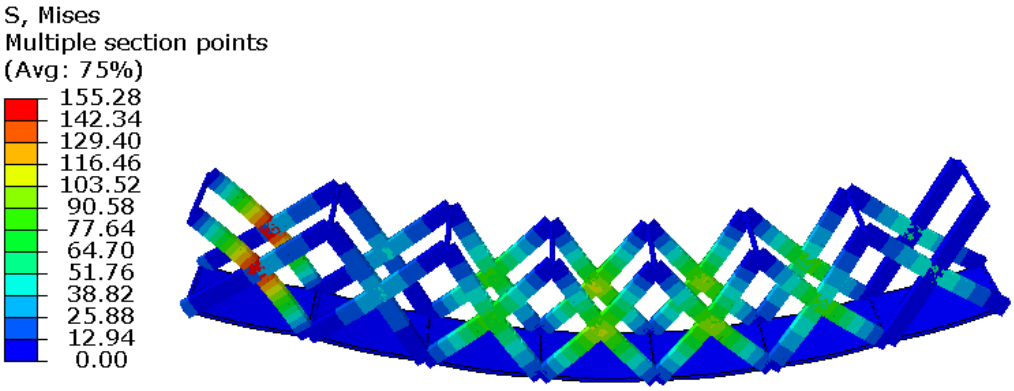
6.2.1. Global Stress Analysis

In Figure 6.7, the deformed stress contour plot of the two material-type bridge models was compared under the extreme load combination, LC4. The two scissor bridge models generally revealed concentrated stresses at the central pivot joints. At the fully restrained scissor unit of the first deck, the pivot joint was higher compared to the remaining units. These joints represented the critical load-transfer locations in the deployable mechanism and therefore experienced the greatest internal force demands.

The scissor members of the FE models were made with beam elements and this made the reported stress in the CFRP model corresponded primarily to the longitudinal fibre direction. Although localized peak stresses occurred around the pivot regions, the maximum stress remained significantly below the design tensile resistance of the CFRP. With a characteristic tensile strength of 1800 MPa and a material reduction factor of 1.8, the design tensile strength was approximately 1000 MPa. By comparing the S11 stress values in Figure 6.7 (a) with the reduced longitudinal tensile strength of the CFRP, the utilization ratio was approximately 11 %. This indicated a substantial strength reserve under the critical loading combination.



(a) CFRP Model



(b) Aluminium Model

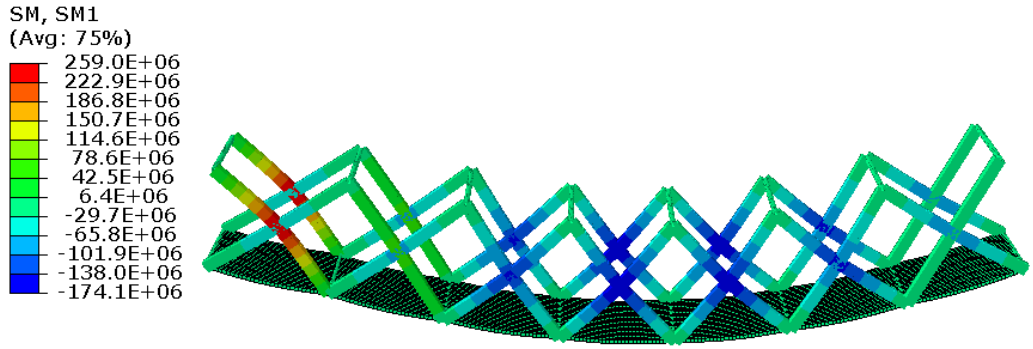
Figure 6.7 : Deformed stress contour plot of bridge models

In contrast, the Aluminium bridge model exhibited a similar stress concentration pattern at the pivot joints but with considerably higher stress utilization because of the lower material strength. Taking an Aluminium yield strength of 185 MPa and a strength reduction factor of 1.5 gave a design yield strength of approximately 123 MPa. The maximum Mises stress in the Aluminium members shown in Figure 6.7 (b) exceeded this design resistance, producing a utilization ratio greater than 100%.

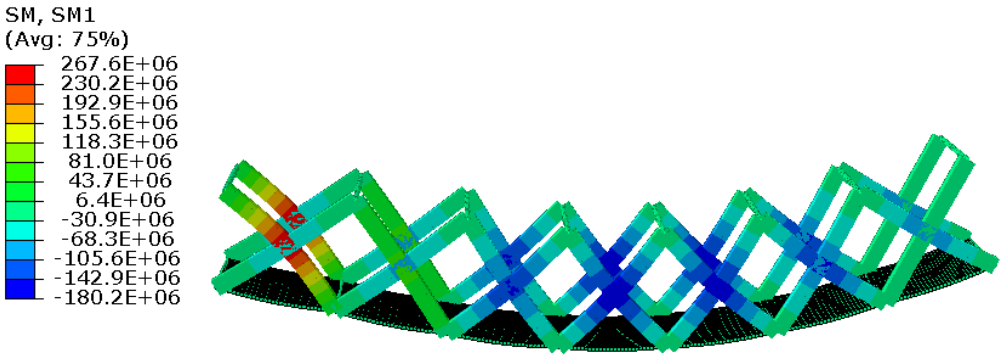
6.2.2. Bending Analysis

This section discusses the comparative bending capacities of the two material-type scissor bridge models as shown in Figure 6.8 as well as bending verification calculation summarized in Table 6.2. The deformed bending contour plots from the FE model presents the distribution of bending moment in the scissor members.

Bending verification was carried out by comparing the maximum bending moments obtained from the global FE results with the design bending capacities of the selected sections.



(a) CFRP Model



(b) Aluminium

Figure 6.8: Deformed bending contour plot of bridge models

The bending resistance of the pultruded CFRP member was governed by its longitudinal compressive strength, as UD profiles typically fail in compression before tensile fibre rupture. Using a characteristic compressive strength of 900 MPa and a material partial factor of 1.65, the resulting design compressive strength was 545.5 MPa. For the 300 × 240 × 10 mm CFRP RHS section, this corresponded to a design bending resistance of 826.2 kN.m. The ABAQUS analysis predicted a maximum bending demand of 259.0 kN.m, giving a utilization ratio of 31.35 %. This satisfied the ULS requirement, leaving approximately 68.35 % reserve bending capacity.

Table 6.2: Comparative bending verification results

Material Type Model	Characteristic Strength (MPa)	Reduction Factor, γ	Design Strength (MPa)	Section Modulus, W_x (mm^3)	Design bending capacity (kN.m)	Max. FE bending moment (kN.m)
Aluminium	185	1.5	123.3	5.16E+05	63.6	267.6
CFRP	900	1.65	545.5	1.51E+06	826.2	259.0

Conversely, the Aluminium bridge member (450 × 250 × 10 mm RHS) provided a design bending resistance of 63. 6 kN.m, obtained by applying the ASM safety factor of 1.5 to the 185 MPa yield strength. In comparison, the FE analysis predicted a bending demand of 267. 60 kN.m, resulting in a utilization ratio greater than 100 %. This indicated that the Aluminium member exceeded its design bending capacity by a wide margin and would yield under the critical load combination.

6.2.3. Buckling Performance

Comparative Global Linear Buckling Analysis

As part of the structural verification of the DCS bridge, a linear eigenvalue buckling analysis was carried out in Abaqus to assess the global stability of the selected Aluminium and CFRP scissor-member sections. Although the serviceability results showed that the CFRP bridge produced smaller vertical deflections than the Aluminium bridge, the slender and highly anisotropic nature of pultruded UD CFRP members makes them more sensitive to instability under compression. Deflection performance alone is therefore insufficient to confirm their structural adequacy. For this reason, a global buckling analysis was performed for both material configurations to evaluate their resistance to elastic instability.

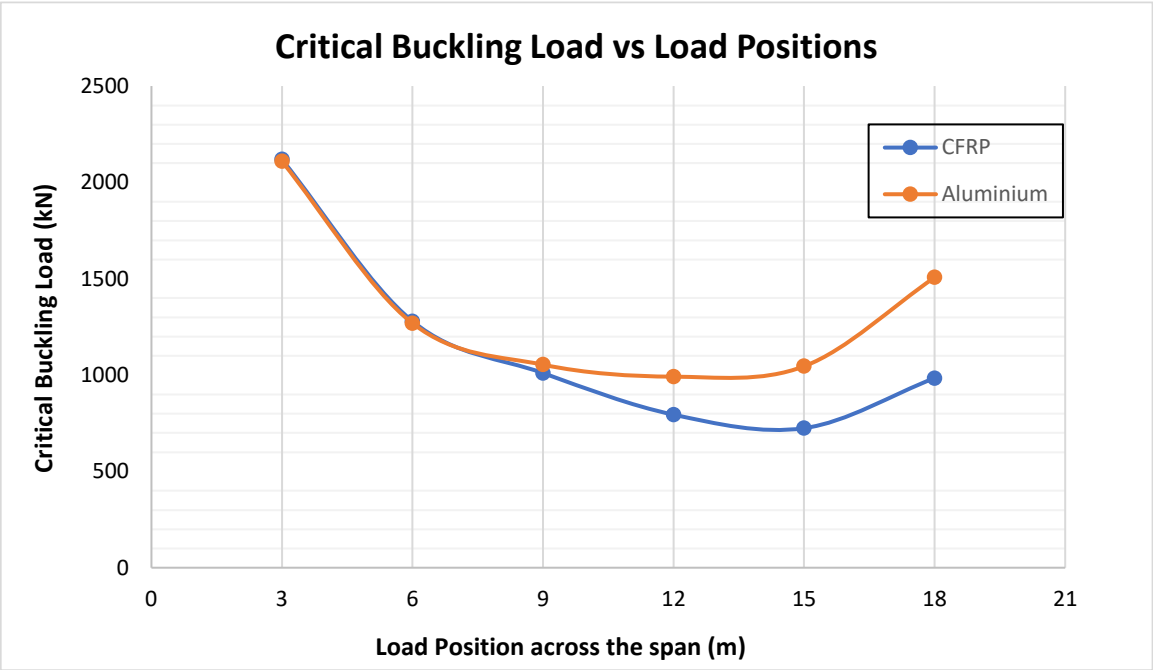


Figure 6.9: Comparative linear buckling response

From the results in Figure 6.9, both material models performed equally at the first two load positions until the Aluminium model consistently produced higher critical buckling loads than the CFRP bridge throughout the remaining traversing load positions. The highest buckling capacity for both materials occurred when the traversing load was positioned at the first intermediate point from the fully constrained edge of the bride, while the lowest buckling capacities occurred when the vehicle was located at around the mid-span, where the compression demand in the diagonal members was greatest.

Design Buckling Verification

The buckling verification from the results in Table 6.3 showed that both Aluminium and the CFRP bridge models satisfied the global stability requirement at every traversing load position. The design compressive load increased as the vehicle approached the mid-span of the bridge and reduced towards the supports. However, all the allowable buckling load remained greater than the applied compressive load.

The utilisation ratio expresses the percentage of the available buckling resistance mobilised by the applied compressive load. A value below 100 % indicates that the member satisfies the buckling requirement, while a value approaching 100 % indicates that the member is nearing

its design buckling capacity. In this study, the maximum buckling utilisations of the CFRP bridge was 21.4 % and 21.1 % around the mid-span load position, whereas the Aluminium bridge reached a maximum utilisation of 16.6 %, demonstrating a greater stability reserve under the same traversing load condition.

Table 6.3: Buckling Verification Results for Aluminium and CFRP for traversing load

	Load Position (m)	**Critical Buckling Load, P_{cr}(kN)**	**Allowable Buckling, $B = \frac{P_{cr}}{\gamma}$ (kN)**	**Design Compressive Load, P_d((kN)**	**Utilization ratio, $\eta = \frac{P_d}{B}$ (%)**
Aluminium	3	2110.00	1406.67	87.82	6.2
	6	1270.00	846.67	107.90	12.7
	9	1055.00	703.33	112.20	16.0
	12	993.00	662.00	109.90	16.6
	15	1047.00	698.00	102.30	14.7
	18	1508.00	1005.33	91.10	9.1
CFRP	3	2120.00	1284.85	79.50	6.2
	6	1280.00	775.76	99.70	12.9
	9	1011.00	612.73	104.00	17.0
	12	795.00	481.82	101.70	21.1
	15	725.00	439.39	94.10	21.4
	18	985.00	596.97	82.80	13.9

Similarly, buckling verification was performed for the two materials at the critical load combination, LC4 as shown in Table 6.4. In these results, the minimum critical buckling load was checked against the critical design compressive load from the FE models. The Aluminium section outperformed the CFRP, however their utilization ratios were less than 100%.

Table 6.4: Buckling verification for Aluminium and CFRP at LC4

	Critical Buckling Load, P_{cr}(kN)	**Allowable Buckling, $B = \frac{P_{cr}}{\gamma}$ (kN)**	**Design Compressive Load, P_d((kN)**	**Utilization ratio, $\eta = \frac{P_d}{B}$ (%)**
Aluminium	993.00	662.00	234.50	35.42
CFRP	725.00	439.39	266.60	60.67

These results highlighted the different roles of serviceability stiffness and stability resistance in the two material systems. The CFRP bridge, which was 19% lighter than the Aluminium bridge (58.59 kN versus 72.24 kN), previously demonstrated lower global vertical deflections under service loading because of its superior stiffness-to-weight efficiency. However, the

Aluminium bridge exhibited a higher buckling resistance because its isotropic material behaviour and larger equivalent section provide greater flexural rigidity against global elastic instability.

Pultruded CFRP members are orthotropic and compression-dominated stability is governed primarily by the longitudinal stiffness and the slenderness of the section rather than by the reduced structural weight alone. Therefore, while CFRP provides a lighter and more displacement-efficient bridge, buckling becomes an essential governing verification criterion.

6.3. Local Structural Response of Connection

The local finite element model was developed to assess the structural behaviour of the two proposed connection solutions under the critical internal actions extracted from the global scissor-bridge analysis. This section examined the stress distribution within the pultruded CFRP members, the metallic pin and bushings, and the bearing pressures generated at the composite-metal interfaces for the simple pin connection. An equivalent evaluation was then presented for the clamped swivel connector. Together, these results formed the basis for a comparative assessment of the two concepts, highlighting their respective strengths, limitations, and suitability for the deployable CFRP scissor mechanism.

6.3.1. Simple metallic pin connection

The contour in Figure 6.10 represented the longitudinal stress parallel to the pultrusion direction of the CFRP members. The highest stresses were concentrated around the pin hole, particularly along the loaded edge where the pin transferred compressive forces into the profile. Away from the connection region, the stresses decreased rapidly and became relatively uniform along the member length, indicating that the pin joint introduced a localised stress concentration while the remainder of the member continued to carry load primarily through axial action. In both diagonal members tensile and compressive action were observed reaching 166 MPa and 283 MPa respectively.

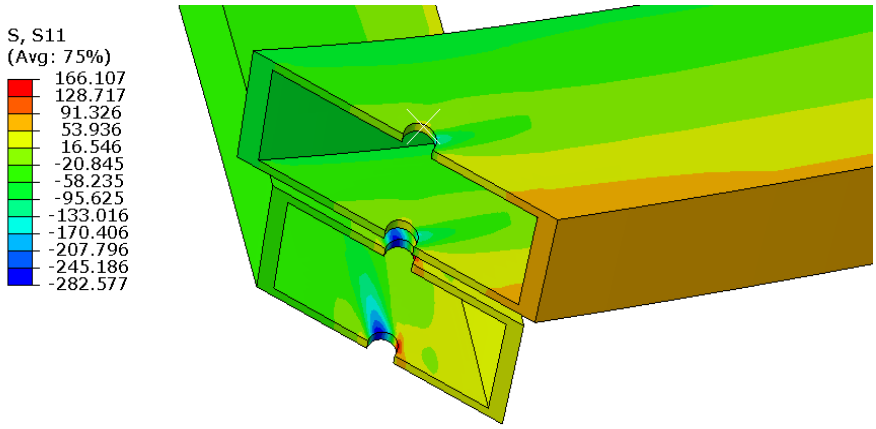


Figure 6.10: Longitudinal stress (S11) distribution around the pin hole

The S22 contour in

Figure 6.11 described the transverse stress acting perpendicular to the pultrusion fibres. As expected for a mechanically fastened pultruded profile, the transverse stress field was highly localised around the pin hole, while the remainder of the member experienced negligible transverse demand. Tensile and compressive stresses developed on opposite sides of the hole as the pin bore against the profile, producing a characteristic band of matrix-dominated stresses around the perforated region.

At the hole edge, the transverse stress rose sharply, reaching approximately 56 MPa in tension and 49 MPa in compression**.** These values were small compared with the fibre-direction stresses but were more structurally significant, since the composite is far weaker across the fibres than along them.

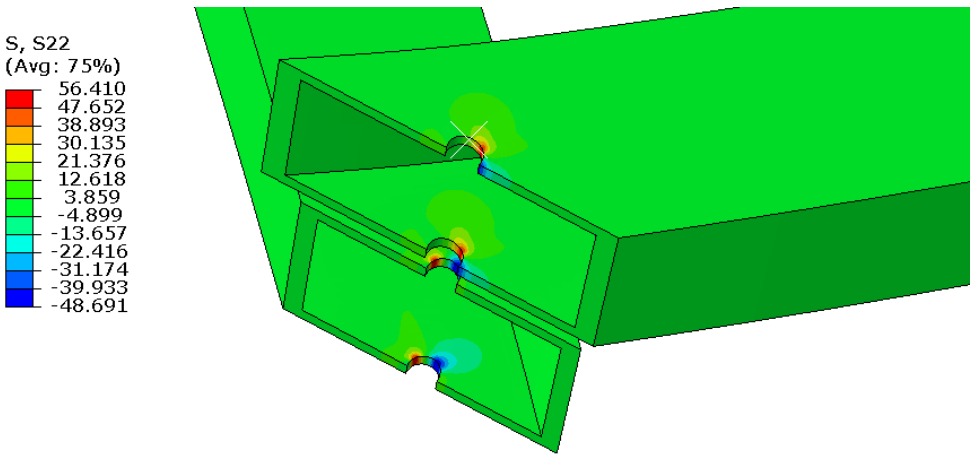


Figure 6.11: Transverse Stress (S22) Distribution around the pin hole

The S12 contour in Figure 6.12 illustrated the in-plane shear stress generated by the interaction between the metallic pin and the pultruded profile. As with the transverse stress response, the shear field was highly localised around the hole, while the remainder of the member experienced negligible shear demand. Peak shear stresses developed at the bearing zone immediately adjacent to the pin, confirming that load transfer occurred through a combination of bearing and in-plane shear. At the hole boundary, the shear stress rose sharply, reaching 59.9 MPa. Away from the connection, the shear stress decayed rapidly, indicating that the shear transfer mechanism was confined to the immediate vicinity of the pin and did not influence the global behaviour of the CFRP member.

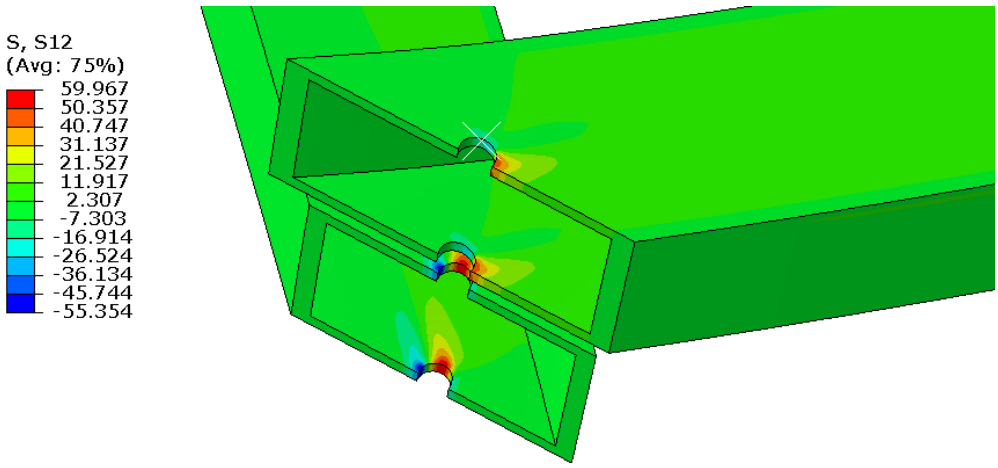


Figure 6.12: In-plane shear stress (S12) distribution in the CFRP connection.

The von Mises stress contour in Figure 6.13 showed that the highest stresses developed at the contact interfaces between the pin and the bushings, where bearing forces entered the metallic components. Along most of its length, the pin remained lightly stressed, generally below 100 MPa**,** indicating that the shank carried minimal load away from the connection zone. Localised stress concentrations formed at two regions. These were the central section of the pin, where it engaged both CFRP members. The peak von Mises stress reached approximately 377 MPa, reflecting the combined bearing and shear transfer occurring at these interfaces.

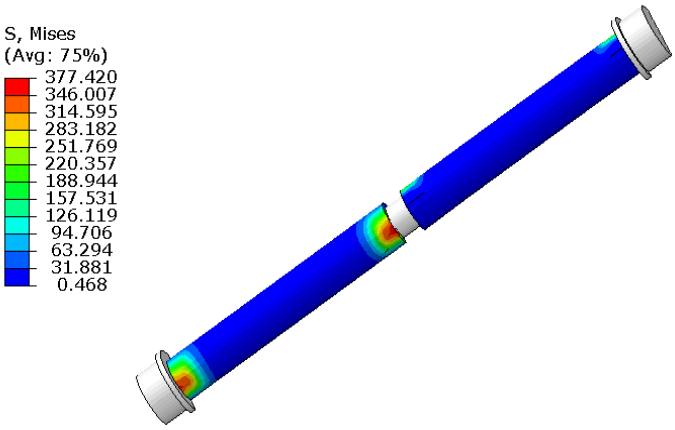
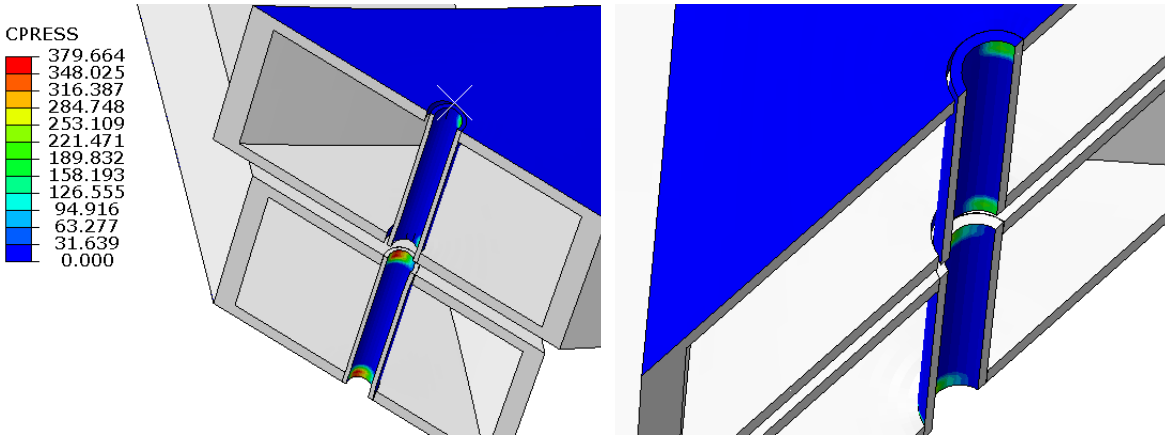


Figure 6.13: Von Mises stress distribution in the steel pin and bushings

The contact pressure results in Figure 6.14 showed how the pin transferred load into the pultrude CFRP RHS profile section. Pressure remained close to zero over most of the pin and bushing surfaces and increased only at a few well-defined regions where the pin bore directly against the drilled hole in each member. At these contact patches, the bearing pressure reached approximately 380 MPa. This behaviour confirmed that the pin did not engage the profile uniformly along its length. Instead, the load was transmitted through small, concentrated bearing zones. The CPRESS contour therefore demonstrated that the connection relied on local bearing rather than distributed contact around the hole circumference.



(a) Critical contact pressure

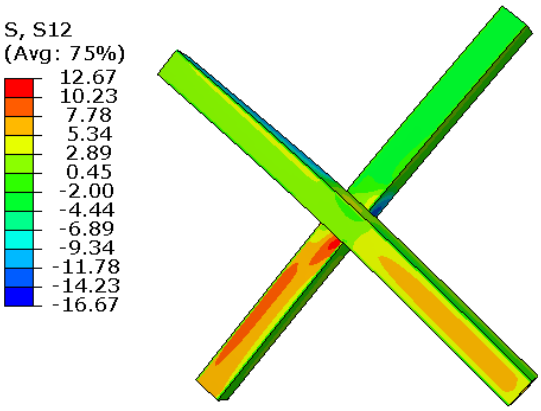
(b) Bearing gap between bushing and member hole

Figure 6.14: Contact pressure (CPRESS) distribution between the bushing and the CFRP hole.

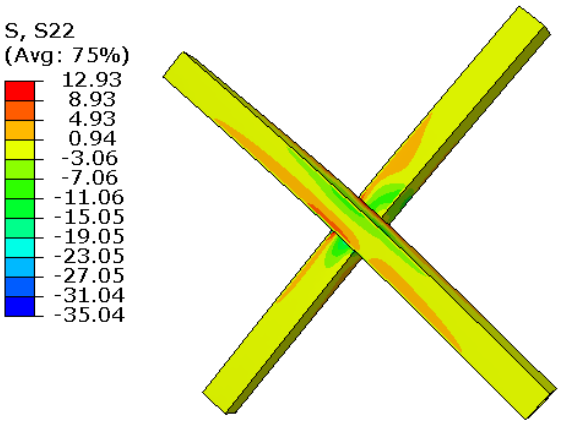
6.3.2. External clamped metallic swivel connector.

In the alternative connection concept, where the pultruded CFRP profiles were not perforated, the stress fields were markedly more uniform than in the simple drilled pin connection solution.

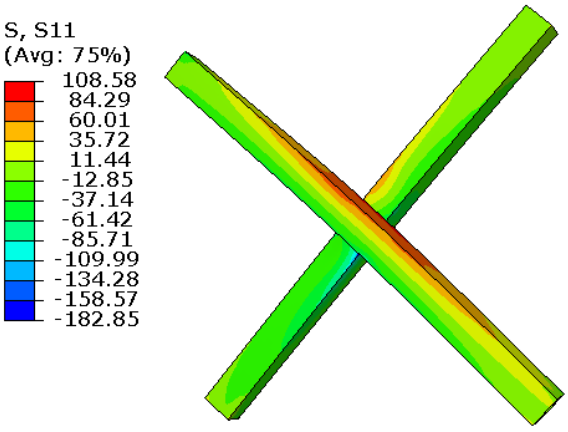
In the non-perforated connection concept, the S11 contour in Figure 6.15 (c) showed a smooth and continuous longitudinal stress field along the CFRP members. Without a drilled hole, no sharp stress concentration developed at the connector interface. Instead, the stresses reflected the combined axial and bending actions inherent to the scissor mechanism. This bending-induced curvature produced noticeable zones of tension and compression along the fibre direction, particularly near the clamped region where rotation was restrained.



(a) In-plane shear stress (S12)



(b) Transverse stress (S22)



(c) Longitudinal stress (S11)

Figure 6.15: Stress distribution of unperforated CFRP pultruded members

The transverse (S22) and in-plane shear (S12) stresses in Figure 6.15 (a) and Figure 6.15 (b) also remained low and broadly distributed, with no sharp concentrations. Both stress components increased only in the immediate clamped region, where the connector engaged the outer surface of the CFRP profile, but their magnitudes stayed modest and decayed rapidly along the member. The absence of a drilled hole eliminated the typical matrix-dominated transverse tension peaks and shear-out paths, resulting in a more uniform and structurally favourable stress state across the profiles.

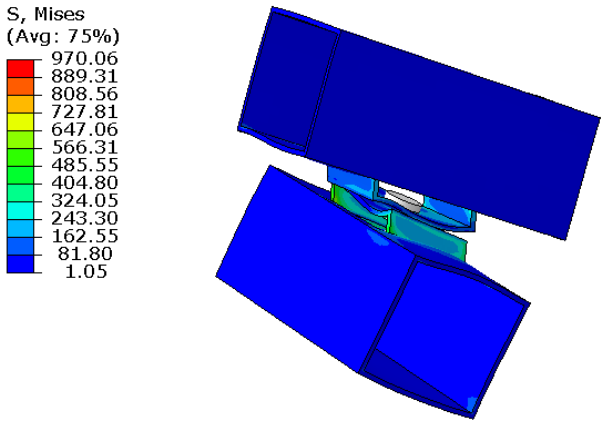


Figure 6.16: Von Mises stress of the swivel connector

The von Mises stress field in the external swivel connector remained highly localised around the metallic joint components as shown in Figure 6.16. The connector plates and the swivel pin exhibited clear stress concentrations at the load-transfer interfaces. The highest stresses occurred at the inner faces of the connector where rotation and bearing forces were introduced. The maximum von Mises stress recorded in the deformed model was approximately 970 MPa, indicating that the connector experienced significant localised demand. Away from these concentrated regions, the stress levels dropped sharply, confirming that the swivel mechanism effectively isolated the CFRP profiles from high local metallic stresses.

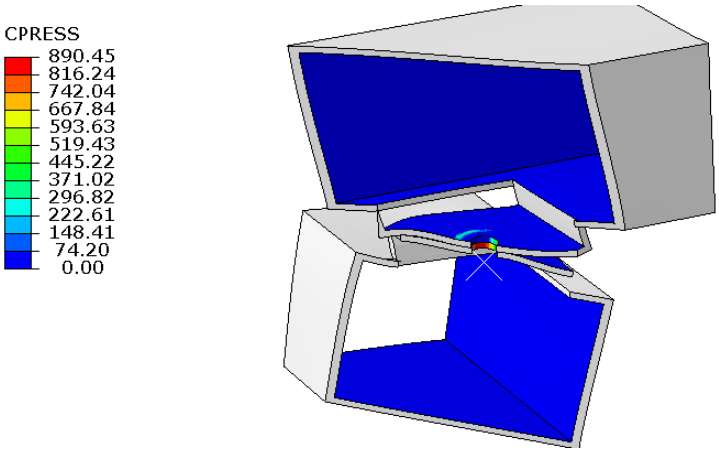


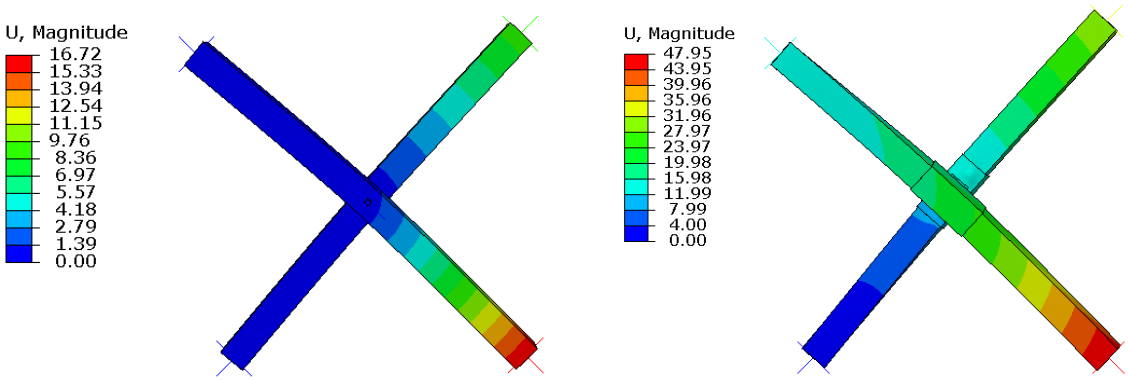
Figure 6.17: Contact Pressure (CPRESS) within the swivel connector

The CPRESS results in Figure 6.17 showed that the two collar halves remained essentially loaded across most of their mating surfaces. The interacting plates of the swivel collars did not bear against each other over the majority of their contact area. A noticeable bearing occurred only along a narrow band at the hinge line where the diagonal collars met at the pivot. In this region, the pressure increased with a peak of approximately 890 MPa, confined to only a few elements at the pin interface. This pattern demonstrated that the swivel transmitted load almost entirely through this small, concentrated contact line rather than through the broader collar faces.

6.3.3. Comparison of Global Displacement Behavior

Under identical loading and boundary conditions, the two connector types exhibited different displacement responses. The perforated CFRP pin connection reached a peak displacement of 16.72 mm in Figure 6.18 (a), concentrated at the free end of the loaded diagonal. The contour bands remained perpendicular to the member axis, revealing deformation governed by axial extension and bending about a concentric pin joint.

In contrast, the undrilled clamped swivel connector reached a significantly larger peak displacement of 47.95 mm in Figure 6.18 (b), approximately 2.9 times that of the pin connection. This confirmed that the swivel introduced joint flexibility, as load was transferred through friction and bearing over the external collar.



(a) Perforated CFRP scissor unit (b) Undrilled CFRP scissor unit

Figure 6.18: Displacement results of the two connection solutions

The swivel-connected member also showed clear torsional rotation, visible in the skewed contour bands across the cross-section. This twisting arose from the eccentric load path created by the external clamp, which did not align with the member's shear centre. The perforated pin connection showed no comparable torsional behaviour.

6.4. Failure Assessment of Connection

Building on the local structural response presented above, a failure assessment was undertaken for each connection concept. This was to check the governing stress and contact-pressure results against the relevant failure modes. Here, the available design allowable were verified against the corresponding material strength. Among the classical composite joint failure modes discussed in the literature, the local FE results showed that bearing was the most critical for the perforated CFRP profile in the simple pin connection.

For the external clamped swivel connector, the evaluation criteria differed because the CFRP profiles were not perforated. The assessment focused on the metallic strength of the connector hardware and the bearing pressure generated at the pivot.

6.4.1. Pin Bearing Failure.

This was the primary critical failure mode observed in both the perforated CFRP profile connection and the metallic swivel connection based on the contact pressure (CPRESS) obtained from the local FE model results. The two-connection solution utilized pins that bore against different surrounding materials. In all cases, the bearing capacity of the surrounding material revealed the extent of bearing failure in the connected region.

For the simple pin connection with perforation in the CFRP, a stress-based local verification was performed against the multidirectional design compressive strength as summarized in Table 6.5 below. The design strengths in all cases accounted for a reduction factor to the characteristic material properties.

Table 6.5: Bearing failure verification results.

Material Strength Property	Symbol	Characteristic strength, $\mathbf{f_{ck}}$ (MPa)	Design strength, $\mathbf{f_d}$(MPa)	Applied CPRESS (MPa)	Bearing Utilization ratio, $\boldsymbol{\eta}$ (%)
Longitudinal Compression	Xc	900.0	600.0	379.0	63.2
Transverse compression	Yc	150.0	100.0	379.0	379.0

Although the CPRESS in Abaqus is nondirectional, the contact pressure had to be checked against the direction-dependent compressive strengths of the pultruded CFRP profile. In the longitudinal compressive direction (Xc), the utilisation reached 63.2%, showing that fibres aligned with the pultrusion direction retained adequate capacity and were not at risk of bearing-induced fibre crushing.

In the transverse compressive direction (Yc), the utilisation rose to 379.0%, meaning the local bearing pressure far exceeded the matrix-dominated transverse compressive resistance. This indicated a clear likelihood of resin crushing and fibre-matrix crushing at the loaded edge of the hole.

6.4.2. Metallic Yielding

In the swivel connector connection, the governing structural risk shifted from the diagonal CFRP members as expected. This solution concept protected the pultruded CFRP members while the metallic hardware was identified as the critical element.

The governing failure in the swivel connector occurred in the metallic lugs that held the pivot pin. These small features at the ends of the collar halves carried the full bearing and shear demand from the hinge action.

The peak von Mises stress in the lug region reached approximately 970 MPa, far above the 503 MPa yield strength of the Al-7075-T6 used in the model. This corresponded to a utilisation of about 193%, confirming that the lugs yielded under the applied load. The observed pivot contact pressure of 890 MPa did not only confirm the failure but the yielding was a clear and immediate indicaton. This showed that the lug geometry including thickness and fillet radius at the pin bore required redesign in addition to any material upgrade.

7. CONCLUSIONS AND FURTHER DEVELOPMENTS

7.1. Main Conclusion

7.1.1. Global Bridge Model

In this project, the scissor mechanism was adopted as a novel deployable lightweight bridge for emergency application. The global analysis validated this choice by demonstrating that its structural behaviour can be reliably quantified under realistic service and ultimate loading.
Both Aluminium and CFRP sections were sized to meet the span/120 serviceability limit, but the CFRP configuration achieved this requirement with approximately 19 % lighter in weight.
In terms of ULS, the CFRP bridge carried the critical load combination with substantial strength reserve of tensile and bending capacity. The Aluminium bridge did not meet the same strength and bending requirements. Although the selected Aluminium section satisfied deflection, it failed to satisfy strength under the same loading.
In terms of buckling performance, the CFRP members mobilised a larger proportion of their buckling capacity, reaching about 61% utilisation compared with 35% for Aluminium. This reflected the compression-sensitive behaviour of pultruded CFRP.
The global structural analysis confirmed that the scissor mechanism, when combined with pultruded CFRP members, was a viable and efficient solution for a lightweight deployable bridge. The CFRP configuration was lighter, met serviceability requirements with a comparable margin to Aluminium, and carried ultimate loads with significant strength reserve. Its main structural limitation was reduced buckling reserve, which must continue to guide section selection.

7.1.2. Local connection model

The joint design study set out to address the adoption of a conventional simple pin in a perforated CFRP profile and an external swivel connector developed specifically to avoid perforation in the CFRP diagonal members of the DSC bridge.

The verification confirmed that the perforated CFRP connection was not governed by longitudinal fibre compression, but by the much weaker transverse compressive properties of the profile. Bearing-induced transverse matrix failure was therefore identified as the governing local failure mechanism, supporting the need for detailed reinforcement or local composite inserts to reduce contact-pressure concentrations around the hole.

The external swivel connector, concept 2, achieved its principal design objective of keeping the CFRP diagonal member itself lightly and diffusely stressed, free of the perforation-related failure modes examined for Concept 1. However, in doing so it shifted the governing structural risk onto the metallic connector hardware, where the connecting lugs were found to exceed the yield strength of the modelled material

7.2. Further developments

For a lightweight deployable composite bridge, future studies should also explore alternative deployment strategies, such as the cable-assisted deployable systems which are adaptable for different bridge spans.

From a numerical modelling perspective, deployable scissor bridge should be developed with a higher-fidelity global finite element model by replacing the beam-element idealisation with shell or solid elements capable of representing local plate behaviour, orthotropic laminate stresses, and cross-sectional distortion.

Instead of drilling holes into the finished pultruded profile, the pivot region should be prefabricated with built-in reinforced perforations or co-cured composite inserts. This preserves the continuity of the main load-carrying fibres, reduces the stress concentrations caused by post-manufacture drilling, and improves the bearing and fatigue performance of the joint.

Future research should focus on building and testing a small-scale laboratory prototype of the deployable composite scissor bridge. This would allow the proposed connection design to be evaluated under real deployment and loading conditions.

7.3. References

[1] D. W. Poppema *et al.*, "Bridge Clogging in Belgium and Germany During the 2021 Floods", doi: 10.1029/2024WR039218.

[2] "2024 European floods," *Wikipedia*. Jun. 22, 2026. Accessed: Jul. 18, 2026. [Online]. Available: https://en.wikipedia.org/w/index.php?title=2024_European_floods&oldid=1360542770

[3] A. Scala *et al.*, "Extreme natural events and bridge collapses: statistical insights in Italy," *Int. J. Disaster Risk Reduct.*, vol. 131, p. 105880, Dec. 2025, doi: 10.1016/j.ijdrr.2025.105880.

[4] "Germany's valley of floods is braced to withstand future disasters | The National." Accessed: Aug. 09, 2026. [Online]. Available: https://www.thenationalnews.com/world/2023/08/03/germanys-valley-of-floods-is-braced-to-withstand-future-disasters/

[5] "Motorway collapses as deadly storms hit France, Portugal and Spain." Accessed: Aug. 09, 2026. [Online]. Available: https://www.bbc.com/news/articles/c20l6d03e1no

[6] "Licensable picture: Aftermath of floods in Valencia," Reuters Connect. Accessed: Aug. 09, 2026. [Online]. Available: https://www.reutersconnect.com/item/aftermath-of-floods-in-valencia/dGFnOnJldXRlcnMuY29tLDIwMjQ6bmV3c21sX1JDMk5WQUFHT0pJSQ

[7] J. J. Moy, C. S. Tan, S. Mohammad, and A. R. Z. Abidin, "State-of-Art review on deployable scissor structure in construction," *Structures*, vol. 42, pp. 160–180, Aug. 2022, doi: 10.1016/j.istruc.2022.05.084.

[8] E. Rivas-Adrover, *Deployable Structures*. 2015.

[9] A. Tanha, A. KR, H. PH, and C. Lonth, "Analysis of deployable bridge," *Sustain. Agri Food Environ. Res.-Discontin.*, Dec. 2023, doi: 10.7770/safer-V12N-art773.

[10] H. T. Ali *et al.*, "Fiber reinforced polymer composites in bridge industry," *Structures*, vol. 30, pp. 774–785, Apr. 2021, doi: 10.1016/j.istruc.2020.12.092.

[11] M. S. Khani, "CONNECTIONS IN STRUCTURAL FRP MEMBERS".

[12] A. Zhou and T. Keller, "Joining techniques for fiber reinforced polymer composite bridge deck systems," *Compos. Struct.*, vol. 69, no. 3, pp. 336–345, Jul. 2005, doi: 10.1016/j.compstruct.2004.07.016.

[13] S. Russo, "On failure modes and design of multi-bolted FRP plate in structural joints," *Compos. Struct.*, vol. 218, pp. 27–38, Jun. 2019, doi: 10.1016/j.compstruct.2019.03.048.

[14] J. L. Clarke and European Structural Polymeric Composites Group, Eds., *Structural design of polymer composites: EUROCOMP design code and handbook*, Transf. to digital printing. London: Spon, 2009.

[15] D. Begbie and G. Roberts, "Bridging in the Second World War: an imperative to victory," *Proc. Inst. Civ. Eng. - Eng. Hist. Herit.*, vol. 167, no. 2, pp. 111–121, Apr. 2014, doi: 10.1680/ehah.13.00022.

[16] "Bailey bridge," *Wikipedia*. Jul. 16, 2026. Accessed: Aug. 09, 2026. [Online]. Available: https://en.wikipedia.org/w/index.php?title=Bailey_bridge&oldid=1364403452

[17] “Bailey bridge,” *Wikipedia*. Jul. 16, 2026. Accessed: Aug. 09, 2026. [Online]. Available: https://en.wikipedia.org/w/index.php?title=Bailey_bridge&oldid=1364403452
[18] F. E. Pallarés, “EMILIO PÉREZ PIÑERO: INVENTOR OF DEPLOYABILITY”.
[19] W. Bettini, J. Quirant, J. Averseng, and B. Maurin, “Self-Deployable Geometries for Space Applications,” *J. Aerosp. Eng.*, vol. 32, no. 1, p. 04018138, Jan. 2019, doi: 10.1061/(ASCE)AS.1943-5525.0000967.
[20] J. Unda, J. Weisz, J. Rivacoba, I. R. Uríen, and R. S. Capitanio, “Family of deployable/retractable structures for space application,” *Acta Astronaut.*, vol. 32, no. 12, pp. 767–784, Dec. 1994, doi: 10.1016/0094-5765(94)90084-1.
[21] M. Muñoz-Vidal, I. López-César, J. Pérez-Valcárcel, and F. Riestra, “A new approach to expandable structures: crossed expandable frames (X-frames). (TSUBOI AWARD 2019 for the most meritorious paper published in the Journal of the IASS).,” *J. Int. Assoc. Shell Spat. Struct.*, vol. 60, pp. 292–303, Dec. 2019, doi: 10.20898/j.iass.2019.202.034.
[22] J. Pérez-Valcárcel and F. Pallares, *1996-7 Maras Recent advances in the analysis of expandable structures*. 2021.
[23] B. R. Russell and A. P. Thrall, “Portable and Rapidly Deployable Bridges: Historical Perspective and Recent Technology Developments,” *J. Bridge Eng.*, 2013, doi: 10.1061/(asce)be.1943-5592.0000454.
[24] T. J. Chai and C. S. Tan, “Review on deployable structure,” *IOP Conf. Ser. Earth Environ. Sci.*, vol. 220, no. 1, p. 012034, Jan. 2019, doi: 10.1088/1755-1315/220/1/012034.
[25] S. Bright, “Briefing: Portable bridging for civil contingency and disaster response: EasiBridge – the future of lightweight bridging,” *Proc. Inst. Civ. Eng. - Civ. Eng.*, vol. 179, no. 1, pp. 6–9, Sep. 2025, doi: 10.1680/jcien.25.00360.
[26] G. R. Thomas and B. J. Sia, “A Rapidly Deployable Bridge System,” in *Structures Congress 2013*, Pittsburgh, Pennsylvania, United States: American Society of Civil Engineers, Apr. 2013, pp. 656–667. doi: 10.1061/9780784412848.058.
[27] G. Lederman, Z. You, and B. Glišić, “A novel deployable tied arch bridge,” *Eng. Struct.*, vol. 70, pp. 1–10, Jul. 2014, doi: 10.1016/j.engstruct.2014.03.015.
[28] J. Szelka and A. Wysoczański, “Modern structures of military logistic bridges,” *Open Eng.*, vol. 12, no. 1, pp. 1106–1112, Dec. 2022, doi: 10.1515/eng-2022-0391.
[29] “M60 AVLB,” *Wikipedia*. Jun. 11, 2026. Accessed: Aug. 09, 2026. [Online]. Available: https://en.wikipedia.org/w/index.php?title=M60_AVLB&oldid=1358799575
[30] “British company WFEL will deliver retrofit kits for Dry Support Bridge system of US army.” Accessed: Aug. 09, 2026. [Online]. Available: https://www.armyrecognition.com/archives/archives-land-defense/2020/british-company-wfel-will-deliver-retrofit-kits-for-dry-support-bridge-system-of-us-army
[31] 메쎄이상-MESSE ESANG, “Line of Communication Bridge (LOCB) - Acrow Bridge,” Linkonbiz. Accessed: Aug. 09, 2026. [Online]. Available: https://linkonbiz.com/product/10669
[32] W.-F. Chen and L. Duan, *Bridge Engineering Handbook, Second Edition: Superstructure Design*. CRC Press, 2014.
[33] N. Farmer, “Book review: Cable Supported Bridges- Concept and Design,” *Proc. Inst. Civ. Eng. - Eng. Comput. Mech.*, vol. 166, no. 4, pp. 229–229, Dec. 2013, doi: 10.1680/eacm.13.00006.
[34] C. P. Quaglia, A. J. Dascanio, and A. P. Thrall, “Bascule shelters: A novel erection strategy for origami-inspired deployable structures,” *Eng. Struct.*, vol. 75, pp. 276–287, Sep. 2014, doi: 10.1016/j.engstruct.2014.06.003.

[35] M. M. R. Komol, A. N. M. Mizanur Rahman, A. K. Podder, M. S. Hasan, and S. Islam, "Design of Automated Bascule Bridge and Collision Avoidance with Water Traffic," *Transp. Telecommun. J.*, vol. 25, no. 1, pp. 54–65, Feb. 2024, doi: 10.2478/ttj-2024-0006.
[36] Y. Zhu and E. T. Filipov, "Large-scale modular and uniformly thick origami-inspired adaptable and load-carrying structures," *Nat. Commun.*, vol. 15, no. 1, p. 2353, Mar. 2024, doi: 10.1038/s41467-024-46667-0.
[37] Y. Zou, "Application, Development and Challenges of Deployable Structures in Bridge Engineering," *Acad. J. Sci. Technol.*, vol. 20, no. 2, pp. 426–430, Mar. 2026, doi: 10.54097/n9phc933.
[38] Q. Yan, "Advances in the Application of Deployable Structures in Bridge Engineering," *Acad. J. Sci. Technol.*, vol. 20, no. 2, pp. 236–240, Mar. 2026, doi: 10.54097/j0g5z582.
[39] I. Ario, Y. Chikahiro, and Y. Tanaka, *Dynamic analysis for the prototype of a new type of Mobilebridge TM*. 2011.
[40] Y. Chikahiro *et al.*, "Experimental and numerical study of full-scale scissor type bridge," *Autom. Constr.*, vol. 71, pp. 171–180, Nov. 2016, doi: 10.1016/j.autcon.2016.05.007.
[41] Y. Chikahiro *et al.*, "Dynamics of the scissors-type Mobile Bridge," *Procedia Eng.*, vol. 199, pp. 2919–2924, Jan. 2017, doi: 10.1016/j.proeng.2017.09.339.
[42] K. Yoshida, I. Ario, M. Zawidzki, and Y. Hama, "Optimization Problem of the size-scale for a Foldable Chain Scissors Structure based on Stress Analysis," *J. Phys. Conf. Ser.*, vol. 2647, no. 4, p. 042005, Jun. 2024, doi: 10.1088/1742-6596/2647/4/042005.
[43] I. Ario, Y. Hama, K. Chanthamanivong, Y. Chikahiro, A. Fujiwara, and H. Ma, "Influence Line-Based Design of Scissors-Type Bridge," *Appl. Sci.*, vol. 12, no. 23, p. 12170, Jan. 2022, doi: 10.3390/app122312170.
[44] Y. Chikahiro, S. Zenzai, and I. Ario, "A new formula for estimation of vertical natural frequency for a scissors-type bridge through hammering tests and numerical simulation," *Meccanica*, vol. 60, no. 8, pp. 2345–2360, Aug. 2025, doi: 10.1007/s11012-025-01972-w.
[45] K. Chanthamanivong, I. Ario, and Y. Chikahiro, "Smart design of coupling scissors-type bridge," *Structures*, vol. 30, pp. 206–216, Apr. 2021, doi: 10.1016/j.istruc.2020.12.044.
[46] E. Georgantzia and M. M. Kashani, "On the use of aluminium alloys in sustainable design, construction and rehabilitation of bridges," *Proc. Inst. Civ. Eng. - Bridge Eng.*, vol. 178, no. 3, pp. 229–241, Jun. 2025, doi: 10.1680/jbren.23.00018.
[47] L. Y. Soh, C. S. Tan, Y. E. Tu, B. F. Yip, and A. Sulaiman, "STRUCTURAL BEHAVIOUR OF ALUMINIUM ALLOY BEAMS TO EUROCODE 9," *ASEAN Eng. J.*, vol. 15, no. 4, pp. 47–58, Dec. 2025, doi: 10.11113/aej.v15.23052.
[48] H. T. Ali *et al.*, "Fiber reinforced polymer composites in bridge industry," *Structures*, vol. 30, pp. 774–785, Apr. 2021, doi: 10.1016/j.istruc.2020.12.092.
[49] W. Hu, Y. Li, and H. Yuan, "Review of Experimental Studies on Application of FRP for Strengthening of Bridge Structures," *Adv. Mater. Sci. Eng.*, vol. 2020, no. 1, p. 8682163, Jan. 2020, doi: 10.1155/2020/8682163.
[50] P. G. Kossakowski and W. Wciślik, "Fiber-Reinforced Polymer Composites in the Construction of Bridges: Opportunities, Problems and Challenges," *Fibers*, vol. 10, no. 4, p. 37, Apr. 2022, doi: 10.3390/fib10040037.
[51] J. Qureshi, "A Review of Fibre Reinforced Polymer Bridges," *Fibers*, vol. 11, no. 5, p. 40, May 2023, doi: 10.3390/fib11050040.

[52] W. Hu, Y. Li, and H. Yuan, "Review of Experimental Studies on Application of FRP for Strengthening of Bridge Structures," *Adv. Mater. Sci. Eng.*, vol. 2020, no. 1, p. 8682163, Jan. 2020, doi: 10.1155/2020/8682163.

[53] M. J. Robinson and J. B. Kosmatka, "Light-Weight Fiber-Reinforced Polymer Composite Deck Panels for Extreme Applications," *J. Compos. Constr.*, vol. 12, no. 3, pp. 344–354, Jun. 2008, doi: 10.1061/(ASCE)1090-0268(2008)12:3(344).

[54] M. S. Pfeil, A. M. A. J. Teixeira, and R. C. Battista, "Experimental tests on GFRP truss modules for dismountable bridges," *Compos. Struct.*, vol. 89, no. 1, pp. 70–76, Jun. 2009, doi: 10.1016/j.compstruct.2008.06.019.

[55] Q. Zhang, Z. Xu, and Y. Hu, "Built-Up Fiber-Reinforced Polymers (FRP) Profiles with Improved Shear Performance for FRP–Concrete Hybrid Section," *Buildings*, vol. 13, no. 9, p. 2298, Sep. 2023, doi: 10.3390/buildings13092298.

[56] G. Sedlacek, H. Trumpf, and U. Castrischer, "Development of a Light-Weight Emergency Bridge," *Struct. Eng. Int.*, vol. 14, no. 4, pp. 282–287, Nov. 2004, doi: 10.2749/101686604777963702.

[57] J. B. Kosmatka, "Structural testing of DARPA/BIR composite army bridge treadway," *Compos. Struct.*, vol. 44, no. 2–3, pp. 99–115, Feb. 1999, doi: 10.1016/S0263-8223(98)00095-6.

[58] J. Xiong, P. Ai, J. Xu, J.-Q. Yang, and P. Feng, "A comprehensive study on CFRP rapid portable bridge: Design, experimental investigation and finite element analysis," *Compos. Struct.*, vol. 289, p. 115439, Jun. 2022, doi: 10.1016/j.compstruct.2022.115439.

[59] D. Zhang *et al.*, "Experimental Characterization of Static Behavior of a New GFRP–Metal Space Truss Deployable Bridge: Comparative Case Study," *J. Bridge Eng.*, vol. 26, no. 1, p. 05020011, Jan. 2021, doi: 10.1061/(ASCE)BE.1943-5592.0001650.

[60] D. Zhang *et al.*, "Experimental Characterization of Static Behavior of a New GFRP–Metal Space Truss Deployable Bridge: Comparative Case Study," *J. Bridge Eng.*, vol. 26, no. 1, p. 05020011, Jan. 2021, doi: 10.1061/(ASCE)BE.1943-5592.0001650.

[61] F.-Y. Yeh, K.-C. Chang, Y.-C. Sung, H.-H. Hung, and C.-C. Chou, "A novel composite bridge for emergency disaster relief: Concept and verification," *Compos. Struct.*, vol. 127, pp. 199–210, Sep. 2015, doi: 10.1016/j.compstruct.2015.03.012.

[62] J. André, R. Beale, and A. Baptista, "Bridge Construction Equipment: An Overview of the Existing Design Guidance," *Struct. Eng. Int.*, vol. 22, no. 3, pp. 365–379, Aug. 2012, doi: 10.2749/101686612X13363869853419.

[63] M. A. Mora Quispe, L. Todisco, and H. Corres Peiretti, "Design Basis of Movable Scaffolding Systems Following American and European Code Provisions and Recommendations," *Balt. J. Road Bridge Eng.*, vol. 16, no. 2, pp. 151–177, Jun. 2021, doi: 10.7250/bjrbe.2021-16.528.

[64] A. Galińska, "Mechanical Joining of Fibre Reinforced Polymer Composites to Metals—A Review. Part I: Bolted Joining," *Polymers*, vol. 12, no. 10, p. 2252, Sep. 2020, doi: 10.3390/polym12102252.

[65] G. Olivier, F. Csillag, E. Tromp, and M. Pavlović, "Static, fatigue and creep performance of blind-bolted connectors in shear experiments on steel-FRP joints," *Eng. Struct.*, vol. 230, p. 111713, Mar. 2021, doi: 10.1016/j.engstruct.2020.111713.

[66] M. S. Pfeil, A. M. A. J. Teixeira, and R. C. Battista, "Experimental tests on GFRP truss modules for dismountable bridges," *Compos. Struct.*, vol. 89, no. 1, pp. 70–76, Jun. 2009, doi: 10.1016/j.compstruct.2008.06.019.

[67] A. M. A. J. Teixeira, M. S. Pfeil, and R. C. Battista, “Structural evaluation of a GFRP truss girder for a deployable bridge,” *Compos. Struct.*, vol. 110, pp. 29–38, Apr. 2014, doi: 10.1016/j.compstruct.2013.11.014.

[68] J. L. Clarke and European Structural Polymeric Composites Group, Eds., *Structural design of polymer composites: EUROCOMP design code and handbook*, Transf. to digital printing. London: Spon, 2009.

[69] R. Q. Bridge, T. Sukkar, I. G. Hayward, and M. van Ommen, “Behaviour and design of structural steel pins,” *Steel Compos. Struct.*, vol. 1, no. 1, pp. 97–110, Mar. 2001, doi: 10.12989/SCS.2001.1.1.097.

[70] G. Li, Y. Lyu, and Y. Wang, “Ductility and Strength of High-strength Bolted Connections for High-strength Constructional Steels,” *ce/papers*, vol. 5, no. 4, pp. 28–35, Sep. 2022, doi: 10.1002/cepa.1724.

[71] J. Conde, L. S. Da Silva, T. Tankova, R. Simões, and T. Abecasis, “Design of pin connections between steel members,” *J. Constr. Steel Res.*, vol. 201, p. 107752, Feb. 2023, doi: 10.1016/j.jcsr.2022.107752.

[72] J. Vičan and M. Farbák, “Analysis of High - Strength Steel Pin Connection,” *Civ. Environ. Eng.*, vol. 16, no. 2, pp. 276–281, Dec. 2020, doi: 10.2478/cee-2020-0027.

[73] L. Liu, X. Wang, Z. Wu, and T. Keller, “Resistance and ductility of FRP composite hybrid joints,” *Compos. Struct.*, vol. 255, p. 113001, Jan. 2021, doi: 10.1016/j.compstruct.2020.113001.

[74] R. Gopalan and P. Narayanan, “Experimental and numerical evaluation of pultruded GFRP double-lap joints with different mechanical fasteners,” *Results Eng.*, vol. 18, p. 101035, Jun. 2023, doi: 10.1016/j.rineng.2023.101035.

[75] F. Csillag and M. Pavlović, “Push-out behaviour of demountable injected vs. blind-bolted connectors in FRP decks,” *Compos. Struct.*, vol. 270, p. 114043, Aug. 2021, doi: 10.1016/j.compstruct.2021.114043.

[76] D. S. E. Abdelkerim, X. Wang, H. A. Ibrahim, and Z. Wu, “Effect of Connection Techniques on the Static and Fatigue Performance of Pultruded Basalt FRP Multibolted Joints,” *J. Compos. Constr.*, vol. 24, no. 5, p. 04020046, Oct. 2020, doi: 10.1061/(ASCE)CC.1943-5614.0001062.

[77] Z. Jiang, S. Wan, Z. Fang, and A. Song, “Static and fatigue behaviours of a bolted GFRP/steel double lap joint,” *Thin-Walled Struct.*, vol. 158, p. 107170, Jan. 2021, doi: 10.1016/j.tws.2020.107170.

[78] Y. Chen, M. Duan, X. Zou, Y. Feng, and G. Li, “Experimental and Numerical Investigation of Joints for a Pultruded Fiber-Reinforced Polymer Truss,” *Polymers*, vol. 14, no. 22, p. 4810, Jan. 2022, doi: 10.3390/polym14224810.

[79] J. J. Moy, C. S. Tan, S. Mohammad, and A. R. Z. Abidin, “State-of-Art review on deployable scissor structure in construction,” *Structures*, vol. 42, pp. 160–180, Aug. 2022, doi: 10.1016/j.istruc.2022.05.084.

[80] M. V. B. Santana, L. I. W. Arnouts, T. J. Massart, P. B. Gonçalves, and P. Z. Berke, “Corotational 3D joint finite element tailored for the simulation of bistable deployable structures,” *Eng. Struct.*, vol. 227, p. 111387, Jan. 2021, doi: 10.1016/j.engstruct.2020.111387.

[81] S. Li, Y. Zheng, J. Zhang, and Y. Luo, “Uncertainty and Sensitivity Analysis of Deployable Structures with Clearance Combining Finite Particle Method and Chebyshev Polynomial Method,” *Int. J. Struct. Stab. Dyn.*, p. 2650415, Sep. 2025, doi: 10.1142/S0219455426504158.

[82] J. R. Correia *et al.*, *Design of Fibre-Polymer Composite Structures: Commentary to European Technical Specification CEN/TS 19101: 2022*, 1st ed. London: CRC Press, 2025. doi: 10.1201/9781032706948.

[83] A. M. Girão Coelho, J. T. Mottram, and K. A. Harries, "Bolted connections of pultruded GFRP: Implications of geometric characteristics on net section failure," *Compos. Struct.*, vol. 131, pp. 878–884, Nov. 2015, doi: 10.1016/j.compstruct.2015.06.048.

[84] J. L. Clarke and European Structural Polymeric Composites Group, Eds., *Structural design of polymer composites: EUROCOMP design code and handbook*, Transf. to digital printing. London: Spon, 2009.

[85] X. Yu, Y. Ji, W. Wang, S. Cheng, and W. Xu, "Static performances of scissor structures," *Structures*, vol. 65, p. 106684, Jul. 2024, doi: 10.1016/j.istruc.2024.106684.

[86] I. Ario *et al.*, "Structural analysis of a scissor structure," *Bull. Pol. Acad. Sci. Tech. Sci.*, pp. 1319–1332, Dec. 2020, doi: 10.24425/bpasts.2020.134623.

[87] X. Yu, Y. Ji, W. Wang, S. Cheng, and W. Xu, "Static performances of scissor structures," *Structures*, vol. 65, p. 106684, Jul. 2024, doi: 10.1016/j.istruc.2024.106684.

[88] "Nissan URVAN - Colors & Dimensions | Nissan Dubai," Nissan. Accessed: Aug. 18, 2026. [Online]. Available: https://en.nissan-dubai.com/vehicles/new/urvan/colors-and-dimensions.html

[89] Y. Chikahiro, I. Ario, and M. Nakazawa, "Theory and Design Study of a Full-Scale Scissors-Type Bridge," *J. Bridge Eng.*, vol. 21, no. 9, p. 04016051, Sep. 2016, doi: 10.1061/(ASCE)BE.1943-5592.0000913.

[90] J. Bergenudd, J.-M. Battini, R. Crocetti, and C. Pacoste, "Dynamic testing and numerical modelling of a pedestrian timber bridge at different construction stages," *Eng. Struct.*, vol. 279, p. 115429, Mar. 2023, doi: 10.1016/j.engstruct.2022.115429.

[91] J. M. Guerrero, A. Sasikumar, J. Llobet, and J. Costa, "A computationally efficient methodology to simulate hybrid bolted joints including thermal effects," *Mech. Adv. Mater. Struct.*, vol. 30, no. 1, pp. 48–66, Jan. 2023, doi: 10.1080/15376494.2021.2007555.

Annex I

Wheeled Pressure			CFRP					H	300	[mm]	
	Load (tons)	Load (kN)						B	240	[mm]	
Mass of Deck	2.41	24.01						t	18	[mm]	
Selfweight (Sections only)	3.5	34.87						Cross-sectional Area	18144	[mm^2]	
Total Selfweight	5.91	58.89									
	Distance (m)	U1 (mm)	U2(mm)	S11 (MPa)		SM (kNm)	Section Force (kN)		Shear Force (kN)	Reaction Force (kN)	Position
							Comp	Tension			
SelfWeight (SW)+wind	0.00	-20.62	45.14	-43.41	29.90	70.20	-62.50	26.70	34.10	57.00	
Case 1 + SW	3.00	-22.77	50.72	-52.67	32.60	85.50	-79.50	28.70	41.50	83.50	Deck 1
Case 2 + SW	6.00	-27.27	62.03	-66.56	39.51	108.00	-99.70	33.30	52.30	91.60	Deck 2
Case 3 + SW	9.00	-31.79	72.24	-73.00	49.50	118.10	-104.00	47.10	57.20	93.70	Deck 3
Case 4 + SW	***12.00***	***35.10***	***81.26***	***-73.03***	***54.76***	***117.90***	***-101.70***	***53.30***	***57.20***	***90.70***	***Deck 4***
Case 5 + SW	15.00	-36.00	77.43	-68.06	53.40	109.80	-94.10	52.20	53.20	83.90	Deck 5
Case 6 + SW	18.00	-33.22	66.29	-59.54	45.06	96.10	-82.80	48.30	46.60	74.20	Deck 6
Case 7 + SW	21.00	-25.58	52.37	-48.89	34.32	79.00	-69.30	37.70	38.30	62.70	Deck 7
Pedestrian Loads+SW+ wind		***77.68***	***168.46***	***-160.03***	***109.96***	***259.00***	***-266.60***	***101.10***	***125.30***	***210.50***	***Total Structure***
Three Convoy		-54.36	118.69	-112.30	77.35	181.70	-159.30	70.50	87.95	142.50	
SelfWeigth as Cantilever			764.00	-186.94	0.00	297.70	-206.10	82.60	143.90	165.30	

Tracked Pressure			CFRP					H	300	[mm]	
	Load (tons)	Load (kN)						B	240	[mm]	
Mass of Deck	2.41	24.01						t	18	[mm]	
Selfweight (Sections only)	3.5	34.87						Cross-sectional Area	18144	[mm^2]	
Total Selfweight	5.91	58.89									
	Distance (m)	U1 (mm)	U2(mm)	S11 (MPa)		SM (kNm)	Section Force (kN)		Shear Force (kN)	Reaction Force (kN)	Position
							Comp	Tension			
SelfWeight (SW)+wind	0.00	-20.62	45.14	-43.41	29.90	70.20	-62.50	26.70	34.10	57.00	
Case 1 + SW+w	3.00	-22.33	49.57	-50.77	32.05	82.40	-76.00	28.30	-39.90	78.60	Deck 1
Case 2 + SW+w	6.00	-26.01	58.85	-62.30	37.30	101.00	-92.90	32.00	49.00	85.30	Deck 2
Case 3 + SW+w	9.00	-24.93	67.40	-67.70	45.49	109.50	-96.60	43.20	53.10	87.20	Deck 3
Case 4 + SW+w	***12.00***	***-32.49***	***78.36***	***-67.80***	***50.22***	***109.52***	***-94.70***	***48.60***	***53.10***	***84.80***	***Deck 4***
Case 5 + SW+w	15.00	-33.27	73.97	-63.78	49.34	102.90	-88.60	47.60	49.90	79.20	Deck 5
Case 6 + SW+w	18.00	-31.05	62.61	-56.81	41.84	91.70	-79.40	44.10	44.40	71.30	Deck 6
Case 7 + SW+w	21.00	-24.84	51.28	-48.07	33.67	77.80	-68.30	35.90	37.70	61.90	Deck 7
Pedestrian Loads+SW+ wind		***77.68***	***168.46***	***-160.03***	***109.96***	***259.00***	***-266.60***	***101.10***	***125.30***	***210.50***	***Total Structure***
Three Convoy+w		-48.32	109.00	-100.08	68.83	161.90	-142.20	62.90	78.40	127.50	
SelfWeigth as Cantilever+w			764.00	-186.94	0.00	297.70	-206.10	82.60	143.90	165.30	

Wheeled Pressure			Aluminium					H	450	[mm]	
	Load (tons)	Load (kN)						B	250	[mm]	
Mass of Deck	2.41	24.01						t	10	[mm]	
Selfweight (Sections only)	4.84	48.23						Cross-sectional Area	13600	[mm^2]	
Total Selfweight	7.25	72.24									
	Distance (m)	U1 (mm)	U2(mm)	S11 (MPa)		SM (kNm)	Section Force (kN)		Shear Force (kN)	Reaction Force (kN)	Position
							Comp	Tension			
SelfWeight (SW)+wind	0.00	-22.65	49.95	**46.02**		79.20	-70.80	30.00	-38.50	64.30	
Case 1 + SW+w	3.00	-24.76	55.41	**54.61**		94.50	-87.82	31.98	45.80	90.80	Deck 1
Case 2 + SW+w	6.00	-29.16	66.51	**67.62**		116.90	-107.90	36.50	56.70	98.90	Deck 2
Case 3 + SW+w	9.00	-33.58	76.53	**73.74**		126.90	-112.20	50.30	61.50	101.10	Deck 3
Case 4 + SW+w	***12.00***	***-36.82***	***85.46***	***73.81***		***126.80***	***-109.90***	***56.51***	***61.51***	***98.07***	***Deck 4***
Case 5 + SW+w	15.00	-37.69	81.59	**69.17**		228.70	-102.30	55.10	57.60	91.10	Deck 5
Case 6 + SW+w	18.00	-23.80	70.75	**61.17**		105.05	-91.10	51.70	50.90	81.48	Deck 6
Case 7 + SW+w	21.00	-27.50	57.05	**51.17**		87.97	-77.65	41.20	42.74	70.00	Deck 7
Pedestrian Loads+SW+ wind		***-78.48***	***171.08***	***155.28***		***267.50***	***-234.50***	***104.00***	***129.40***	***217.60***	***Total Structure***
Three Convoy+w		-55.67	122.21	**110.57**		190.50	-167.40	73.70	92.20	149.70	
SelfWeigth as Cantilever+w			919.74	**216.89**		365.30	-252.80	101.60	176.70	202.70	